

A SOLUTION OF THE NONHOMOGENEOUS BIHARMONIC
EQUATION BY THE BOUNDARY ELEMENT METHOD

By

CHARLES VIPPERMAN CAMP

Bachelor of Science in Civil Engineering
Auburn University
Auburn, Alabama
1981

Master of Science
Auburn University
Auburn, Alabama
1986

Submitted to the Faculty of the Graduate College
of the Oklahoma State University
in partial fulfillment of the requirements
for the Degree of
DOCTOR OF PHILOSOPHY
December, 1987

Thesis
1987D
C1865
cop.2



COPYRIGHT

by

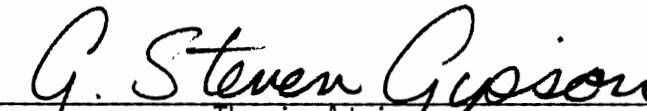
Charles Vipperman Camp

December 1987

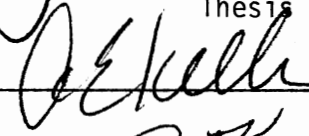
1307083

A SOLUTION OF THE NONHOMOGENEOUS BIHARMONIC
EQUATION BY THE BOUNDARY ELEMENT METHOD

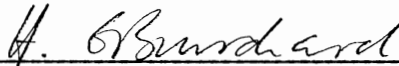
Thesis Approved:




Thesis Adviser









Dean of the Graduate College

ACKNOWLEDGMENTS

There are many people I wish to thank for their individual contributions to my education and the successful completion of this work. First, I wish to express my sincere appreciation and gratitude to my major adviser, Dr. G. Steven Gipson, for his guidance and encouragement throughout my graduate work. His devotion to quality education and the enthusiasm he shows in his research activities have greatly influenced me. Also, I wish to thank Dr. Allen E. Kelly, Dr. James K. Good, and Dr. Herman G. Burchard for their efforts as members of my graduate committee.

I wish to thank the faculty and staff of the Computer Graphics Research and Applications Laboratory (CGRAL) at Louisiana State University, especially Dr. John A. Brewer III, Jeffrey N. Jortner, and Alaric Hagg, for providing an excellent environment in which to learn and grow as a researcher. A special thanks goes to former members of CGRAL who are now students at Oklahoma State University, Juan C. Ortiz and Harold G. Walters, for their friendship and insightful contributions to this work. The many hours we spent together discussing and criticizing our collective research efforts have been an important part of my education. Also, I would like to extend a very special thanks to Ms. Charlene Fries for all her time and effort in helping me prepare this manuscript.

I would like to express my appreciation to Mr. Paul K. Senter and Dr. N. Radhakrishnan of the Information Technology Laboratory of the Waterways Experiment Station for providing support for this work under Purchase Order No. DACW39-87-P-0771. Also acknowledged is the Oklahoma State University Center for Energy Research for providing additional support under Grant No. 1-1-50728. Finally, in the way of financial aid, I would like to thank the School of Civil Engineering at Oklahoma State University for its provision of a teaching assistantship during the last two years.

A very special expression of gratitude goes to the most important person in my life, my wife, Kay. In her love and compassion I have found more strength and confidence than I had believed to be possible. Her devotion and unending encouragement have been a constant inspiration to me especially when times were rough. Her considerable editorial skills helped turn the difficult task of preparing this manuscript into a relatively painless experience.

Finally, I wish to thank the people who gave me every opportunity in life and who are responsible for my success: my parents, Barbara and Billy; and my grandmother, Elizabeth Vipperman. The love and support my parents give to each other and to every member of our family is a never ending source of strength to me. Their unwavering faith continues to influence my life everyday. In my grandmother's beautiful spirit and wonderful outlook on life I have always found comfort and love. It is to my family that I dedicate this work.

TABLE OF CONTENTS

Chapter	Page
I. INTRODUCTION	1
II. BOUNDARY INTEGRAL EQUATION FORMULATION	5
Boundary Element Formulation	14
Summary	18
III. BOUNDARY DISCRETIZATION	20
Isoparametric Linear Elements	20
Quadratic Element	28
Isoparametric Quadratic Elements	29
Subparametric Quadratic Elements	37
Overhauser Element	43
Isoparametric Overhauser Elements	44
Subparametric Overhauser Elements	49
Summary	54
IV. DOMAIN DISCRETIZATION AND INTERNAL POINT CALCULATIONS	55
Domain Discretization	55
Integral Transformations	56
Linear Elements	59
General Isoparametric Element	62
Domain Fanning	63
Iterative Solution	66
Internal Point Calculations	69
Linear Isoparametric Elements	70
Higher Order Elements	76
Summary	77
V. EXAMPLE ANALYSES	79
Deflections of Thin Plates	79
Circular Clamped Plates	82
Concentrated Load at Plate Center	82
Uniform Load	86
Quadratic Load	86
Asymmetric Loading	88
Elastic Foundations	90

Chapter	Page
Simply Supported Rectangular Plates	92
Edge Moments	94
Thermal Loads	94
Concentrated Load	95
Uniform Load	97
Hydrostatic Load	99
Quadratic Load	99
Cubic Load	104
Elastic Foundations	104
In-Plane Forces	106
Variable Thickness	109
Rectangular Plates with Various Edge Conditions	111
One Clamped Edge	111
Two Opposite Edges Clamped	111
All Edges Clamped	113
All Edges Clamped on an Elastic Foundation	113
Plates of Various Shapes	117
Simply Supported Triangular Plates	117
Triangular Plates with Two or Three Edges Clamped	117
Skewed Plates	120
Rhombic Plates	120
Hexagonal Plates	120
Corner Plates	120
Incompressible Viscous Fluid Flow at Low Reynolds Numbers	123
Moving-Wall Problem	126
Inflow-Outflow Problem	126
Flow Through a Fibrous Filter	133
Flow in Bearings of Arbitrary Geometries	133
Concluding Remark	138
 VI. SUMMARY AND CONCLUSIONS	 143
Summary	143
Conclusion	144
Recommendations	146
 REFERENCES	 148

LIST OF TABLES

Table	Page
1. Deflection and Moment Function for a Clamped Circular Plate With a Concentrated Load P at its Center	85
2. Deflection and Moment Function for a Clamped Circular Plate Under a Uniform Load $P(r) = q$	87
3. Deflection and Moment Function for a Clamped Circular Plate Under a Quadratic Load $P(r) = q(r/a)^2$	89
4. Deflection and Moment Function for a Clamped Circular Plate Under an Asymmetric Load $P(r) = q_0 + q_1 \cos(\theta)$	91
5. Deflection and Moment Function for a Clamped Circular Plate Under a Uniform Load q on a Winkler Elastic Foundation	91
6. Edge Moments for a Clamped Circular Plate Under a Uniform Load q on a Winkler Elastic Foundation	93
7. Center Deflection and Moment Function for a Simply Supported Rectangular Plate Bent by Moments Distributed Along Two Parallel Edges	93
8. Center Deflection for Simply Supported Rectangular Plate Bent by Thermal Loads	96
9. Center Deflection for a Simply Supported Rectangular Plate Bent by a Concentrated Load, P , Located at Its Center	96
10. Deflection, Moment Function, and Their Derivatives at Various Points on a Uniformly Loaded Square Plate	100
11. Deflection, Moment Function, and Their Derivatives at Various Points on a Square Plate Under a Hydrostatic Load	101
12. Deflection, Moment Function, and Their Derivatives at Various Points on a Square Plate Under a Quadratic Load	102

Table	Page
13. Deflection, Moment Function, and Their Derivatives at Various Points on Square Plate Under a Cubic Load	105
14. Center Deflection for a Simply Supported Plate Under a Uniform Load q on a Winkler Elastic Foundation	107
15. Center Deflection for a Simply Supported Plate Under a Hydrostatic Load $q(x/a)$, on a Winkler Elastic Foundation	107
16. Center Deflection for a Simply Supported Plate Under a Quadratic Load $q(xy/a^2)$, on a Winkler Elastic Foundation	108
17. Center Deflection for a Simply Supported Rectangular Plate Under the Combined Action of Uniform Lateral and Uniform In-Plane Forces	108
18. Center Deflection and Moment Function for a Simply Supported Rectangular Plate with One Edge Clamped Bent by a Uniform Load q	112
19. Center Deflection and Moment Function for a Simply Supported Rectangular Plate with One Edge Clamped Bent by a Hydrostatic Load $q(x/a)$	112
20. Center Deflection and Moment Function for a Rectangular Plate with Two Opposite Edges Clamped and the Other Two Simply Supported Bent by a Uniform Load q	114
21. Center Deflection and Moment Function for a Rectangular Plate with Two Opposite Edges Clamped and the Other Two Simply Supported Bent by a Hydrostatic Load $q(x/a)$	114
22. Center Deflection and Moment Function for a Rectangular Plate with All Edges Clamped Bent by a Uniform Load q	115
23. Center Deflection and Moment Function for a Rectangular Plate with All Edges Clamped Bent by a Hydrostatic Load $q(x/a)$	115
24. Center Deflection for a Simply Supported Skewed Plate Bent by a Uniform Load q	115
25. Center Deflection and Moment Function for a Simply Supported Rhombic Plate Under a Uniform Load q	122
26. Center Deflection and Moment Function for a Simply Supported Hexagonal Plate Under a Uniform Load q	122

LIST OF FIGURES

Figure	Page
1. Biharmonic Problem Definition	7
2. Linear Element Nomenclature	22
3. Definitions for Exact Analysis of Linear Elements	24
4. Quadratic Element Nomenclature	30
5. Overhauser Element Nomenclature	43
6. Behavior of Overhauser Element with Abnormal Node Spacing	50
7. Distribution of Triangular Quadrature Regions for the "Fanning" Domain Integration Technique Related to a Particular Source Point	65
8. Internal Point Locations for a Solution Map for an Arbitrary Domain	68
9. Example Models Using Various Element Types	84
10. Absolute Percent Error for the Center Deflection of a Clamped Circular Plate with a Concentrated Load at the Center	85
11. Absolute Percent Error for the Center Deflection of a Clamped Circular Plate Under a Uniform Load	87
12. Absolute Percent Error for the Center Deflection of a Clamped Circular Plate Under a Quadratic Load	89
13. Absolute Percent Error for the Center Deflection of a Simply Supported Square Plate Under a Uniform Load	98
14. Absolute Percent Error for the Center Deflection of a Simply Supported Square Plate Under a Quadratic Load	103
15. Deflection Along the Centerline, $x = a/2$, for a Simply Supported Plate of Variable Thickness	110

Figure	Page
16. Moment Function Along the Centerline, $x = a/2$, for a Simply Supported Plate of Variable Thickness	110
17. Center Deflection for a Clamped Rectangular Plate on an Elastic Foundation	116
18. Maximum Edge Moment for a Clamped Rectangular Plate on an Elastic Foundation	116
19. Deflection Along the Centerline of a Simply Supported Triangular Plate Bent by Uniform Edge Moments	118
20. Deflection Along the Centerline of a Simply Supported Triangular Plate Bent by a Uniform Load	118
21. Deflection Along the Centerline of a Triangular Plate With Two Sides Clamped	119
22. Deflection Along the Centerline of a Triangular Plate With All Edges Clamped	119
23. Skewed Plate Geometry	121
24. Rhombic and Hexagonal Plate Geometries	121
25. Corner Plates of Different Angles	124
26. Corner Plate Problem Domain Incorporating Symmetry	124
27. Deflection Across the Diagonal for Corner Plates of Different Angles	125
28. Moment Function Across the Diagonal for Corner Plates of Different Angles	125
29. Moving-Wall Problem Definition, $r = 2.0$, $\alpha = 0.0$, and $\beta = \pi$	127
30. Streamline Plot for the Moving-Wall Problem, $R_1 = 0.0$. . .	128
31. Streamline Plot for the Moving-Wall Problem, $R_1 = 10.0$. . .	129
32. Streamline Plot for the Moving-Wall Problem, $R_1 = 20.0$. . .	130
33. Inflow-Outflow Problem Definition, $r = 2.0$, $\alpha = \pi/8$, $\beta = \pi$, and $\epsilon = \epsilon_1 = \pi/32$	131
34. Streamlines Plot for the Inflow-Outflow Problem, $R = 0.0$. .	132
35. Problem Definition for Flow Through an Infinite Rectangular Array of Cylinders	134

Figure	Page
36. Streamline Plot for Flow Through an Infinite Rectangular Array of Cylinders, $R = 0.0$	135
37. Streamline Plot for Flow Through an Infinite Rectangular Array of Cylinders, $R = 10.0$	136
38. Streamline Plot for Flow Through an Infinite Rectangular Array of Cylinders, $R = 20.0$	137
39. Streamline and Vorticity Contours for an Eccentric Bearing, $e = 0.5$	139
40. Streamline and Vorticity Contours for an Eccentric Bearing, $e = 0.8$	140
41. Streamline and Vorticity Contours for an Elliptical Eccentric Bearing, $e = 0.5$	141
42. Streamline and Vorticity Contours for an Elliptical Eccentric Bearing, $e = 0.8$	142

CHAPTER I

INTRODUCTION

In the past decade there has been an enormous increase in the amount of research activity in boundary integral equation techniques. Known as "boundary element" methods (Brebbia, 1978), the subject has received considerable attention in the current literature and has gained popularity as an alternative to more traditional numerical procedures such as finite difference and finite element techniques. The major advantage of the boundary element method over other techniques, as its name would indicate, is that in many important cases only the boundary of the problem domain needs to be modeled. A boundary element formulation for a three-dimensional problem is represented by a discrete surface and for a two-dimensional problem by a discrete curve. As a result the time required to construct the discrete model and solve the boundary element approximation for a particular problem is significantly reduced.

Two major applications of the boundary element method to biharmonic analysis are found in the theory of thin plates and the flow of an incompressible viscous fluid. Considerable work has been done in applying the boundary element method to the biharmonic equation governing the theory of thin plates. Jaswon, Maiti, and Symm (1967) developed a boundary integral equation technique for biharmonic analysis with applications in two dimensional stress problems. In their work,

the biharmonic function was presented as a quadratic combination of two Laplacian functions. The resulting solution is calculated from boundary integrals involving harmonic potentials. Jaswon and Maiti (1968) extended their previous work on integral equations to the problem of clamped and simply supported plates. Other authors have presented formulations in which the biharmonic form of the fundamental solution is incorporated and applied to a variety of plate problems (Segedin and Brickell, 1968; Maiti and Chakrabarty, 1974; Altiero and Sikarskie, 1978; Stern 1979, Wu and Altiero, 1979; and Guo-Shu and Mukherjee, 1986). The approximation of the boundary in these early works was generally limited to linear variations in the geometry and a piecewise constant distribution of the biharmonic function. In most cases, the nonhomogeneous term involving the loading function was either evaluated using some form of explicit domain quadrature or separated from the numerical analysis by some change of variable.

Determining the flow field of an incompressible viscous fluid using the boundary element method was presented in a series of papers by Kelmanson, 1983(a) and 1983(b), Ingham and Kelmanson, 1984; and Hildyard et al. 1985. However, these works were limited to very slow flows which are governed adequately by the homogeneous form of the biharmonic equation. Also, the approximation of the boundary was restricted to a simple constant element formulation. If a non-zero Reynolds number flow is assumed, the governing equation becomes nonlinear and some type of iterative solution involving domain quadrature is required (Mills, 1977, and Banerjee and Butterfield, 1981).

In general there are two types of integrals required for a boundary element method solution: integrations over the surface of the

problem and domain integrations involving "body force" effects or the nonhomogeneous term of the governing equation. The accuracy of the surface integrations depends greatly on the level of representation of the geometry of each boundary segment. By improving the approximation of the actual surface geometry, the accumulation of any "discretization error" is reduced. Integrations involving the body force terms over the domain are equally important in developing a formulation which produces accurate results. Originally, this type of integration was performed using a variety of volume cell quadrature schemes all requiring explicit domain discretization.

Increasing the order of both the discrete approximation of the surface geometry and the distribution of the field variables over each segment provides greater accuracy in evaluating boundary integrals. Recently, a new boundary approximation, the Overhauser element, which provides intrinsic first derivative continuity between elements in both its representation of the geometry and the variation of the function has been developed (Ortiz, 1986; Walters, 1986).

In this work, the performance of the Overhauser element for bi-harmonic analysis will be compared to both a linear and a quadratic element formulation for a variety of boundary conditions and geometries. A series of analytic expressions will be derived for an isoparametric linear element and for the subparametric form of both the quadratic and Overhauser elements for the required surface integrations.

Several techniques are available which eliminate the need for explicit domain discretization when evaluating the integrations involving the nonhomogeneous terms. Domain integrations of special

forms of the source function may be transformed into an equivalent series of surface integrations using the appropriate form of Green's identity. However, the evaluation of the domain integrals for a general function requires some form of numerical volume quadrature. The method presented in this work will avoid any form of explicit domain discretization and will be intrinsically sensitive to the singular nature of the integrations. The resulting formulation will reduce both the modeling and the execution time of the formulation as well as improve the accuracy of the solution at both the boundary and internal points.

The objective of this work is to develop a general boundary element formulation for the nonhomogeneous biharmonic equation of higher accuracy than affordable with earlier methods for equivalent computational effort. In doing so, several numerical improvements will be developed to increase the accuracy of the solution and reduce the execution time of the formulation. In addition, a scheme for dealing with nonhomogeneous terms that are a function of the field variables and their derivatives will be implemented which will provide an efficient way to calculate iterative and nonlinear solutions of the biharmonic equations.

CHAPTER II

BOUNDARY INTEGRAL EQUATION FORMULATION

The integral equation form of the nonhomogeneous biharmonic equation may be derived several different ways. A general approach, common to many boundary element researchers, is the weighted residual technique. From this general principle, a variety of approximation schemes have developed. Some of the more widely used methods can be found in Lapidus and Pinder (1982). All weighted residual methods are similar in the respect that the unknown function is replaced by an approximation in the form of a finite linear combination of basis functions. In the finite element method, the basis functions are constructed to satisfy certain behavioral requirements over each "element" of the problem domain. The result is a polynomial form of the basis functions referred to also as a shape function or interpolation function. In a boundary element method, the finite sum approximation is represented by a combination of a shape function set and a weighting function of a particular form, referred to as the Green's function or the fundamental solution. The derivation of the fundamental solution for the biharmonic equation will be discussed later in this section.

The development of the boundary integral formulation for a nonhomogeneous biharmonic equation from a weighted residual technique is not difficult. However, it is quite cumbersome, particularly in per-

forming the integration by parts necessary to convert the domain integrals into exclusive boundary integrals. The result of this operation is to form the "inverse" problem where the biharmonic operator has been transformed from the field variable to the weighting function (Brebbia and Walker, 1980). However, the dual problem can be achieved much faster and in a more mathematically elegant fashion by using the Rayleigh-Green identity for two biharmonic functions (Jaswon and Symm, 1977). The method employed in this work will be based upon a boundary integral equation derived from the Rayleigh-Green identity.

Referring to Figure 1, consider the general nonhomogeneous biharmonic equation in a two-dimensional domain V ,

$$\nabla^4 \psi = f(x,y) \quad (1)$$

The nonhomogenous function $f(x,y)$ is a known function of the spatial coordinates. In Chapter III of this work, the possibility of $f(x,y)$ being a function of both the coordinates and the field variable will be explored. The boundary conditions for a general biharmonic problem are of four types:

$$\begin{aligned} \psi &= \bar{\psi} \text{ on } S_1 & \psi' &= \frac{\partial \bar{\psi}}{\partial n} = \bar{\psi}' \text{ on } S_2 \\ \omega &= \nabla^2 \bar{\psi} = \bar{\omega} \text{ on } S_3 & \omega' &= \frac{\partial (\nabla^2 \bar{\psi})}{\partial n} = \bar{\omega}' \text{ on } S_4 \end{aligned} \quad (2)$$

The partial derivative with respect to n denotes the normal derivative with respect to the outward normal. For a general well-posed boundary value problem involving the biharmonic operator, two of the four types of boundary conditions are prescribed at each point. The remaining two boundary quantities require another functional constraint in addi-

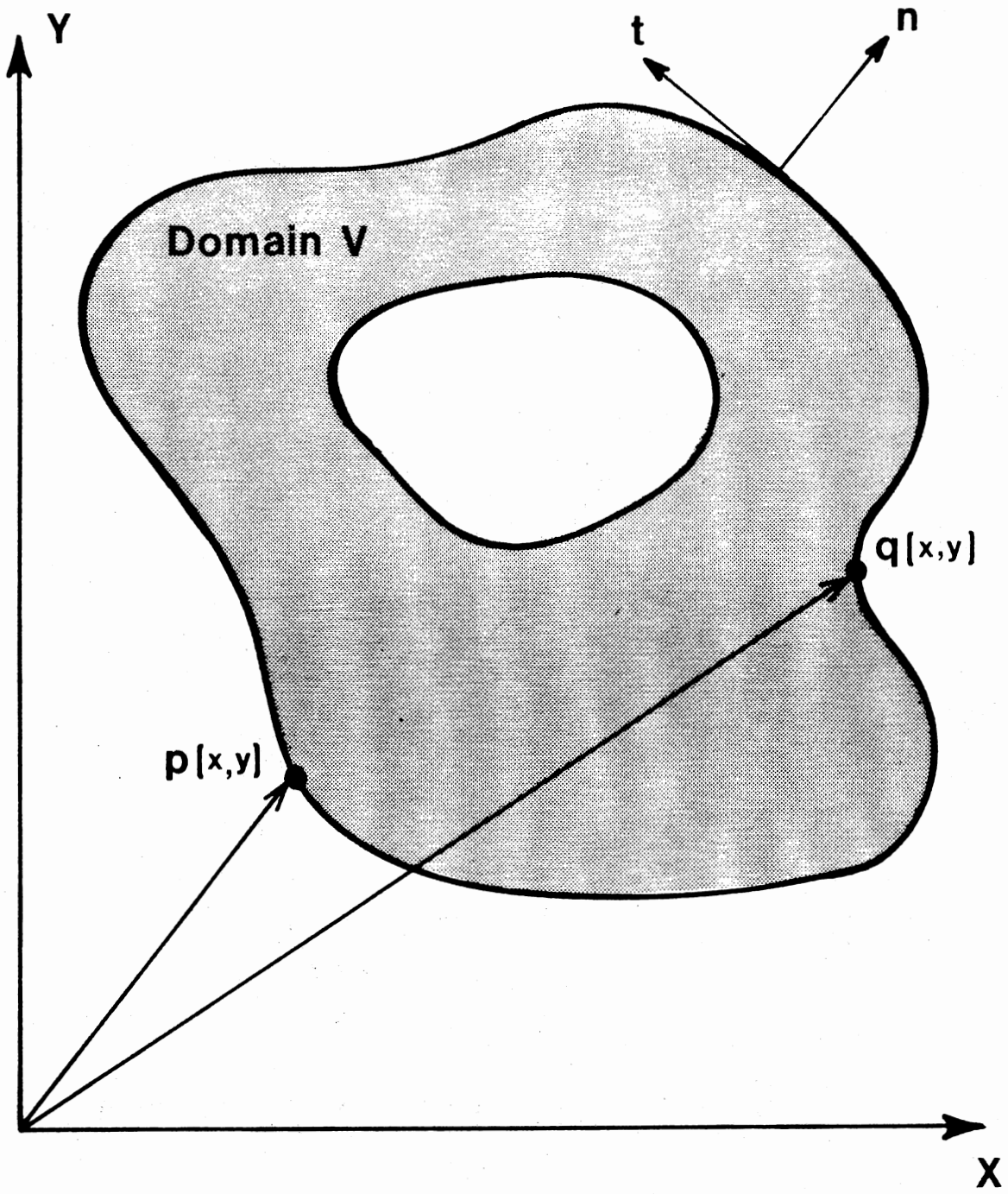


Figure 1. Biharmonic Problem Definition

tion to Equation (1). In other words, two equations are necessary in order to solve for the two remaining unknown boundary quantities. Because of the nature of the boundary conditions it is practical to introduce the Laplacian ω of the field function ψ explicitly.

Equation (1) may be transformed to an equivalent set of coupled Poisson-type equations by employing the relationship between the field variable ψ and its Laplacian, ω :

$$\nabla^2 \psi = \omega \quad (3)$$

$$\nabla^2 \omega = f(x,y) \quad (4)$$

The result, Equation (4), constitutes the second functional constraint on the biharmonic problem.

The first step in transforming Equations (1) and (4) into appropriate integral representations is the application of the Rayleigh-Green identity for two biharmonic functions to Equation (1) and Green's second identity for two Laplacian functions to Equation (4). The Rayleigh-Green identity for two biharmonic functions ψ and λ which are continuous in the domain V bounded by a closed surface S and differentiable to the fourth order in V is given as (Jawson and Symm, 1977)

$$\int_V (\psi \nabla^4 \lambda - \lambda \nabla^4 \psi) dV = \int_S \left[\psi \frac{\partial}{\partial n} (\nabla^2 \lambda) - \nabla^2 \lambda \frac{\partial \psi}{\partial n} + \nabla^2 \psi \frac{\partial \lambda}{\partial n} - \lambda \frac{\partial}{\partial n} (\nabla^2 \psi) \right] dS \quad (5)$$

Equation (5) defines the relationship between the biharmonic operator as a domain integral and a series of surface integrations. Notice that the surface integral terms are combinations of the two biharmonic

functions ψ and λ and that their derivatives are in a form identical to that of the above mentioned boundary conditions.

Green's second identity for two Laplacian functions ω and ϕ in a domain V bounded by a closed surface S , where the functions have continuous second derivatives, is (Jaswon and Symm, 1977)

$$\int_V (\omega \nabla^2 \phi - \phi \nabla^2 \omega) dV = \int_S (\omega \frac{\partial \phi}{\partial n} - \phi \frac{\partial \omega}{\partial n}) dS \quad (6)$$

The terms involved in the surface integrals on the right-hand side of Equation (6) are, like their counterparts in Equation (5), in the form of the previously defined boundary conditions.

An intermediate integral representation of the biharmonic equation may be accomplished by a direct and straightforward application of the Rayleigh-Green identity. The left-hand side of Equation (5) contains the biharmonic operator acting on both ψ and λ . The $\lambda \nabla^4 \psi$ term may be viewed as the biharmonic operator acting on the field variable ψ multiplied by a weighting function λ . The second term $\psi \nabla^4 \lambda$ characterizes the inverse problem, in which the biharmonic operator is acting on the weighting function. The volume integrals of Equation (6) contain two terms: the first term, $\phi \nabla^2 \omega$, is the Laplacian of ω multiplied by a different weighting function, and the second term, $\omega \nabla^2 \phi$, is the inverse relationship.

The final step in transforming Equations (1) and (4) into an integral equation form is the determination of the appropriate weighting functions. In boundary element analysis, the weighting functions are the fundamental solutions or the Green's functions for the operators in question. In general, the determination of the Green's function for a particular operator may be difficult.

Consider the vector \vec{p} as the position of a variable field point where the solution is desired and the vector \vec{q} as the general location of a point on the boundary or in the domain. In terms of this notation the required Green's functions are defined as the solutions to the following relationships (Brebbia, 1978):

$$\nabla^2 G_1(\vec{p}, \vec{q}) = \delta(|\vec{p} - \vec{q}|) \quad (7)$$

$$\nabla^4 G_2(\vec{p}, \vec{q}) = \delta(|\vec{p} - \vec{q}|) \quad (8)$$

where δ is the Dirac delta function. Solving Equations (7) and (8) defines the biharmonic and the Laplacian fundamental solutions for unbounded space:

$$G_1(\vec{p}, \vec{q}) = \frac{1}{2\pi} \ln|\vec{p} - \vec{q}| \quad (9)$$

$$G_2(\vec{p}, \vec{q}) = \frac{1}{8\pi} |\vec{p} - \vec{q}|^2 [\ln|\vec{p} - \vec{q}| - 1] \quad (10)$$

The integral representation of Equation (1) can now be obtained by using the Rayleigh-Green identity for the biharmonic function ψ and substituting G_2 for the biharmonic function λ . Applying Green's second identity to Equation (4) with G_1 substituted for the Laplacian function ϕ defines the integral expression of the second equation. The resulting set of coupled integral equations for a general field point are

$$\begin{aligned} \beta(\vec{p})\psi(\vec{p}) &= \int_S [\psi(\vec{q})G_1'(\vec{p}, \vec{q}) - \psi'(\vec{q})G_1(\vec{p}, \vec{q}) \\ &\quad + \omega(\vec{q})G_2'(\vec{p}, \vec{q}) - \omega'(\vec{q})G_2(\vec{p}, \vec{q})] dS \\ &\quad + \int_V f(x, y)G_2(\vec{p}, \vec{q})dV \end{aligned} \quad (11)$$

$$\begin{aligned} \beta(\vec{p})\omega(\vec{p}) &= \int_S [\omega(\vec{q})G_1'(\vec{p}, \vec{q}) - \omega'(\vec{q})G_1(\vec{p}, \vec{q})] dS \\ &\quad + \int_V f(x, y)G_1(\vec{p}, \vec{q})dV \end{aligned} \quad (12)$$

where the primes denote differentiation with respect to the outward normal of the boundary S defining a region V . The normal derivative of each Green's function can be calculated in a very straight-forward manner and are defined as

$$G_1'(\vec{p}, \vec{q}) = \frac{(x-x_p)n_x + (y-y_p)n_y}{2\pi|\vec{p}-\vec{q}|^2} \quad (13)$$

$$G_2'(\vec{p}, \vec{q}) = \frac{\ln|\vec{p}-\vec{q}|^2}{8\pi} [(x-x_p)n_x + (y-y_p)n_y] \quad (14)$$

The value of the generalized function $\beta(\vec{p})$ shown in Equations (11) and (12) is 1.0 for a point inside the domain, some fractional value on the boundary, and is zero outside the domain (Brebbia, 1978). The solution of the two coupled integral Equations (11) and (12) requires information on the boundary for $\psi(\vec{q})$, $\psi'(\vec{q})$, $\omega(\vec{q})$, and $\omega'(\vec{q})$. Two of these quantities are defined at each boundary point \vec{q} by the boundary conditions of the biharmonic problem under consideration, as shown in Figure 1. The remaining two quantities are determined by applying Equations (11) and (12) at points \vec{q} along the boundary. Once the remaining two boundary values are determined, the values for ψ and ω may be obtained at any point within the domain.

The derivatives of ψ and ω may be calculated by differentiating the integral Equations (11) and (12) with respect to the appropriate spatial coordinate. The location of the field point where the derivatives are sought is defined by the vector $\vec{p}(x,y)$. Therefore, the spatial differential operator acts on components which are functions of \vec{p} only. For example, the first derivative with respect to the x -coordinate of the functions ψ and ω are calculated as follows:

$$\begin{aligned} \frac{\partial \psi}{\partial x_p} = & \int_S \left(\psi \frac{\partial G_1'}{\partial x_p} - \psi' \frac{\partial G_1}{\partial x_p} + \omega \frac{\partial G_2'}{\partial x_p} - \omega' \frac{\partial G_2}{\partial x_p} \right) dS \\ & + \int_V f(x,y) \frac{\partial G_2}{\partial x_p} dV \end{aligned} \quad (15)$$

$$\frac{\partial \omega}{\partial x_p} = \int_S \left(\omega \frac{\partial G_1'}{\partial x_p} - \omega' \frac{\partial G_1}{\partial x_p} \right) dS + \int_V f(x,y) \frac{\partial G_1}{\partial x_p} dV \quad (16)$$

where the derivative of the Green's functions G_1 , G_1' , G_2 , and G_2' with respect to the x -coordinate are calculated as

$$\frac{\partial G_1}{\partial x_p} = \frac{1}{2\pi} \frac{(x-x_p)}{|\vec{p}-\vec{q}|^2} \quad (17)$$

$$\begin{aligned} \frac{\partial G_1'}{\partial x_p} = & -\frac{1}{2\pi} \left(\frac{2[(x-x_p)^2 n_x + (x-x_p)(y-y_p)n_y]}{|\vec{p}-\vec{q}|^4} \right. \\ & \left. - \frac{n_x}{|\vec{p}-\vec{q}|^2} \right) \end{aligned} \quad (18)$$

$$\frac{\partial G_2}{\partial x_p} = \frac{1}{8\pi} [(x-x_p)(\ln|\vec{p}-\vec{q}|^2 - 1)] \quad (19)$$

$$\begin{aligned} \frac{\partial G_2'}{\partial x_p} = & \frac{1}{8\pi} \left(\frac{2(x-x_p)}{|\vec{p}-\vec{q}|^2} [(x-x_p)n_p + (y-y_p)n_y] \right. \\ & \left. + n_x [\ln|\vec{p}-\vec{q}|^2 - 1] \right) \end{aligned} \quad (20)$$

In a similar manner, the first derivative of ψ and ω with respect to the y -coordinate may be determined from the following expressions:

$$\begin{aligned} \frac{\partial \psi}{\partial y_p} = & \int_S \left(\psi \frac{\partial G_1'}{\partial y_p} - \psi' \frac{\partial G_1}{\partial y_p} + \omega \frac{\partial G_2'}{\partial y_p} - \right. \\ & \left. - \omega' \frac{\partial G_2}{\partial y_p} \right) dS + \int_V f(x,y) \frac{\partial G_2}{\partial y_p} dV \end{aligned} \quad (21)$$

$$\frac{\partial \omega}{\partial y_p} = \int_S \left(\omega \frac{\partial G_1'}{\partial y_p} - \omega' \frac{\partial G_1}{\partial y_p} \right) dS + \int_V f(x,y) \frac{\partial G_1}{\partial y_p} dV \quad (22)$$

where the derivative of the Green's functions G_1 , G_1' , G_2 , and G_2' with respect to the y -coordinate are calculated as

$$\frac{\partial G_1}{\partial y_p} = \frac{1}{2\pi} \frac{(x-x_p)}{|\vec{p}-\vec{q}|^2} \quad (23)$$

$$\begin{aligned} \frac{\partial G_1'}{\partial y_p} = & -\frac{1}{2\pi} \left(\frac{2[(x-x_p)(y-y_p)n_x + (y-y_p)^2 n_y]}{|\vec{p}-\vec{q}|^4} \right. \\ & \left. - \frac{n_y}{|\vec{p}-\vec{q}|^2} \right) \quad (24) \end{aligned}$$

$$\frac{\partial G_2}{\partial y_p} = \frac{1}{8\pi} [(y-y_p)(\ln|\vec{p}-\vec{q}|^2 - 1)] \quad (25)$$

$$\begin{aligned} \frac{\partial G_2'}{\partial y_p} = & \frac{1}{8\pi} \left(\frac{2(y-y_p)}{|\vec{p}-\vec{q}|^2} [(x-x_p)n_x + (y-y_p)n_y] \right. \\ & \left. + n_y [\ln|\vec{p}-\vec{q}|^2 - 1] \right) \quad (26) \end{aligned}$$

The value of any order spatial derivative in the domain interior is a function of the same four boundary quantities, $\psi(\vec{q})$, $\psi'(\vec{q})$, $\omega(\vec{q})$, and $\omega'(\vec{q})$, and the nonhomogeneous function $f(x,y)$ that are used in the calculation of field variables ψ and ω at any point. The calculation of any order derivative with respect to any spatial coordinate at an internal point may be accomplished by determining the appropriate derivative forms of the Green's functions and substituting them into Equations (11) and (12).

Boundary Element Formulation

The term "boundary elements" was first used in association with the boundary integral equation method to indicate a technique whereby the boundary of a problem domain is subdivided into a series of elements over which a field variable is approximated (Brebbia, 1978). The obvious advantage of boundary elements over more traditional methods such as finite element and finite difference techniques is a reduction in the order of the dimensionality of the problem by one. A general multi-dimensional boundary value problem may be approximated through a series of surface integrations rather than a set of domain integrations. The resulting integral equations require information on the geometry and the field variables at points along the problem surface, thereby reducing the amount of information necessary to accurately describe the physical problem.

The first approximation in the boundary element method is the discretization of the problem surface into a series of elements. The behavior of the field variables ψ and ω and their normal derivatives ψ' and ω' in Equations (11) and (12) over each boundary element is characterized by an assumed interpolation function. As in finite element methods, these interpolation functions or shape functions can be of many different forms and result in varying degrees of accuracy for the field variables and the surface geometry. If the shape function defining the distribution of the field variable and the geometry over an element are the same, the element is called isoparametric. An element where the variation of the geometry is defined by a lower order shape function than that used to describe the field variable is termed

subparametric. A third element type is superparametric, in which the order of the shape function defining the geometry is higher than that used to distribute the field variable over the element. Advantages and disadvantages associated with each element type will be discussed in Chapter III.

By defining the interpolation function as a shape function set $\{N\}$, a column vector, the distribution of ψ , ω , ψ' , and ω' over each element may be established as

$$\begin{aligned}\psi &= \langle \psi \rangle \{N\} & \psi' &= \langle \psi' \rangle \{N\} \\ \omega &= \langle \omega \rangle \{N\} & \omega' &= \langle \omega' \rangle \{N\}\end{aligned}\tag{27}$$

where $\langle \psi \rangle$, $\langle \omega \rangle$, $\langle \psi' \rangle$, and $\langle \omega' \rangle$ are row vectors containing the discrete values of ψ , ω , ψ' , and ω' respectively at nodes defining each element. Substituting these approximations into Equations (11) and (12) results in the following discrete expressions for the governing set of coupled integral equations

$$\begin{aligned}\sum_{j=1}^n & \left(\int_{S_j} [\langle N \rangle G_1'(\vec{p}, \vec{q}) \{\psi\} - \langle N \rangle G_1(\vec{p}, \vec{q}) \{\psi'\}] \right. \\ & \left. + \langle N \rangle G_2'(\vec{p}, \vec{q}) \{\omega\} - \langle N \rangle G_2(\vec{p}, \vec{q}) \{\omega'\} \right] dS_j \\ & + \int_V F(x, y) G_2(\vec{p}, \vec{q}) dV - \beta(\vec{p}) \psi(\vec{p}) = 0\end{aligned}\tag{29}$$

$$\begin{aligned}\sum_{j=1}^n & \left(\int_{S_j} [\langle N \rangle G_1'(\vec{p}, \vec{q}) \{\omega\} - \langle N \rangle G_1(\vec{p}, \vec{q}) \{\omega'\}] dS_j \right) \\ & + \int_V f(x, y) G_1(\vec{p}, \vec{q}) dV - \beta(\vec{p}) \omega(\vec{p}) = 0\end{aligned}\tag{29}$$

where the summation is over n elements that define the boundary. The integrands of Equations (28) and (29) may be rewritten by introducing the following terms

$$H_{ij} = \frac{1}{2\pi} \int_{S_j} \langle N \rangle \ln |\vec{q}_i - \vec{q}| dS_j - \beta(\vec{p}) \delta(|\vec{q}_i - \vec{q}|) \quad (30)$$

$$G_{ij} = \frac{1}{2\pi} \int_{S_j} \langle N \rangle \ln |\vec{q}_i - \vec{q}| dS_j \quad (31)$$

$$L_{ij} = \frac{1}{8\pi} \int_{S_j} \langle N \rangle (|\vec{q}_i - \vec{q}|^2 [\ln |\vec{q}_i - \vec{q}| - 1]) dS_j \quad (32)$$

$$K_{ij} = \frac{1}{8\pi} \int_{S_j} \langle N \rangle (|\vec{q}_i - \vec{q}|^2 [\ln |\vec{q}_i - \vec{q}| - 1]) dS_j \quad (33)$$

$$B1_i = \frac{1}{8\pi} \int_V f(x,y) (|\vec{q}_i - \vec{q}|^2 [\ln |\vec{q}_i - \vec{q}| - 1]) dV \quad (34)$$

$$B2_i = \frac{1}{2\pi} \int_V f(x,y) \ln |\vec{q}_i - \vec{q}| dV \quad (35)$$

The integrals in Equations (30) - (35) may be evaluated analytically for linear isoparametric and higher order subparametric elements, and for certain forms of the nonhomogeneous function $f(x,y)$. The exact evaluations avoid the error introduced by numerical quadrature schemes and generally decrease computational time while increasing the accuracy of the integration. Unless specially formulated, most numerical quadrature schemes become inaccurate at small values of $|\vec{q}_i - \vec{q}|$. This type of error is especially evident at internal point calculations very close to the boundary. The reader is referred to Chapter III for the details of the analysis involved in obtaining the exact expressions for Equations (30) - (35) for the above mentioned elements.

Substituting Equations (30) - (35) into Equations (28) and (29) reduces the problem formulation to a coupled set of vector equations with the form

$$[H]\{\psi\} + [G]\{\psi'\} + [L]\{\omega\} + [K]\{\omega'\} = \{B1\} \quad (36)$$

$$[H]\{\omega\} + [G]\{\omega'\} = \{B2\} \quad (37)$$

where the column vectors $\{\psi\}$, $\{\psi'\}$, $\{\omega\}$, and $\{\omega'\}$ represent the values of ψ , ψ' , ω , ω' at each node. The diagonal terms of the $[H]$ matrix contain the constant $\beta(\vec{p})$, but there is no need to explicitly perform the integrations to obtain this value. The diagonal terms of $[H]$ may be calculated from the homogeneous form of Equation (37) by applying the fact that when a uniform potential, say unity, is applied over the entire boundary, the normal derivatives on the boundary must be zero everywhere. Therefore, Equation (37) becomes

$$[H] \{1\} = \{0\} \quad (38)$$

This equation states that the sum of the elements in each row of the $[H]$ matrix must be zero. Therefore, the diagonal term of a row in $[H]$ is the negative of the sum of all nondiagonal terms of that row (Brebbia, 1978).

Equations (36) and (37) may be rewritten in a more compact form as a single vector equation by combining terms involving the functions ψ and ω into one matrix, and the normal derivative terms ψ' and ω' into a second matrix:

$$\begin{vmatrix} [H] & [L] \\ 0 & [H] \end{vmatrix} \begin{vmatrix} \{\psi\} \\ \{\omega\} \end{vmatrix} = \begin{vmatrix} [G] & [K] \\ 0 & [G] \end{vmatrix} \begin{vmatrix} \{\psi'\} \\ \{\omega'\} \end{vmatrix} + \begin{vmatrix} \{B1\} \\ \{B2\} \end{vmatrix} \quad (39)$$

At any point on the boundary at least two of the four quantities ψ , ω , ψ' , and ω' are specified. Depending on the combination of boundary conditions prescribed at a discrete point, the columns of the matrices in Equation (39) may be rearranged such that all the unknown boundary

quantities are on one side of the equation. The result is the construction of a matrix equation of the form

$$[A]\{x\} = \{B\} \quad (40)$$

where $[A]$ is a nonsymmetric matrix, $\{x\}$ is a column vector of unknown boundary quantities, and $\{B\}$ is a column vector calculated from the prescribed boundary conditions and their appropriated matrix components combined with the domain integral terms.

Summary

A boundary element formulation for the nonhomogeneous biharmonic equation has been presented in this chapter. Boundary element analysis has many appealing advantages over the more traditional domain type formulations such as the finite element and finite difference techniques. Since only the boundary surface is modeled, the dimensionality of the problem is reduced by one. Consequently, both the input information necessary to define the problem and the simultaneous equations required for a solution are generally reduced. Another advantage is that for certain types of problems, the accuracy and consistency of the results from a boundary element solution can be considerably better than those obtained from either a finite element or a finite difference method (Connor and Brebbia, 1986).

Some major disadvantages of the boundary element method are the nonsymmetric form of the assembly matrices, the complex nature of the fundamental solution, and the possibility of additional domain discretization to handle the domain terms.

The next chapter will introduce several different types of elements for use in the boundary discretization and the derivation of some analytical expressions for the integrals defined in Equations (30) - (33). Also presented are various techniques to calculate the domain integrals of Equations (34) and (35) which avoid the disadvantages associated with domain cell methods. The resulting numerical analysis will be capable of solving the nonhomogeneous problem as easily as the homogeneous form.

CHAPTER III

BOUNDARY DISCRETIZATION

In Chapter II, a boundary integral equation representation of the nonhomogeneous biharmonic equation was formulated in terms of the field variables ψ and ω , their normal derivatives ψ' and ω' , and the nonhomogeneous function $f(x,y)$. An assumed set of shape functions were defined over each boundary element which characterized the distribution of the four boundary quantities along the surface. In this work, three isoparametric shape function sets are presented: a two node linear element, a three node quadratic element, and a two node Overhauser element defined by four nodes. In addition, for rectilinear geometries a subparametric version of both the quadratic and Overhauser elements will be defined.

Analytic expressions for the integrations of Equations (30) - (33) are derived for an isoparametric linear element and the subparametric form of both the quadratic and the Overhauser elements. For all other cases, a general numerical form of the integrations of Equations (30) - (33) are presented for quadratic and Overhauser elements.

Isoparametric Linear Elements

The boundary will be divided into n straight line segments, and a linear distribution of the boundary quantities over each element will

be assumed. A general linear element defined by two endpoints, node "i" and node "j", as shown in Figure 2, can be transformed into a one dimensional space of a single parameter, t . The resulting isoparametric element is C_0 continuous in each of the four boundary quantities ψ , ω , ψ' , and ω' . The values of any one of the boundary quantities at any point t along the element is defined in terms of their discrete nodal values and a shape function set $\langle N \rangle$. For example, the linear distribution of the field variables ψ and ω is given as

$$\psi(t) = N_i \psi_i + N_j \psi_j = \langle N_i \ N_j \rangle \begin{matrix} \psi_i \\ \psi_j \end{matrix} \quad (41)$$

$$\omega(t) = N_i \omega_i + N_j \omega_j = \langle N_i \ N_j \rangle \begin{matrix} \omega_i \\ \omega_j \end{matrix}$$

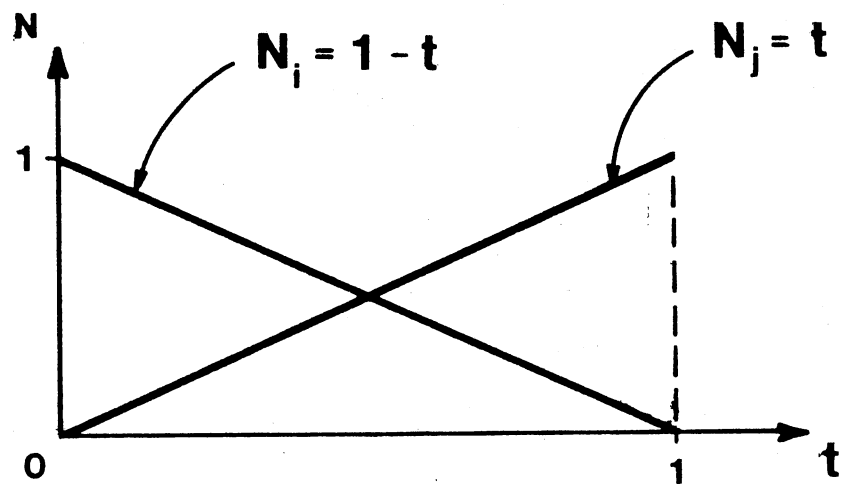
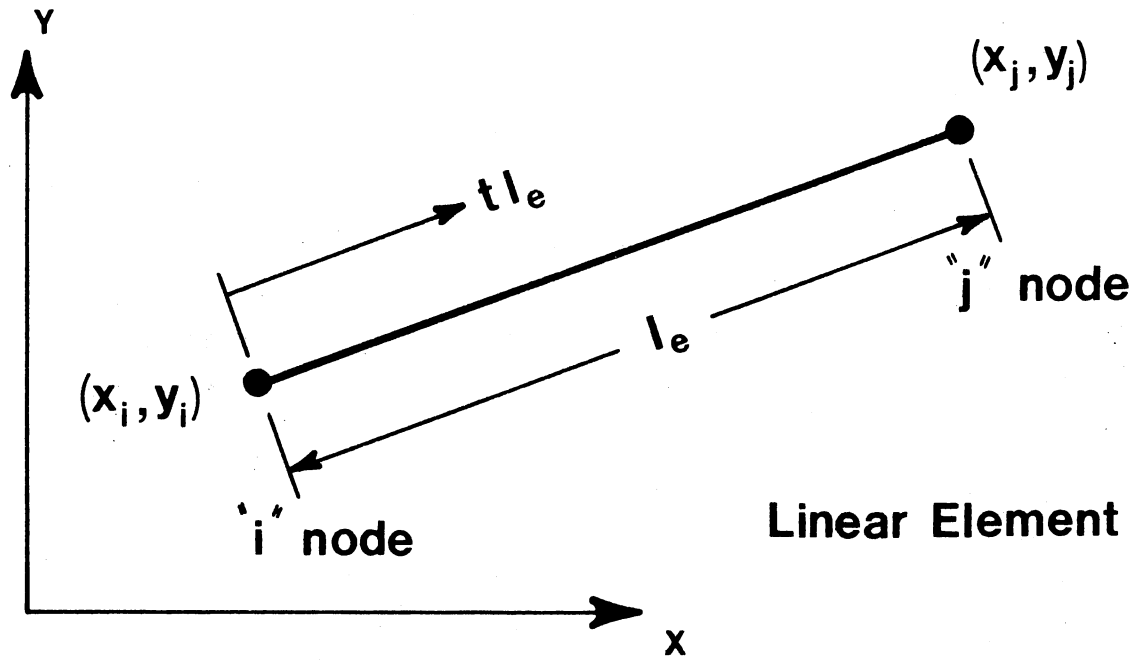
The shape functions N_i and N_j are

$$N_i = t \quad N_j = 1-t \quad (42)$$

The form of the integrals in Equations (30) - (33) are transformed into the parameter space reducing the order of the integration by one. Using the shape functions defined in Equation (42), the variation over an element of the two-dimensional coordinates x and y can be written as

$$x = x_i(1-t) + x_j t \quad y = y_i(1-t) + y_j t \quad (43)$$

The transformation of the differential length dS is accomplished by using the following simple one dimensional Jacobian:



Shape Functions

Figure 2. Linear Element Nomenclature

$$|J| = \sqrt{\left(\frac{dx}{dt}\right)^2 + \left(\frac{dy}{dt}\right)^2} = \frac{dS}{dt} \quad (44)$$

$$dS = |J|dt = l_e dt \quad l_e \equiv \text{Element Length} \quad (45)$$

The argument of the fundamental solution for each integrand of Equations (30) - (33) are of the form $|q_p - q|$. For a linear element, the argument may be replaced using the following relationships:

$$|\vec{q}_i - \vec{q}|^2 = (x(t) - x_p)^2 + (y(t) - y_p)^2 \quad (46)$$

where (x_p, y_p) are the coordinates which locate a variable field point. Expanding Equation (46) in terms of the parameter t results in the following expression for $|\vec{q}_p - \vec{q}|^2$:

$$\begin{aligned} |\vec{q}_p - \vec{q}|^2 &= ((x_j - x_i)t + x_i - x_p)^2 + ((y_j - y_i) \\ &\quad + y_i - y_p)^2 \end{aligned} \quad (47)$$

Equation (47) may be rewritten as

$$|\vec{q}_p - \vec{q}|^2 = At^2 + Bt + C \equiv X \quad (48)$$

where the constants A , B , and C , graphically shown in Figure 3, are defined as

$$\begin{aligned} A &= A_x^2 + A_y^2 & B &= 2(A_x B_x + A_y B_y) & C &= B_x^2 + B_y^2 \\ A_x &= x_j - x_i & B_x &= x_i - x_p \\ A_y &= y_j - y_i & B_y &= y_i - y_p \end{aligned} \quad (49)$$

Substituting the above expression into the integrals of Equations (30) - (33) result in the following parametrized forms:

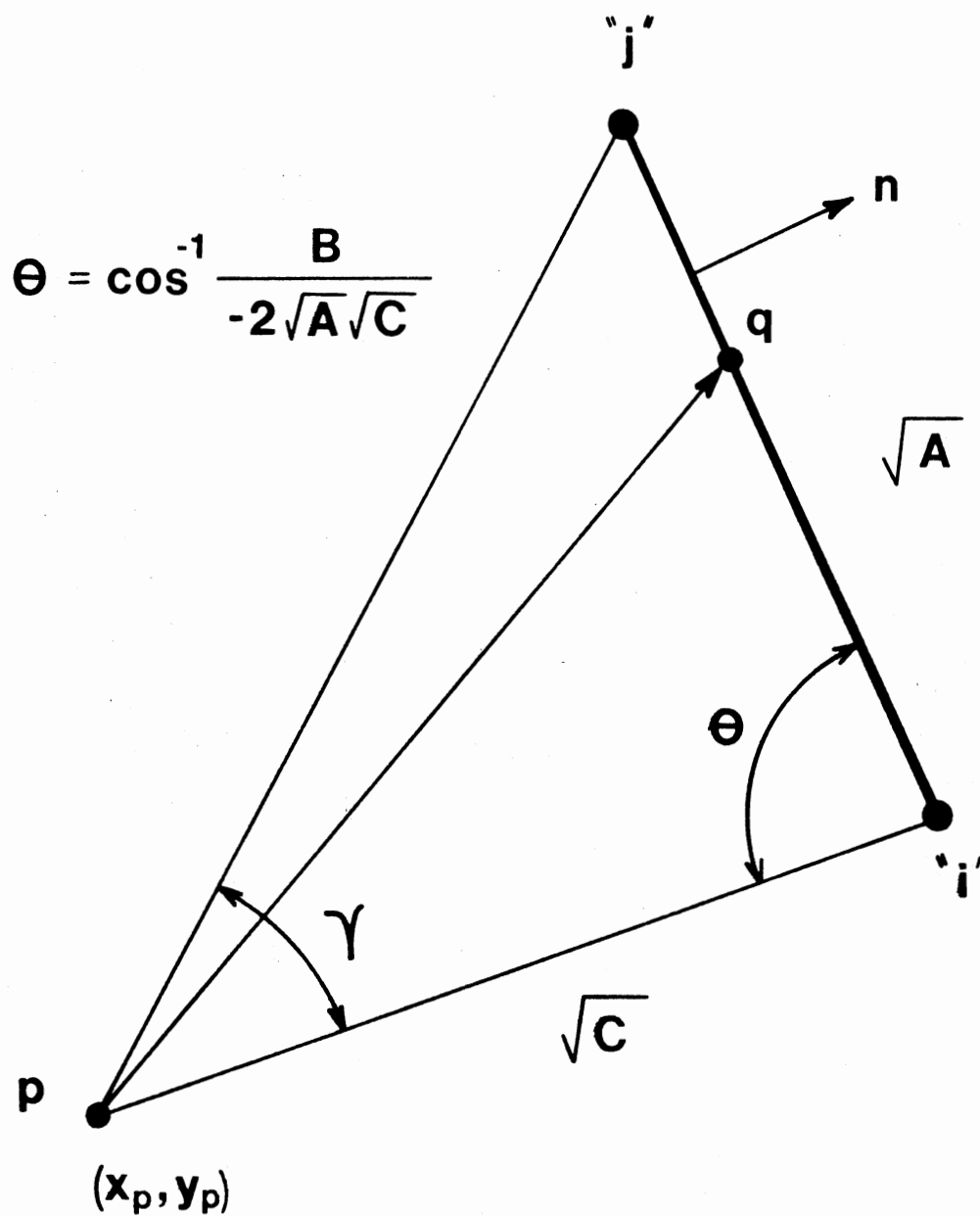


Figure 3. Definitions for Exact Analysis of Linear Elements

$$H_{pe} = \frac{1}{2\pi} \int_0^1 \langle t, 1-t \rangle \frac{Dt+E}{X} \{\psi_e\} dt - \beta(\vec{p}) \delta(|\vec{q}_p - \vec{q}|) \quad (50)$$

$$G_{pe} = \frac{1}{4\pi} \int_0^1 \langle t, 1-t \rangle \ln X \{\psi_e'\} dt \quad (51)$$

$$L_{pe} = \frac{1}{8\pi} \int_0^1 \langle t, 1-t \rangle (\ln X - 1) (Dt+E) \{\omega_e\} dt \quad (52)$$

$$K_{pe} = \frac{1}{16\pi} \int_0^1 \langle t, 1-t \rangle X (\ln X - 2) \{\omega_e'\} dt \quad (53)$$

where constants D and E are defined as

$$D = A_x n_x + A_y n_y \equiv 0 \quad E = B_x n_x + B_y n_y \quad (54)$$

For the linear element under consideration, the constant D (which is the dot product of the vector \vec{A} defining the length of the element and the unit normal vector, as shown in Figure 3) is identically zero.

The integrands of the one dimensional integrations defined in Equations (50) - (53) are combinations of the functions $t^n \ln X$, t^n/X , and t^n all of which may be evaluated analytically. Therefore, the following integration table may be compiled:

$$I_0 = \int_0^1 \frac{dt}{X} = \frac{2\gamma}{(4AC - B^2)^{1/2}} \quad 4AC - B^2 > 0$$

$$= \frac{2}{B(1 + B/2C)} \quad 4AC - B^2 = 0 \quad (55)$$

where the angle γ is defined in Figure 3:

$$I_1 = \int_0^1 \frac{t}{X} dt = (\ln(A+B+C) - \ln C - BI_0) / 2A \quad (56)$$

$$I_2 = \int_0^1 \frac{t^2}{X} dt = (1 - BI_1 - CI_0) / A \quad (57)$$

$$I_3 = \int_0^1 \frac{t^3}{X} dt = (\frac{1}{2} - BI_2 - CI_1) / A \quad (58)$$

$$I_4 = \int_0^1 \frac{t^4}{X} dt = (\frac{1}{3} - BI_3 - CI_2) / A \quad (59)$$

$$I_5 = \int_0^1 \frac{t^5}{X} dt = (\frac{1}{4} - BI_4 - CI_3) / A \quad (60)$$

Analytic expressions for the integration of terms of the form $t^n \ln X$ may be listed as

$$L_0 = \int_0^1 \ln X dt = \ln(A+B+C) - 2AI_2 - BI_1 \quad (61)$$

$$L_1 = \int_0^1 t \ln X dt = \frac{1}{2} (\ln(A+B+C) - 2AI_3 - BI_2) \quad (62)$$

$$L_2 = \int_0^1 t^2 \ln X dt = \frac{1}{3} (\ln(A+B+C) - 2AI_4 - BI_3) \quad (63)$$

$$L_3 = \int_0^1 t^3 \ln X dt = \frac{1}{4} (\ln(A+B+C) - 2AI_5 - BI_4) \quad (64)$$

Each of the parametrized integrations in Equations (50) - (53) have individual values associated with each discrete end node of the linear element being integrated. Therefore, two values are determined for each of the four integrations. In terms of the element constants

A, B, C, and E, and the integration table defined previously, the exact integrations for the expression in Equations (50) - (53) may be defined as

$$H_{pe} = \frac{1}{2\pi} e (H_i \psi_i + H_j \psi_j) \quad (65)$$

$$G_{pe} = \frac{1}{4\pi} e (G_i \psi'_i + G_j \psi'_j) \quad (66)$$

$$L_{pe} = \frac{1}{8\pi} e (L_i \omega_i + L_j \omega_j) \quad (67)$$

$$K_{pe} = \frac{1}{16\pi} e (K_i \omega'_i + K_j \omega'_j) \quad (68)$$

where

$$H_i = E(I_0 - I_1) \quad H_j = EI_1 \quad (69)$$

$$G_i = L_0 - L_1 \quad G_j = L_1 \quad (70)$$

$$L_i = E(L_0 - L_1 - \frac{1}{2}) \quad L_j = E(L_1 - \frac{1}{2}) \quad (71)$$

$$K_j = AL_3 + BL_2 + CL_1 - 2(\frac{A}{4} + \frac{B}{3} + \frac{C}{2}) \quad (72)$$

$$K_i = AL_2 + BL_1 + CL_0 - 2(\frac{A}{3} + \frac{B}{2} + C) - K_j$$

The preceding analytical expressions for the integrations required for biharmonic analysis using linear elements have many advantages. The source point (x_p, y_p) may be at any location, even occupy a point on the element itself without loss of generality. Normally, if numerical quadrature were used, special care would have to be taken if the source point was a member of or colinear with the element to handle the singular part of the integral. Also, depending on discrete mesh size, values of the field variables calculated by

numerical quadrature at points very near an element where the natural logarithm terms of the Green's functions approach their singular point may be inconsistent and inaccurate. The presented exact analysis implicitly handles the singular terms without any adjustment in the formulation. This is particularly important in calculating the system matrices and in accurately evaluating values of the field variables at internal points near the boundary. Unlike numerical procedures, the exact formulation is not iterative by nature, and therefore considerably reduces the time required to formulate the system matrices and calculate internal points.

A linear element formulation for the required integrations using analytic expressions has obvious advantages over the more commonly used subparametric constant element. Not only is the order of the approximation increased by one, from a constant to a linear function, but more importantly, the linear shape functions provide C_0 continuity for all four boundary quantities ψ , ω , ψ' , and ω' between elements.

The major disadvantage intrinsic to linear elements is their inability to accurately describe complex geometries and rapidly varying functions. Higher order elements are required to better represent the geometry of the domain and consequently increase the accuracy of the approximation.

Quadratic Element

Quadratic elements are often used to achieve a more accurate representation of the geometry of the problem domain and provide a second order approximation of the function over each element.

Isoparametric Quadratic Elements

The boundary is defined by a series of n discrete nodal points. A general quadratic element will be defined by a continuous set of three nodal points as shown in Figure 4. A second order distribution of the boundary quantities and the geometry will be assumed over each element. The resulting quadratic element is C_0 continuous in each of the four boundary quantities ψ , ω , ψ' , and ω' between elements.

The quadratic element is transformed from two-dimensional Cartesian coordinates (x,y) into a single parameter curvilinear coordinate, t . The values of any of the boundary quantities ψ , ω , ψ' , and ω' as well as the Cartesian coordinates of the approximate geometry are defined in terms of their discrete nodal values and a shape function set $\langle N \rangle$. The shape functions for a quadratic element in terms of the parameter t are given as

$$\begin{aligned} N_i &= 2t^2 - 3t + 1 & N_j &= -4t^2 + 4t \\ N_k &= 2t^2 - t \end{aligned} \quad (73)$$

Using the shape functions defined in Equation (73), the variation of the Cartesian coordinates x and y as a function of the parameter t may be written as

$$\begin{aligned} x(t) &= N_i x_i + N_j x_j + N_k x_k \\ y(t) &= N_i y_i + N_j y_j + N_k y_k \end{aligned} \quad (74)$$

The evaluation of the integrations in Equations (30) - (33) in the parameter space requires a transformation using a simple Jacobian

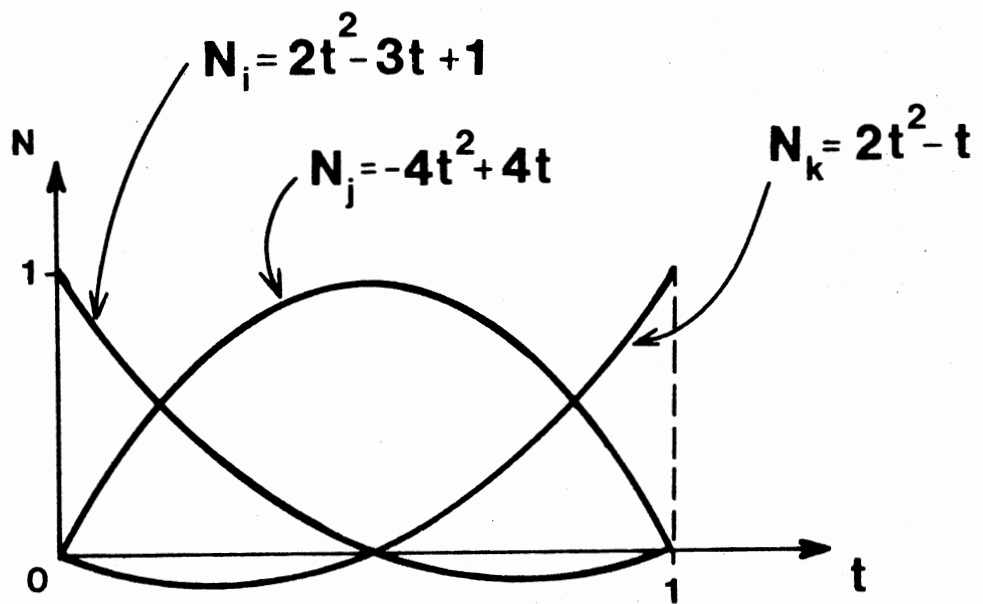
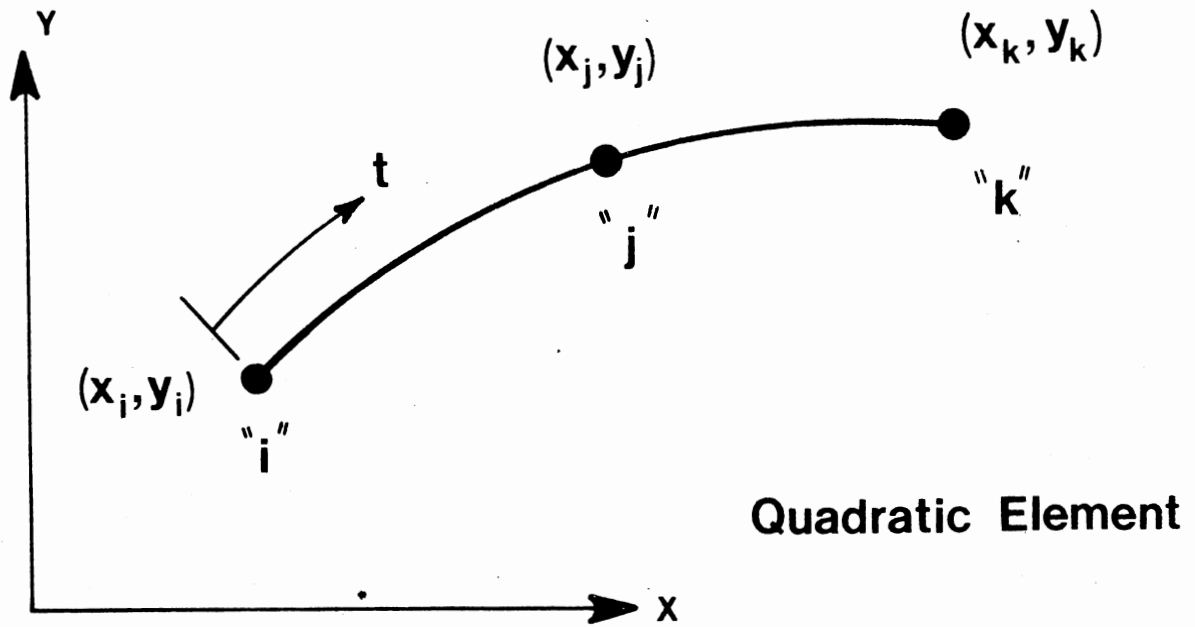


Figure 4. Quadratic Element Nomenclature

defined as

$$|J| = \sqrt{\left(\frac{dx}{dt}\right)^2 + \left(\frac{dy}{dt}\right)^2} = \frac{dS}{dt} \quad (75)$$

Unlike the linear element the Jacobian for a quadratic formulation is a function of the parameter t . An elemental form of the Jacobian may be derived from the discrete nodal coordinates and the shape functions. Equation (74) may be rewritten in the following form:

$$\begin{aligned} x(t) &= A_x t^2 + B_x t + x_i \\ y(t) &= A_y t^2 + B_y t + y_i \end{aligned} \quad (76)$$

where the element constants A_x , A_y , B_x , and B_y are defined as

$$\begin{aligned} A_x &= 2x_i - 4x_j + 2x_k & B_x &= -3x_i + 4x_j - x_k \\ A_y &= 2y_i - 4y_j + 2y_k & B_y &= -3y_i + 4y_j - y_k \end{aligned} \quad (77)$$

The derivatives of the x and y with respect to t are calculated and substituted into the expression for the Jacobian. The resulting form of the Jacobian is

$$|J| = (4At^2 + 2Bt + C)^{1/2} \quad (78)$$

where the constants A , B , and C are defined as

$$\begin{aligned} A &= A_x^2 + A_y^2 & B &= 2(A_x B_x + A_y B_y) \\ C &= B_x^2 + B_y^2 \end{aligned} \quad (79)$$

The position vector $|\vec{q}_p - \vec{q}|$ is transformed into a function of the parameter t by the relationship defined in Equation (46). Substituting the quadratic form of $x(t)$ and $y(t)$ into Equation (46) results in

$$|\vec{q}_p - \vec{q}|^2 = At^4 + Bt^3 + (C+E)t^2 + Ft + D \equiv X \quad (80)$$

where the constants D , E , and F are defined as

$$\begin{aligned} D &= D_x^2 + D_y^2 & E &= 2(A_x D_x + A_y D_y) \\ F &= 2(B_x D_x + B_y D_y) \end{aligned} \quad (81)$$

$$D_x = x_i - x_p \quad D_y = y_i - y_p$$

Substituting the relationships for the Jacobian, the position vector, and the quadratic shape functions into the integrals defined in Equations (30) - (33) result in the following expressions:

$$\begin{aligned} H_{pe} &= \frac{1}{2\pi} \int_0^1 (N_i \psi_i + N_j \psi_j + N_k \psi_k) \\ &\cdot \frac{(A_x t^2 + B_x t + D_x) n_x + (A_y t^2 + B_y t + D_y) n_y}{X} |J| dt \end{aligned} \quad (82)$$

$$G_{pe} = \frac{1}{4\pi} \int_0^1 (N_i \psi_i' + N_j \psi_j' + N_k \psi_k') \ln X |J| dt \quad (83)$$

$$\begin{aligned} L_{pe} &= \frac{1}{8\pi} \int_0^1 (N_i \omega_i + N_j \omega_j + N_k \omega_k) (\ln X - 1) \\ &\cdot ((A_x t^2 + B_x t + D_x) n_x + (A_y t^2 + B_y t + D_y) n_y) |J| dt \end{aligned} \quad (84)$$

$$\begin{aligned} K_{pe} &= \frac{1}{16\pi} \int_0^1 (N_i \omega_i' + N_j \omega_j' + N_k \omega_k') \\ &\cdot X (\ln X - 2) |J| dt \end{aligned} \quad (85)$$

The direction cosines n_x and n_y are functions of the parameter t , the Jacobian, and the element constants, and are defined as

$$n_x = \frac{2A_y t + B_y}{|J|} \quad n_y = - \frac{2A_x t + B_x}{|J|} \quad (86)$$

Equations (82) - (85) may be evaluated numerically for a general source point (x_p, y_p) . However, a special form of Equation (83) is required when the source point is a member of the element being integrated since the natural logarithmic part of the Green's function is singular at that point. Since a quadratic element is located by three discrete nodal points, there are three locations where Equation (83) will become singular. If the source point (x_p, y_p) is equal to the nodal point (x_i, y_i) , Equation (80) reduces to

$$x = At^4 + Bt^3 + Ct^2 \quad (87)$$

Therefore Equation (83) may be rewritten as

$$G_{pe} = \frac{1}{4\pi} \int_0^1 \langle N \rangle \{ \psi' \} \ln(At^4 + Bt^3 + Ct^2) |J| dt \quad (88)$$

By factoring a t^2 from the logarithmic function the integral may be separated into a singular part and a non-singular part

$$G_{pe} = \frac{1}{4\pi} \int_0^1 \langle N \rangle \{ \psi' \} \ln(At^2 + Bt + C) |J| dt \\ + \frac{1}{2\pi} \int_0^1 \langle N \rangle \{ \psi' \} \ln t |J| dt \quad (89)$$

The second term in Equation (89) may be integrated using any appropriate logarithmic quadrature scheme (Stroud and Secrest, 1966).

Evaluating the singular integral for a quadratic element when the source point (x_p, y_p) is equal to the nodal point (x_j, y_j) requires a different approach. The position vector definition, Equation (80), cannot be factored as before. Instead, the shape functions will be rewritten as a function of a new parameter s , that varies from -1 to 1. This effectively divides the integration in half where each piece contains a term that becomes singular at $s = 0$. The transformation from t space to s space is given as

$$s = 2t - 1 \quad (90)$$

The new shape functions in s space are

$$N_i^* = \frac{1}{2} (s^2 - s) \quad N_j^* = 1 - s^2 \quad N_k^* = \frac{1}{2} (s^2 + s) \quad (91)$$

Substituting the change of variables for s into the position vector and the Jacobian result in

$$X^* = \frac{A}{16} s^4 + \left(\frac{A}{4} + \frac{B}{8}\right) s^3 + \left(\frac{3(A+B)}{8} + \frac{(C+E)}{4}\right) s^2 \quad (92)$$

$$|J^*| = \left(A s^2 + (2A+B) s + A + B + C \right)^{1/2} \quad (93)$$

Equation (83) may be rewritten in the new parameter s as

$$G_{pe} = \frac{1}{8\pi} \int_0^1 \langle N^* \rangle_{\{\psi'\}} \ln X^* |J^*| ds \\ - \frac{1}{8\pi} \int_0^{-1} \langle N^* \rangle_{\{\psi'\}} \ln X^* |J^*| ds \quad (94)$$

Another change of variable is required to transform the limits of the second integral of Equation (94). A new parameter u is defined by $u = -s$. The shape functions, the position vector, and the Jacobian are rewritten as functions of the parameter u , and defined as

$$N_i^{**} = \frac{1}{2} (u^2 + u) \quad N_j^{**} = 1 - u^2 \quad N_k^{**} = \frac{1}{2} (u^2 - u) \quad (95)$$

$$\chi^{**} = \frac{A}{16} u^4 - \left(\frac{A}{4} + \frac{B}{8}\right) u^3 + \left(\frac{3(A+B)}{8} + \frac{(C+E)}{4}\right) u^2 \quad (96)$$

$$|J^{**}| = (Au^2 - (2A+B)u + A + B + C)^{1/2} \quad (97)$$

Substituting Equations (95) - (97) into the second integral of Equation (94) yields the final form of the required integration:

$$G_{pe} = \frac{1}{8\pi} \int_0^1 \langle N^* \rangle_{\{\psi'\}} \ln \chi^* |J^*| ds + \frac{1}{8\pi} \int_0^1 \langle N^{**} \rangle_{\{\psi'\}} \ln \chi^{**} |J^{**}| du \quad (98)$$

Both integrals of Equation (98) are identical in form to previous analysis. Each may be decomposed into a singular part and nonsingular part similar to Equation (89) and evaluated with the appropriate numerical quadrature scheme.

The final case is when the source point (x_p, y_p) is equal to the nodal point (x_k, y_k) . The logarithmic terms become singular at $t = 1$. Defining a change of variable, $t = 1 - v$, effectively reverses the limits of the integration. The shape functions, the position vector, and the Jacobian are redefined as

$$N_i^{***} = 2v^2 - v \quad N_j^{***} = -4v^2 + 4v \quad N_k^{***} = 2v^2 - 3v + 1 \quad (99)$$

$$X^{***} = Av^4 - (4A+B)v^3 + (6A+3B+C+E)v^2 \quad (100)$$

$$|J^{***}| = (4Av^2 + (2B+8A)v + 4A + 2B + C)^{1/2} \quad (101)$$

The substitution of Equations (99) - (101) into Equation (83) allows the integrations to be rewritten as

$$G_{pe} = \frac{1}{8\pi} \int_0^1 \langle N^{***} \rangle_{\{\psi'\}} \ln X^{***} |J^{***}| dv \quad (102)$$

By factoring a v^2 out of the logarithmic term in Equation (102) the integral may be written as two separate integrals, of which only one is singular. This is identical to the previous analysis when the source point is equal to (x_i, y_i) except the shape functions are reversed and the position vector and the Jacobian have slightly different forms.

Boundary element analysis using general quadratic elements presents some of the same problems as do their finite element counterparts. Irregular spacing of the element nodes can lead to the development of "overspill" whereby the distribution of the geometry is characterized by kinks and spurious wiggles (Zienkiewicz, 1977). Errors associated with the evaluation of the integrals over a general quadratic element by numerical quadrature are minimal. However, the calculation of internal points very near a quadratic element suffers from the same inconsistencies and inaccuracies as those associated with a general linear element.

Subparametric Quadratic Elements

A subparametric form of the quadratic element has certain advantages over the isoparametric form. If the geometry of the problem domain is linear or a lower order approximation of the surface is assumed, the Jacobian operator becomes a constant and may be factored from the integrations of Equations (82) - (85). The resulting subparametric form may be evaluated analytically. The additional intrinsic advantages of an exact analysis may offset some of the disadvantages associated with a lower order approximation of the geometry.

The boundary is divided into n straight line segments where the distribution of each of the boundary quantities ψ , ω , ψ' , and ω' is a function of three equally spaced discrete nodal values and the shape functions given in Equation (73). The resulting subparametric formulation is C_0 continuous between elements. Since the geometry is linear over each element, Equation (74) may be rewritten as

$$x(t) = (1-t)x_i + tx_k \quad y(t) = (1-t)y_i + ty_k \quad (103)$$

The Jacobian and the position vector defined in Equations (75) and (80) must be rewritten using the relationships in Equation (103). The resulting subparameteric form of the Jacobian and the position vector is identical to that of a linear element, given in Equations (45) and (48), except for the element constants. The Jacobian and the position vector are defined as

$$|J| = \sqrt{A} = l_e \quad l_e \equiv \text{Element Length} \quad (104)$$

$$X = At^2 + Bt + C \quad (105)$$

where the element constants A, B, and C are given by Equation (79) with the following corrections:

$$A_x = x_k - x_i \quad A_y = y_k - y_i \quad (106)$$

At this point, the procedure continues in the same way as the analytic analysis for the linear element. The linear shape functions in Equations (50) - (53) are replaced by their quadratic counterparts. The resulting integrands are of the form t^n , t^n/X , and $t^n \ln X$. Complementing the previous integration table defined in Equations (55) - (64) with the following additions will provide the necessary components for an exact analysis:

$$I_6 = \int_0^1 \frac{t^6}{X} dt = \left(\frac{1}{5} - BI_5 - CI_4 \right) / A \quad (107)$$

$$L_4 = \int_0^1 t^3 \ln X dt = \frac{1}{5} (\ln(A+B+C) - 2AI_6 - BI_5) \quad (108)$$

The analytic expressions for the integration over a subparametric quadratic element of the integrals defined in Equations (30) - (33) are

$$H_{pe} = \frac{1}{2\pi} (H_i \psi_i + H_j \psi_j + H_k \psi_k) \quad (109)$$

$$G_{pe} = \frac{1}{4\pi} (G_i \psi_i' + G_j \psi_j' + G_k \psi_k') \quad (110)$$

$$L_{pe} = \frac{1}{8\pi} (L_i \omega_i + L_j \omega_j + L_k \omega_k) \quad (111)$$

$$K_{pe} = \frac{1}{16\pi} (K_i \omega_i' + K_j \omega_j' + K_k \omega_k') \quad (112)$$

where

$$\begin{aligned}
 H_i &= E(2I_2 - 3I_1 + I_0) \\
 H_j &= 4E(-I_2 + I_1) \\
 H_k &= E(2I_2 - I_1)
 \end{aligned} \tag{113}$$

$$\begin{aligned}
 G_i &= 2L_2 - 3L_1 + L_0 \\
 G_j &= 4(-L_2 + L_1) \\
 G_k &= 2L_2 - L_1
 \end{aligned} \tag{114}$$

$$\begin{aligned}
 L_i &= E(2L_2 - 3L_1 + L_0 - \frac{1}{6}) \\
 L_j &= 4E(-L_2 + L_1 - \frac{1}{6}) \\
 L_k &= E(2L_2 - L_1 - \frac{1}{6})
 \end{aligned} \tag{115}$$

$$\begin{aligned}
 K_i &= 2A(L_4 - \frac{2}{5}) + (2B-3A)(L_3 - \frac{1}{2}) \\
 &\quad + (A-3B+2C)(L_2 - \frac{2}{3}) + (B-3C)(L_1 - 1) \\
 &\quad + C(L_0 - 2) \\
 K_j &= -A(L_4 - \frac{2}{5}) + (A-B)(L_3 - \frac{1}{2}) \\
 &\quad + (B-C)(L_2 - \frac{2}{3}) + C(L_1 - 1) \\
 K_k &= 2A(L_4 - \frac{2}{5}) + (2B-A)(L_3 - \frac{1}{2}) \\
 &\quad + (2C-B)(L_2 - \frac{2}{3}) - C(L_1 - 1)
 \end{aligned} \tag{116}$$

Unlike the isoparametric form, the analytic subparametric formulation explicitly handles the logarithmic singularity when the source point is at an end node. However, if the source point (x_p, y_p) coin-

cides with the middle node (x_j, y_j) , the shape functions must be transformed like their isoparametric counterparts. The element is divided in two about the (x_j, y_j) point. The transformed shape functions for each segment are previously defined in Equations (91) and (95). The form of the analytic expression for this case is the same as that defined in Equations (109) - (112). However, the integration table must be recompiled with the change of variable resulting in a different form of the integration components given in Equations (113) - (116). The element constants are redefined for this particular case in the following form:

$$A_1 = \frac{A}{16} \quad B_1 = \frac{A}{4} + \frac{B}{8} \quad C_1 = \frac{3(A+C)}{8} + \frac{B+C}{4} \quad (117)$$

$$A_2 = A_1 \quad B_2 = -B_1 \quad C_2 = C_1 \quad (118)$$

The integration table may now be recompiled with the new form of the element constants and is listed below:

$$I_{01} = \frac{2\gamma}{(4A_1C_1 - B_1^2)^{1/2}} \quad I_{02} = \frac{2\gamma}{(4A_2C_2 - B_2^2)^{1/2}} \quad (119)$$

$$I_{1i} = (\ln(A_i + B_i + C_i) - \ln C_i - B_i I_{0i}) / 2A_i \quad (120)$$

$$I_{ni} = \frac{1}{n-1} - B_i I_{n-1,i} - C_i I_{n-2,i} \quad (121)$$

$$L_{ni} = \frac{1}{n+1} (\ln(A_i + B_i + C_i) - 2A_i I_{n+2,i} - B_i I_{n+1,i}) \quad \text{where } i = 1, 2 \quad (122)$$

The original set of integration components, Equations (113) - (116), are redefined as

$$\begin{aligned}
 H_i &= \frac{E}{2} (I_{21} - I_{11} + I_{22} + I_{12}) \\
 H_j &= E (I_{01} - I_{21} + I_{02} - I_{22}) \\
 H_k &= \frac{E}{2} (I_{21} + I_{11} + I_{22} - I_{12})
 \end{aligned} \tag{123}$$

$$\begin{aligned}
 G_i &= \frac{1}{2} (L_{21} - L_{11} + L_{22} + L_{12}) \\
 G_j &= L_{01} - L_{21} + L_{02} - L_{22} \\
 G_k &= \frac{1}{2} (L_{21} + L_{11} + L_{22} - L_{12})
 \end{aligned} \tag{124}$$

$$\begin{aligned}
 L_i &= \frac{E}{2} (L_{21} - L_{11} + L_{22} + L_{12} - \frac{2}{3}) \\
 L_j &= E (L_{01} - L_{21} + L_{02} - L_{22} - \frac{4}{3}) \\
 L_k &= \frac{E}{2} (L_{21} + L_{11} + L_{22} - L_{12} - \frac{2}{3})
 \end{aligned} \tag{125}$$

$$\begin{aligned}
 K_i &= \frac{1}{2} (A_1 (L_{41} + L_{42} - \frac{4}{5}) + (B_1 - A_1) \\
 &\quad \cdot (L_{31} - L_{32}) + (C_1 - B_1) (L_{21} + L_{22} - \frac{4}{3}) \\
 &\quad - C_1 (L_{11} - L_{12})) \\
 K_j &= -A_1 (L_{41} + L_{42} - \frac{4}{5}) - B_1 (L_{31} - L_{32}) \\
 &\quad + (A_1 - C_1) (L_{21} + L_{22} - \frac{4}{3}) \\
 &\quad + B_1 (L_{11} - L_{12}) + C_1 (L_{01} + L_{02} - 4) \\
 K_k &= \frac{1}{2} (A_1 (L_{41} + L_{42} - \frac{4}{5}) + (B_1 + A_1) \\
 &\quad \cdot (L_{31} - L_{32}) + (C_1 + B_1) (L_{21} + L_{22} - \frac{4}{3}) \\
 &\quad + C_1 (L_{11} - L_{12}))
 \end{aligned} \tag{126}$$

The analytic expressions for the integrations over a quadratic subparametric element presented, although lengthy, reduce the time required to formulate system matrices as compared to the isoparametric version. Accuracy of the calculation of the field variables at internal points very close to boundary is also improved. This type of element is very useful when the geometry of the problem is composed of linear segments. In this particular case, the subparametric quadratic element is on the same order as an isoparametric element.

Overhauser Elements

Linear and quadratic elements are generally sufficiently accurate to describe many engineering problems. A variety of curved geometries are well represented by a standard quadratic element or a combination of quadratic and linear elements. A common drawback to both types of formulations is the lack of derivative continuity between elements. Several different types of spline elements that are C_1 continuous have been used for various purposes (Kreyszig, 1983).

Cubic splines provide derivative continuity, but are computationally inefficient and cumbersome (Liggett and Salmon, 1981). Most types of formulations require an additional variable at each end node which enforces the prescribed derivative continuity.

Overhauser (1968) introduced a cubic parametric representation of a curve by blending two parametric quadratic curves. Derivative continuity is implicitly defined by the curve. In this section, a formulation of the Overhauser curve developed by Brewer (1977; Brewer and Anderson, 1977), as shown in Figure 5, will be implemented. The parametric curve, $c(t)$, is a blend of two quadratic curves, $p(r)$ and

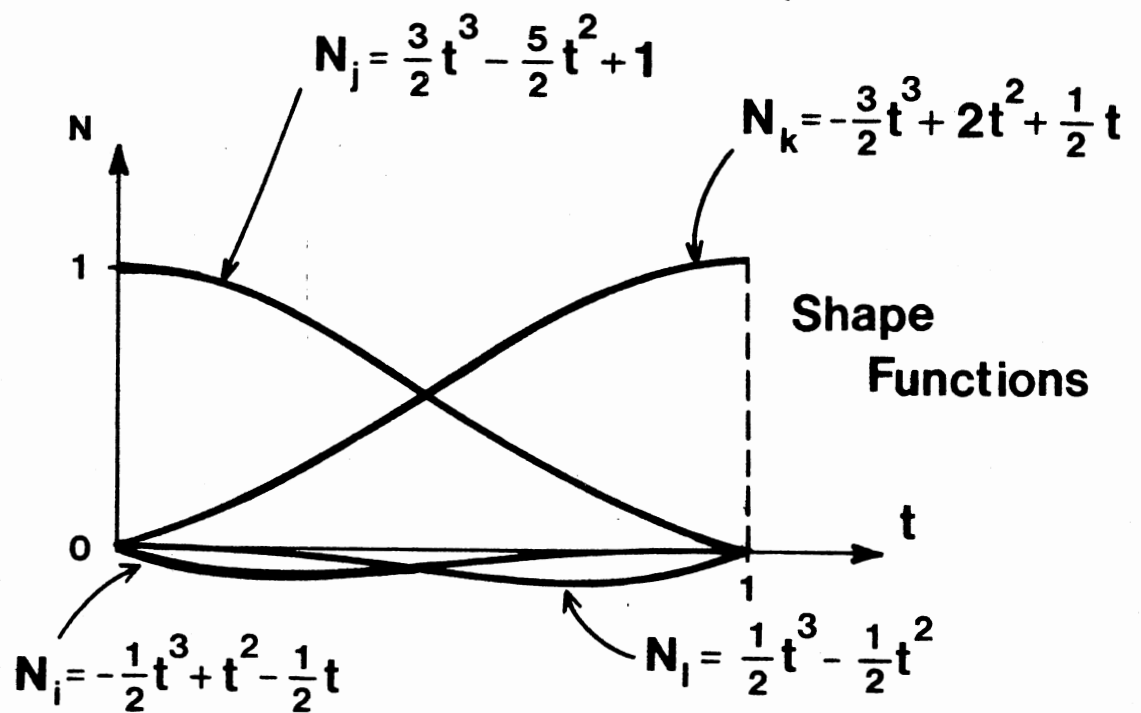
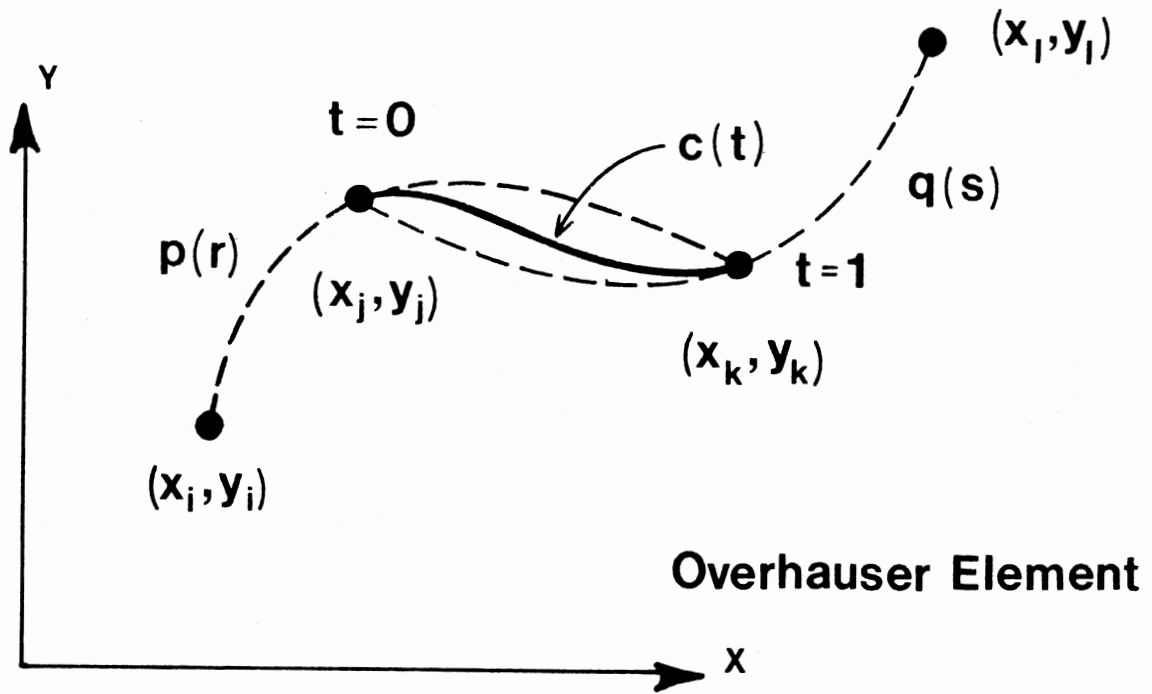


Figure 5. Overhauser Element Nomenclature

$q(s)$, where t , r , and s are curvilinear parameters along their respective curves. Note that the Overhauser curve is defined between "regular" points j and k . The "extra" nodes i and l are used to maintain the derivative continuity.

Isoparametric Overhauser Element

The boundary is divided into a series of n discrete nodal points similar to a quadratic element. The value of any of the boundary quantities ψ , ω , ψ' , ω' as well as the Cartesian coordinates of the approximate geometry are defined in terms of four consecutive discrete nodal values and the shape functions. In terms of the parameter t , the shape functions are given as

$$\begin{aligned} N_i &= -\frac{1}{2}t^3 + t^2 - \frac{1}{2}t & N_j &= \frac{3}{2}t^3 - \frac{5}{2}t^2 + 1 \\ N_k &= -\frac{3}{2}t^3 + 2t^2 + \frac{1}{2}t & N_l &= \frac{1}{2}t^3 - \frac{1}{2}t^2 \end{aligned} \quad (127)$$

Using these shape functions the of the Cartesian coordinates x and y as a function of the parameter t are written as

$$\begin{aligned} x(t) &= N_i x_i + N_j x_j + N_k x_k + N_l x_l \\ y(t) &= N_i y_i + N_j y_j + N_k y_k + N_l y_l \end{aligned} \quad (128)$$

The development of the Overhauser element follows the same procedure as the quadratic element formulation. Therefore, the necessary form of the position vector and the Jacobian operator are defined as

$$|J| = (9At^4 + 6A_b t^3 + (3A_c + 4B)t^2 + 2B_c + C)^{1/2} \quad (129)$$

$$\begin{aligned}
X = & At^6 + A_b t^5 + (A_c + B)t^4 + (A_c + A_d)t^3 \\
& + (B_c + C)t^2 + C_d t + D
\end{aligned} \tag{130}$$

where the element constants A , B , C , D , A_b , A_c , A_d , B_c , B_d , and C_d are given as

$$\begin{aligned}
A &= A_x^2 + A_y^2 & B &= B_x^2 + B_y^2 & C &= C_x^2 + C_y^2 \\
A_b &= 2(A_x B_x + A_y B_y) & A_c &= 2(A_x C_x + A_y C_y) \\
A_d &= 2(A_x D_x + A_y D_y) & B_c &= 2(B_x C_x + B_y C_y) \\
B_d &= 2(B_x D_x + B_y D_y) & C_d &= 2(C_x D_x + C_y D_y) \\
A_x &= -\frac{1}{2} x_i + \frac{3}{2} x_j - \frac{3}{2} x_k + \frac{1}{2} x_l & & & & (131) \\
B_x &= x_i - \frac{5}{2} x_j + 2 x_k - \frac{1}{2} x_l \\
C_x &= -\frac{1}{2} x_i + \frac{1}{2} x_k & D_x &= x_j - x_p \\
A_y &= -\frac{1}{2} y_i + \frac{3}{2} y_j - \frac{3}{2} y_k + \frac{1}{2} y_l \\
B_y &= y_i - \frac{5}{2} y_j + 2 y_k - \frac{1}{2} y_l \\
C_y &= -\frac{1}{2} y_i + \frac{1}{2} y_k & D_y &= y_j - y_p
\end{aligned}$$

Substituting the Overhauser shape functions, the Jacobian, and position vector relationships of Equations (129) and (130) into Equations (30) - (33) result in the following expressions for the required integrations:

$$H_{pe} = \frac{1}{2\pi} \int_0^1 (N_i \psi_i + N_j \psi_j + N_k \psi_k + N_l \psi_l) \cdot \frac{X_p n_x + Y_p n_y}{X} |J| dt \quad (132)$$

$$G_{pe} = \frac{1}{4\pi} \int_0^1 (N_i \psi'_i + N_j \psi'_j + N_k \psi'_k + N_l \psi_l) \ln X |J| dt \quad (133)$$

$$L_{pe} = \frac{1}{8\pi} \int_0^1 (N_i \omega_i + N_j \omega_j + N_k \omega_k + N_l \omega_l) \cdot (X_p n_x + Y_p n_y) |J| dt \quad (134)$$

$$K_{pe} = \frac{1}{16\pi} \int_0^1 (N_i \omega'_i + N_j \omega'_j + N_k \omega'_k + N_l \omega'_l) \cdot X (\ln X - 2) |J| dt \quad (135)$$

where X_p , Y_p , and the direction cosine are functions of the parameter t , the Jacobian, and the element constants:

$$\begin{aligned} X_p &= A_x t^3 + B_x t^2 + C_x t + D_x \\ Y_p &= A_y t^3 + B_y t^2 + C_y t + D_y \\ n_x &= \frac{3A_y t^2 + 2B_y t + C_y}{|J|} \\ n_y &= - \frac{3A_x t^2 + 2B_x t + C_x}{|J|} \end{aligned} \quad (136)$$

Equations (132) - (135) may be evaluated numerically for a general source point (x_p, y_p) . However, a special form of Equation (133) is necessary when the source point is equal to either point (x_j, y_j) or

(x_k, y_k) . When this occurs the natural logarithmic terms of the Green's function become singular, identical to the preceding linear and quadratic formulations. If the source point (x_p, y_p) is equal to the nodal point (x_j, y_j) the expression for the position vector, Equation (130), reduces to

$$x = At^6 + A_b t^5 + (A_c + B)t^4 + B_c t^3 + Ct^2 \quad (137)$$

By factoring a t^2 from the logarithmic function the integral in Equation (133) is separated into a singular part and a nonsingular part:

$$\begin{aligned} G_{pe} = & \frac{1}{4\pi} \int_0^1 \langle N \rangle \{ \psi' \} \ln(At^4 + A_b t^3 + \\ & + (A_c + B)t^2 + B_c t + C) |J| dt \\ & + \frac{1}{2\pi} \int_0^1 \langle N \rangle \{ \psi' \} \ln t |J| dt \end{aligned} \quad (138)$$

The second integral of Equation (138) has effectively isolated the singularity and may be evaluated using any logarithmic quadrature scheme. Another singularity occurs in Equation (133) at $t = 1$, when the source point (x_p, y_p) is equal to the nodal point (x_k, y_k) . A change of variables, $t = 1 - u$, will reverse the limits of the integration such that the singularity occurs at $u = 0$. The shape functions, the position vector, and the Jacobian may be redefined in terms of the parameter u as

$$\begin{aligned} N_i^* &= \frac{1}{2} (s^3 - s^2) & N_j^* &= -\frac{3}{2} s^3 + 2s^2 + \frac{1}{2} s \\ N_k^* &= \frac{3}{2} s^3 - \frac{5}{2} s^2 + 1 & N_l^* &= -\frac{1}{2} s^3 + s^2 - \frac{1}{2} s \end{aligned} \quad (139)$$

$$\begin{aligned}
X^* &= A s^6 + (A_b - 6A) s^5 + (15A + A_b + A_c \\
&\quad + B) s^4 + (-20A - 10A_b - 4(A_c + B) \\
&\quad - A_d + B_c) s^3 + (15A + 10A_b + 6(A_c + B) \\
&\quad + 3(A_d + B_c) + B_c + C) s^2
\end{aligned} \tag{140}$$

$$\begin{aligned}
|J^*| &= (9A s^4 - (36A + 6A_b) s^3 + (54A + 4B + 3A_c \\
&\quad + 18A_c) s^2 - (36A + 8B + 6A_c \\
&\quad + 2B_c + 18A_d) s + (9A + 4B + C \\
&\quad + 3A_c + 2B_c + 6A_b))^{1/2}
\end{aligned} \tag{141}$$

By substituting Equations (139) - (140) into Equation (133) the integration is rewritten in the following form:

$$G_{ps} = \frac{1}{4\pi} \int_0^1 \langle N^* \rangle \{\psi'\} \ln X^* |J^*| ds \tag{142}$$

By factoring the s^2 out of the logarithmic term of Equation (142) the integral may be separated into a singular part and a nonsingular part. The result is similar to Equation (138), except the shape functions are reversed, and the Jacobian and the position vector have different forms. As before, the singular part of the integration may be evaluated with any appropriate logarithmic quadrature scheme.

Boundary element analysis using Overhauser elements provide many interesting advantages over other spline elements or lower order elements. The approximation to the distribution of the field variables and the geometry over an element is represented by cubic order shape functions which are C_1 continuous between elements. The com-

putational implementation of an Overhauser element is much simpler than a standard quadratic or a cubic type element. The characteristic of "overspill" evident in higher order elements is far less pronounced in the Overhauser formulation. This is demonstrated in Figure 6, where several cases of abnormal node spacing are presented. However, it is advisable to avoid abrupt changes in the noding spacing.

The main disadvantage of the Overhauser element occurs when modeling discontinuities in the geometry such as corners. Since the element is designed to model C_1 continuous surfaces, it does not accurately represent abrupt changes in the geometry. Therefore, a special form of the Overhauser element is used for modeling corners. This is accomplished by "double noding" where one of the "extra" nodes is defined to be at the same location as one of the regular nodes. Equally accurate results are obtained when the Overhauser is linked to either a quadratic or a linear element to describe a corner.

Subparameteric Overhauser Elements

The subparameteric form of the Overhauser element has the same advantages as its quadratic counterpart. If the problem under consideration is segmentally linear or the geometry is assumed linear, the Jacobian operator becomes a constant and can be factored from the required integrations. The resulting integrals may be evaluated analytically. Therefore, it is possible to have the intrinsic advantage of an exact analysis with a cubic order C_1 continuous approximation for the boundary quantities.

The boundary is divided into n straight line segments. The subparameteric form of the Overhauser element will be defined by four

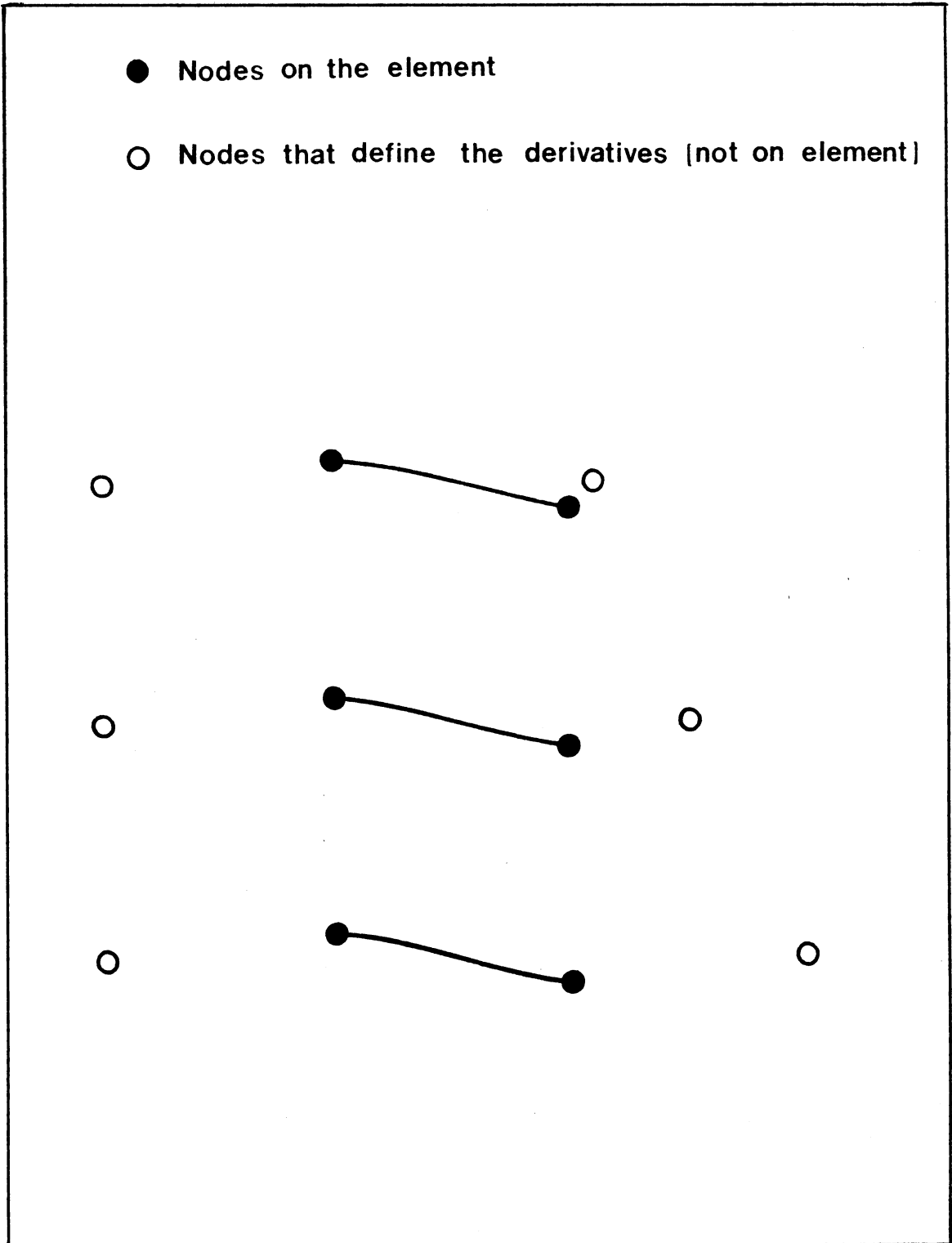


Figure 6. Behavior of Overhauser Element with Abnormal Node Spacing

consecutive equally spaced nodes. Since the geometry is linear, the variation of the Cartesian coordinates with the parameter t given in Equation (128) is redefined as

$$x(t) = (1-t)x_j + tx_k \quad y(t) = (1-t)y_j + ty_k \quad (143)$$

The Jacobian and the position vector defined in Equations (129) and (130) are recalculated using the relationship in Equation (143). The resulting subparametric form of the Jacobian and the position vector are similar to those defined for a subparametric quadratic element, given in Equations (104) and (105), except that the element constants are different. The Jacobian and the position vector are

$$|J| = \sqrt{A} = l_e \quad l_e \equiv \text{Element Length} \quad (144)$$

$$x = At^2 + Bt + C \quad (145)$$

where the element constants A , B , and C are given in Equation (79) with the following corrections

$$A_x = x_k - x_j \quad A_y = y_k - y_j \quad (146)$$

$$B_x = x_j - x_p \quad B_y = y_j - y_p$$

At this point, the procedure continues in an identical manner to that of the linear element. The linear shape function in Equations (50) - (53) are replaced by the Overhauser shape functions given in Equation (127). The resulting integral contains terms of the form t^n , t^n/x , and $t^n \ln x$, identical to the linear element, except to a higher degree. Therefore, the integration table defined in Equations (55) -

(64) is supplemented with the following additions to provide a complete set of components for an exact analysis:

$$I_7 = \int_0^1 \frac{t^7}{x} dt = \left(\frac{1}{6} - BI_6 - CI_5 \right) / A \quad (147)$$

$$L_5 = \int_0^1 t^5 \ln x dt = \frac{1}{6} \left(\ln(A+B+C) - 2AI_7 - BI_6 \right) \quad (148)$$

The analytic expression for the integrations defined in Equations (30) - (33) using a subparametric Overhauser element are

$$H_{pe} = \frac{1}{2\pi} e \left(H_i \psi_i + H_j \psi_j + H_k \psi_k + H_l \psi_l \right) \quad (149)$$

$$G_{pe} = \frac{1}{4\pi} e \left(G_i \psi_i' + G_j \psi_j' + G_k \psi_k' + G_l \psi_l' \right) \quad (150)$$

$$L_{pe} = \frac{1}{8\pi} e \left(L_i \omega_i + L_j \omega_j + L_k \omega_k + L_l \omega_l \right) \quad (151)$$

$$K_{pe} = \frac{1}{16\pi} e \left(K_i \omega_i' + K_j \omega_j' + K_k \omega_k' + K_l \omega_l' \right) \quad (152)$$

where

$$\begin{aligned} H_i &= \frac{E}{2} \left(-I_3 + 2I_2 - I_1 \right) \\ H_j &= \frac{E}{2} \left(3I_3 - 5I_2 + 2I_0 \right) \\ H_k &= \frac{E}{2} \left(-3I_3 + 4I_2 + I_1 \right) \\ H_l &= \frac{E}{2} \left(I_3 - I_2 \right) \end{aligned} \quad (153)$$

$$\begin{aligned} G_i &= \frac{1}{2} \left(-L_3 + 2L_2 - L_1 \right) \\ G_j &= \frac{1}{2} \left(3L_3 - 5L_2 + 2L_0 \right) \\ G_k &= \frac{1}{2} \left(-3L_3 + 4L_2 + L_1 \right) \\ G_l &= \frac{1}{2} \left(L_3 - L_2 \right) \end{aligned} \quad (154)$$

$$\begin{aligned}
L_i &= \frac{E}{2} \left(-L_3 + 2L_2 - L_1 + \frac{1}{12} \right) \\
L_j &= \frac{E}{2} \left(3L_3 - 5L_2 + 2L_0 - \frac{13}{12} \right) \\
L_k &= \frac{E}{2} \left(-3L_3 + 4L_2 + L_1 - \frac{13}{12} \right) \\
L_l &= \frac{E}{2} \left(L_3 - L_2 + \frac{1}{12} \right)
\end{aligned} \tag{155}$$

$$\begin{aligned}
K_i &= \frac{1}{2} \left(-A \left(L_5 - \frac{1}{3} \right) + (2A-B) \left(L_4 - \frac{2}{5} \right) \right. \\
&\quad \left. + (2B-A-C) \left(L_3 - \frac{1}{2} \right) + (2C-B) \left(L_2 - \frac{2}{3} \right) \right. \\
&\quad \left. - C \left(L_1 - 1 \right) \right) \\
K_j &= \frac{1}{2} \left(3A \left(L_5 - \frac{1}{3} \right) + (3B-5A) \left(L_4 - \frac{2}{5} \right) \right. \\
&\quad \left. + (3C-5B) \left(L_3 - \frac{1}{2} \right) + (2A-5C) \left(L_2 - \frac{2}{3} \right) \right. \\
&\quad \left. + 2B \left(L_1 - 1 \right) + 2C \left(L_0 - 2 \right) \right) \\
K_k &= \frac{1}{2} \left(-3A \left(L_5 - \frac{1}{3} \right) + (4A-3B) \left(L_4 - \frac{2}{5} \right) \right. \\
&\quad \left. + (A+4B-3C) \left(L_3 - \frac{1}{2} \right) + (B+4C) \right. \\
&\quad \left. \cdot \left(L_2 - \frac{2}{3} \right) + C \left(L_1 - 1 \right) \right) \\
K_l &= \frac{1}{2} \left(A \left(L_5 - \frac{1}{3} \right) + (B-A) \left(L_4 - \frac{2}{3} \right) \right. \\
&\quad \left. + (C-B) \left(L_3 - \frac{1}{2} \right) - C \left(L_2 - \frac{2}{3} \right) \right)
\end{aligned} \tag{156}$$

The analytical expressions for the integrations over the subparametric Overhauser element presented significantly reduce the time required to formulate system matrices as compared to the isoparametric version. As with all analytical formulations presented, the calculation of the field variables at internal points very near the boundary are consistent and accurate. Since the Overhauser curve is a cubic,

it often requires far fewer discrete nodes to effectively model the geometry and provide accurate reliable solutions. The analytic form of the element suffers the same restriction at abrupt changes in the geometry as the isoparametric version. The use of double noding and element linking with quadratic or linear elements provides a number of different ways to effectively model a corner.

Summary

Three general element types have been presented as possible representations for both the distribution of the field variables over the surface and the approximation of the boundary geometry. Analytic expressions for the required integrations over a linear element were given as well as the exact form for a special case of the quadratic and Overhauser elements.

Analytic analysis provides improved accuracy at internal point calculations, especially at points very near the boundary. The time required to compile the system matrices is greatly reduced while maintaining a high degree of accuracy in the solution. The subparametric assumption for the quadratic and Overhauser elements, which may reduce the order of the approximation for the geometry, is compensated by the increased accuracy of an exact formulation. In Chapter V, numerical examples will be presented comparing the three types of elements for both linear and curved geometries.

CHAPTER IV

DOMAIN DISCRETIZATION AND INTERNAL POINT CALCULATIONS

The nonhomogeneous form of Equations (28) and (29) contains domain integrations as well as the surface integrals. Several ways of evaluating the domain integration which will avoid any type of explicit domain discretization will be developed in this chapter. This effort is an attempt to maintain the purity of the boundary element formulation in the sense that only surface geometries need be modeled.

Calculation of the values of the field variables ψ and ω at internal points requires the evaluation of Equations (28) and (29). Analytic expressions for the surface integrals in these equations have been presented in Chapter III. Values of derivatives of the field variables ψ and ω at points in the domain require the evaluation of a different set of integrals defined in Equations (17) - (20) and (23) - (26). An exact analysis for a linear isoparametric element will be developed. Both a general numerical form and an analytic subparametric version of the quadratic and the Overhauser elements are given.

Domain Discretization

Two methods of evaluating the nonhomogeneous terms defined in Equations (34) and (35) are presented. The first technique uses a series of Green's identities to transform special forms of the integration of the function $f(x,y)$ over the domain V to a set of surface

integrations. The second, more general technique uses a "domain faning" quadrature scheme that does not require implicit volume discretization.

Integral Transformations

The nonhomogeneous function $f(x,y)$ in Equations (34) and (35) may be transformed from its domain integral form to an equivalent set of integration over the surface when the function $f(x,y)$ is harmonic or biharmonic in the domain V . In this case, either Green's second identity for harmonic functions or the Rayleigh-Green identity for two biharmonic functions is used for the transformation. Consider the case where the function $f(x,y)$ is harmonic in the domain V , $\nabla^2 f(x,y) = 0$. Equation (34) can be rewritten using Green's second identity, Equation (6), in the following form

$$\begin{aligned} \int_V (f(x,y) \nabla^2 z - z \nabla^2 f(x,y)) dV \\ = \int_S (f(x,y) \frac{\partial z}{\partial n} - z \frac{\partial}{\partial n} f(x,y)) dS \end{aligned} \quad (157)$$

The second term of the domain integration is identically zero. Therefore, if the function $\nabla^2 z$ is set equal to the Green's function G_2 , a relationship between the domain integral of Equation (34) and a set of equivalent surface integrals is defined. All that is necessary to complete this transformation is the determination of the function z defined by

$$\nabla^2 z(\vec{p}, \vec{q}) = \frac{1}{r} \frac{\partial}{\partial r} \left(r \frac{\partial}{\partial r} \right) = G_2(\vec{p}, \vec{q}) \quad (158)$$

Renaming $z(\vec{p}, \vec{q})$ to $G_3(\vec{p}, \vec{q})$ and solving Equation (158) for the new function results in

$$G_3(\vec{p}, \vec{q}) = z(\vec{p}, \vec{q}) = \frac{|\vec{p}-\vec{q}|^4}{128\pi} \left(\ln|\vec{p}-\vec{q}| - \frac{3}{2} \right) \quad (159)$$

The normal derivative of G_3 is calculated as

$$G_3'(\vec{p}, \vec{q}) = \frac{|\vec{p}-\vec{q}|^2}{32\pi} \left(\ln|\vec{p}-\vec{q}| - \frac{5}{4} \right) \cdot \left((x-x_p)n_x + (y-y_p)n_y \right) \quad (160)$$

By substituting Equations (159) and (160) into Equation (157) the domain integrations are transformed into a set of surface integrals of the form

$$\int_V f(x,y)G_2(\vec{p}, \vec{q})dV = \int_S (fG_3' - f'G_3)dS \quad (161)$$

A similar transformation is found for the domain integral of Equation (35) and is defined as

$$\int_V f(x,y)G_1(\vec{p}, \vec{q})dV = \int_S (fG_2' - f'G_2)dS, \quad (162)$$

where the Green's function G_2 is previously defined in Equation (10).

Consider the case when the function $f(x,y)$ is biharmonic over the domain V , $\nabla^4 f(x,y) = 0$. In this case, the Rayleigh-Green identity for two biharmonic functions, Equation (5), is used to transform Equations (34) and (35). Therefore, the following form of the identity may be written:

$$\int_V (f(x,y)\nabla^4 w - w\nabla^4 f(x,y))dV = \int_S \left(f \frac{\partial}{\partial n} (\nabla^2 w) - \frac{\partial f}{\partial n} \nabla^2 w + \frac{\partial w}{\partial n} \nabla^2 f - w \frac{\partial}{\partial n} (\nabla^2 f) \right) dS \quad (163)$$

The second term of the domain integration of Equation (163) is identically zero. If the term $\nabla^4 w$ is set equal to the Green's function G_2 , the transformation of the domain integrations of Equation (34) into a set of surface integrals is defined. The function $w(p,q)$ is determined for the relationship

$$\nabla^4 w(\vec{p}, \vec{q}) = \frac{1}{r} \frac{\partial}{\partial r} \left(r \frac{\partial}{\partial r} \left(\frac{1}{r} \frac{\partial}{\partial r} \left(r \frac{\partial w}{\partial r} \right) \right) \right) = G_2(\vec{p}, \vec{q}) \quad (164)$$

Solving Equation (164) for the function $w(p,q)$ and renaming it $G_4(p,q)$ results in

$$G_4(\vec{p}, \vec{q}) = \frac{|\vec{p}-\vec{q}|^6}{4608\pi} \left(\ln|\vec{p}-\vec{q}| - \frac{11}{6} \right) \quad (165)$$

The normal derivative of G_4 is calculated as

$$G_4'(\vec{p}, \vec{q}) = \frac{|\vec{p}-\vec{q}|^4}{768\pi} \left(\ln|\vec{p}-\vec{q}| - \frac{5}{3} \right) \cdot \left((x-x_p)n_x + (y-y_p)n_y \right) \quad (166)$$

Substituting the above expressions into Equation (163) defines the complete transformation for Equation (34) into a set of surface integrations as

$$\int_V f(x,y)G_2(\vec{p}, \vec{q})dV = \int_S \left(fG_3' - f'G_3 + G_4'\nabla^2 f - G_4(\nabla^2 f)' \right) dS \quad (167)$$

A similar transformation for the domain integral of Equation (35) is

$$\int_V f(x,y)G_1(\vec{p}, \vec{q})dV = \int_S \left(fG_2' - f'G_2 + G_3'\nabla^2 f - G_3(\nabla^2 f)' \right) dS \quad (168)$$

In general, this type of transformation can be continued to any n order harmonic for the function $f(x,y)$. The form of the Green's function and its normal derivative may be written in a general form as (Gipson and Reible, 1987)

$$G_k(\vec{p}, \vec{q}) = \frac{|\vec{p}-\vec{q}|^{2k-2}}{2^{2k-1} ((k-1)!)^2 \pi} \left(\sum_{j=1}^{k-1} \frac{1}{j} - \ln|\vec{p}-\vec{q}| \right) \quad (169)$$

$$G'_k(\vec{p}, \vec{q}) = \frac{2(k-1)|\vec{p}-\vec{q}|^{2(k-2)}}{2^{2k-1} ((k-1)!)^2 \pi} \left(\ln|\vec{p}-\vec{q}| + \frac{1}{2(k-1)} - \sum_{j=1}^{k-1} \frac{1}{j} \right) \left((x-x_p)n_x + (y-y_p)n_y \right) \quad (170)$$

This type of integral transformation eliminates the domain integrations completely for special forms of the function $f(x,y)$. Note that the transformations determined in Equations (167) and (168) reduce to those defined for the harmonic form of $f(x,y)$. Therefore, this transformation is sufficient to convert both the harmonic and biharmonic forms of the function $f(x,y)$ to a set of surface integrals. Nonetheless, a general function approximated by a finite series can be transformed using the appropriate order of a Green's type identity and the expression in Equations (169) - (170). Numerical examples for both harmonic and biharmonic types of the function $f(x,y)$ are presented in Chapter V.

Linear Elements

Exact integration of Equations (34) and (35) for certain harmonic forms of the function $f(x,y)$ are determined for a linear boundary element. A numerical formulation is also developed for the general bi-

harmonic form of $f(x,y)$. By predetermining a general form for the harmonic function $f(x,y)$ the transformed domain integrations defined in Equations (34) and (35) may be performed analytically. The form of the harmonic function is assumed as

$$f(x,y) = C_1xy + C_2x + C_3y + C_4 \quad (171)$$

For a linear element analysis, the Cartesian coordinates x and y may be defined using the relationship in Equation (43). Substituting the parametrized coordinates into Equation (171) redefines $f(x,y)$ as a function of the parameter t , the element constants given in Equation (49), and discrete linear end-nodes.

$$f(t) = R_1t^2 + R_2t + R_3 \quad (172)$$

where R_1 , R_2 , and R_3 are defined as

$$R_1 = C_1A_xA_y \quad R_2 = C_1(A_xy_i + A_yx_i) + C_2A_x + C_3A_y \quad (173)$$

$$R_3 = C_1x_iy_i + C_2x_i + C_3y_i + C_4$$

In a similar manner, the normal derivative of the general harmonic function, defined in Equation (171), is calculated as

$$\frac{\partial f(t)}{\partial n} = S_1t + S_2 \quad (174)$$

where S_1 and S_2 are defined as

$$S_1 = C_1(A_y n_x + A_x n_y) \quad (175)$$

$$S_2 = (C_1y_i + C_2)n_x + (C_1x_i + C_3)n_y$$

Substituting this special form of $f(x,y)$ into Equation (161) results in the following form of the required surface integrations

$$\int_V f(x,y)G_2(\vec{p},\vec{q}) dV = \frac{1}{64\pi} \sum_e \int_0^1 (E(R_1t^2 + R_2t + R_3)X(\ln X - \frac{5}{2}) - \frac{1}{4}(S_1t + S_2)X^2(\ln X - 3))dt \quad (176)$$

where the position vector X and the element constant E are given in Equations (48) and (54), respectively. The integration table defined in Equations (55) - (64) and complemented by Equations (107), (108), (147) and (148) provide all the necessary components to define the analytic expression for the integration as a summation over n linear elements:

$$\begin{aligned} \int_V f(x,y)G_2(\vec{p},\vec{q})dV = & \frac{1}{64\pi} \sum_e \left(-\frac{S_1P_1}{4} L_5 \right. \\ & + (R_1AE - \frac{1}{4}(S_1P_2 + S_2P_1))L_4 \\ & + (E(R_1B + R_2A) - \frac{1}{4}(S_1P_3 + S_2P_2))L_3 \\ & + (E(R_1C + R_2B + R_3A) - \frac{1}{4}(S_1P_4 + S_2P_3))L_2 \\ & + (E(R_2C + R_3B) - \frac{1}{4}(S_1P_5 + S_2P_4))L_1 \\ & + (ER_3C - \frac{1}{4}S_2P_5)L_0 - \frac{5E}{2}(R_1T_3 + R_2T_2 + R_3T_1) \\ & \left. + \frac{3}{4}(S_1U_2 + S_2U_1) \right) \quad (177) \end{aligned}$$

where

$$\begin{aligned}
 P_1 &= A^2 & P_2 &= 2AB & P_3 &= 2AC + B^2 \\
 P_4 &= 2BC & P_5 &= C^2 & T_n &= \frac{A}{n+2} + \frac{B}{n+1} + \frac{C}{n} \\
 U_n &= \frac{P_1}{n+4} + \frac{P_2}{n+3} + \frac{P_3}{n+2} + \frac{P_4}{n+1} + \frac{P_5}{n}
 \end{aligned} \tag{178}$$

The element constants A, B, and C are previously defined for a linear element in Equation (49). The analytic expression for the domain integral of Equation (35) based on the same set of element constants, the complete integration table, and the constants of Equation (178) is calculated as

$$\begin{aligned}
 \int_V f(x,y) G_1(p,q) dV &= \frac{1}{8\pi} \int_0^e \int_0^e \left(-\frac{S_1 A}{2} L_3 \right. \\
 &+ (R_1 E - \frac{1}{2}(S_1 B + S_2 A)) L_2 \\
 &+ (R_2 E - \frac{1}{2}(S_1 C + S_2 B)) L_1 + (R_3 E - \frac{1}{2} S_2 C) L_0 \\
 &\left. - E \left(\frac{R_1}{3} + \frac{R_2}{2} + R_3 \right) + S_1 T_2 + S_2 T_1 \right)
 \end{aligned} \tag{179}$$

The analytic expressions for the domain integrals of Equations (34) and (35) provide a very accurate technique to work a wide range of nonhomogeneous biharmonic problems. Although the exact analysis is restricted to functions of the form given in Equation (171), any general biharmonic function may be transformed and evaluated numerically.

General Isoparametric Element

Equations (167) and (168) may be rewritten to accommodate any type or combination of elements. In Chapter III, an extensive analy-

sis of linear and high order elements was presented. By substituting the appropriate form of the position vector and the Jacobian for the desired element into Equations (167) and (168), the domain integral is expressed in terms of a series of parametric surface integrations. The general forms of the integrations for any element type are given as

$$\int_V f(x,y) G_2(\vec{p}, \vec{q}) dV = \sum_e \int_0^1 (f G_3' - f' G_3 + \\ + \nabla^2 f G_4' - G_4 (\nabla^2 f)') |J| dt \quad (180)$$

$$\int_V f(x,y) G_1(\vec{p}, \vec{q}) dV = \sum_e \int_0^1 (f G_2' - f' G_2 \\ + \nabla^2 f G_3' - G_3 (\nabla^2 f)') |J| dt \quad (181)$$

where the summation is over the number of elements, e , used to describe the discrete surface.

Domain Fanning

The nonhomogeneous terms of the integral equations defined in Equations (28) and (29) must be evaluated over the region V , the problem domain. The evaluation of these domain integrations may be handled in a number of ways. A popular technique is the use of internal cells where the domain is subdivided into a series of volume elements over each of which a numerical quadrature scheme is applied. This type of procedure requires a discretization of the problem domain and can be difficult to implement for a general region. Monte Carlo quadrature techniques, which have been successfully used to evaluate domain integrations associated with the Poisson equation (Gipson,

1985; Gipson and Camp, 1985), do not require domain discretization. The fundamental disadvantage of Monte Carlo integration is that its accuracy increases only on the order of the inverse square root of the number of sampling points. Neither the volume cell nor the Monte Carlo method is intrinsically sensitive to the singular nature of the Green's function associated with the domain terms of Equations (28) and (29) near the source point.

In this work, an improved domain quadrature technique similar to that used by Telles (1983) is implemented. The method combines the convenience of higher order numerical integration over a triangular area with the inherent advantages of nondiscretization of the domain. This technique divides the domain into a series of triangular areas, each formed implicitly by a set of three vertices; two are consecutive discrete nodal points of a boundary element describing the surface of the domain and the other is the source point (x_p, y_p) under consideration. Each of the elemental triangular regions is divided into a series of smaller triangular areas, as shown in Figure 7. The effect is to concentrate quadrature points in a region close to the source point (x_p, y_p) where the Green's function is singular, and relax the intensity of the quadrature in areas where the function is more well-behaved. Each of the domain integrals defined in Equations (34) and (35) are referenced to a discrete source point. By maintaining the source point as a vertex of the triangular area, the integration scheme automatically distributes its quadrature points in a way that is sensitive to the singularity of the Green's functions as the other two vertices move from element to element around the boundary. The effect is to "fan" the region about the point in question. Another

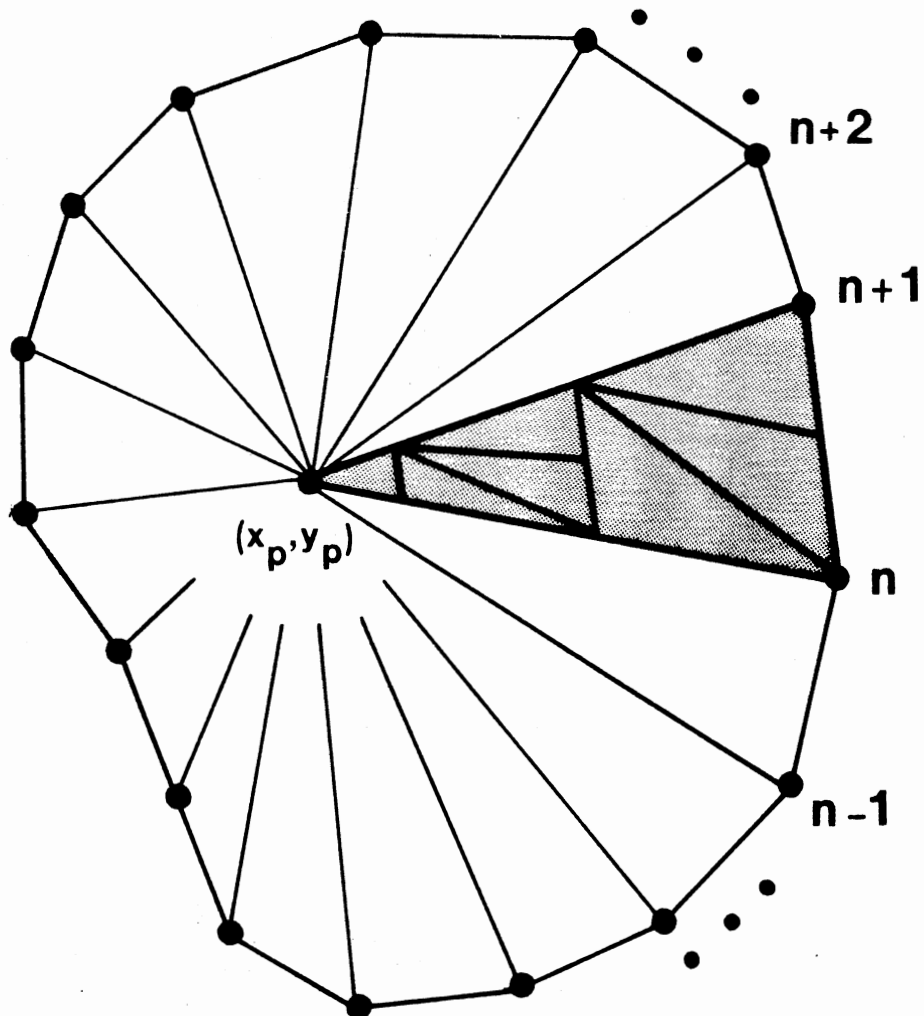


Figure 7. Distribution of Triangular Quadrature Regions for the "Fanning" Domain Integration Technique Related to a Particular Source Point. The Shaded Area Isolates the Distribution Over a Single Elemental Triangle.

advantage of this method is that it is equally applicable to source points on the interior of the domain. This feature is important in the evaluation of the domain integrals of Equations (11) and (12) which define the internal solution of the field variables.

Iterative Solution

If the nonhomogeneous source term $f(x,y)$ is also a function of the field variables and their derivatives, the solution to the governing coupled boundary integral expressions, Equations (28) and (29), is obtained by an iterative technique. The first iteration solves the homogeneous form of the governing equations and uses that solution to update the domain source terms, Equations (34) and (35), for the second iteration. After all the source terms are calculated, Equations (28) and (29) are solved to determine an intermediate solution of ψ , ψ' , ω , and ω' . The updated solution for each preceding iteration is obtained by relaxing the intermediate solution and adding that to either the homogeneous solution or to the previous intermediate solution. For example, the $k+1$ iteration for ψ and ω would be

$$\psi^{k+1} = \theta \psi^k + (1 - \theta) \psi^{k+1} \quad (182a)$$

$$\omega^{k+1} = \theta_1 \omega^k + (1 - \theta_1) \omega^{k+1} \quad (182b)$$

where ψ^k and ω^k are the solutions to the k th iteration or the homogeneous form of Equations (28) and (29) and θ and θ_1 are the appropriate relaxation factors. The iteration procedure is continued until a suitable convergence criterion is satisfied.

Evaluation of the terms in Equations (34) and (35) for an itera-

tive solution will be accomplished using the domain "fanning" integration technique discussed earlier. The form of the function f may involve the field variables ψ and ω and their derivatives in any combination. The "fanning" integration scheme requires the values of these functions at every quadrature point in the domain. In this work, the form of the function f will be restricted to functions of the form ψ , ω , $d\psi/dx$, $d\psi/dy$, $d\omega/dx$, and $d\omega/dy$. Values of these functions are automatically calculated at an array of uniformly distributed points in the domain and are combined with the boundary solution to create a series of solution maps, one for each of the six functions. When the integration scheme calls for a value of a particular function at an arbitrary triangular quadrature point, the point in question is located geometrically within each solution map array. Between two and four points in closest proximity to the quadrature point are located. The value of the function is then determined through linear interpolation of the set of field values associated with these points in the array map.

The location of the points in each solution map are implicitly defined within the formulation. Cartesian coordinates of each array point are defined in terms of the maximum and minimum spatial coordinates of the problem domain under consideration. Dividing the difference between the maximum and minimum points in each coordinate direction by a prescribed number of division defines the solution map point spacing, as shown in Figure 8. Each point is checked to determine if it actually lies within the domain using a residue theorem technique (Gipson, 1986). When an array point is found to be outside the do-

● Points inside the domain

⊕ Points outside the domain

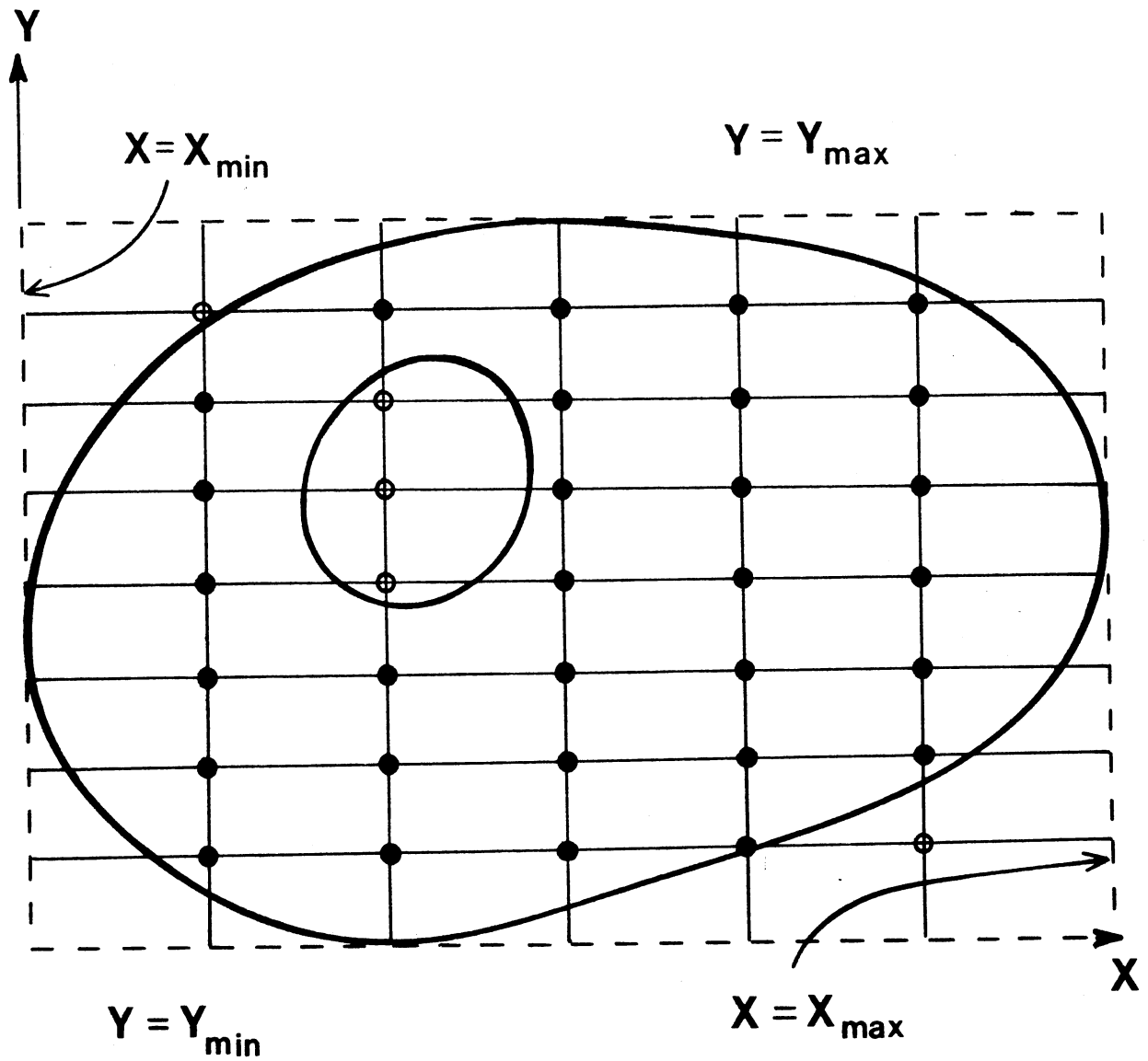


Figure 8. Internal Point Locations for a Solution Map for an Arbitrary Domain

main, it is not considered by either the "fanning" integration or the solution map interpolation techniques.

The advantage of the solution map scheme is that it requires relatively few internal point calculations for the values of the functions ψ , ω , and their derivatives. The execution time of the technique is much faster than it would be if the function were calculated at every triangular quadrature point. Any additional error introduced by the interpolation algorithm is minimal and offset by the decreases in run time. Overall, an iterative solution based on the solution map technique performs consistently and accurately. Several examples of iterative solutions for various combination of the functions ψ , ω and their derivatives are presented in Chapter V.

Internal Point Calculation

Boundary element formulations generally consist of a series of integrations over the surface of the problem domain. The values of the field variables at any points interior to the surface are calculated from a set of surface integrations that require a "complete" solution on the boundary. For a biharmonic analysis, the integral relationships that defined the values of the functions ψ and ω at any internal point are given in Equations (11) and (12). The first derivatives of ψ and ω with respect to both Cartesian coordinates x and y were previously defined in Equations (15), (16), (21), and (22). If linear isoparametric elements are used to describe the surface geometry, the integrations necessary to calculate the values of ψ , ω , and their derivatives may be performed analytically. Subparametric forms of both the quadratic and the Overhauser elements may also be evaluat-

ed analytically if the geometry is piecewise linear. Integrations over curved geometries using quadratic or Overhauser formulations may be performed using any appropriate numerical quadrature.

Linear Isoparametric Elements

Evaluation of the functions ψ and ω at any internal point in the domain V are calculated using Equations (28) and (29), respectively. The integrations defined in these equations are determined through analytical expressions derived in Chapter III. Since the source point (x_p, y_p) for an internal point calculation is never located on the element itself, the logarithmic singularity encountered previously is no longer a concern. Therefore, the appropriate components of the exact expression for the required integrations are given in Equations (65) - (72).

The value of the first derivatives of the functions ψ and ω are calculated from the relationships in Equations (15), (16), (21), and (22). The derivative operator acts exclusively upon the Green's functions as shown in Equations (17) - (20) and (23) - (26). The field variables may be approximated by a series of discrete nodal values and a corresponding shape function set. Substitution of the linear shape functions previously defined in Chapter III into the expressions defining the derivatives results in integrands of the form t^n , t^n/X , t^n/X^2 , and $t^n \ln X$. Only the integrations involving terms of the form t^n/X^2 have not been previously defined. Therefore, the following additions to the integration table are given as

$$\begin{aligned}
M_0 &= \int_0^1 \frac{dt}{x^2} = \left(\frac{2A+B}{A+B+C} - \frac{B}{C} + 2AI_0 \right) / \Delta \quad \Delta > 0 \\
&= \frac{1}{3A^2} \left(\left(\frac{2A}{B} \right)^3 - \frac{1}{\left(1 + \frac{B}{2A} \right)^3} \right) \quad \Delta = 0
\end{aligned} \tag{183}$$

$$\begin{aligned}
M_1 &= \int_0^1 \frac{t}{x^2} dt = - \left(\frac{2C+B}{A+B+C} - 2BI_0 \right) / \Delta \quad \Delta > 0 \\
&= - \left(\frac{1}{2} + \frac{B}{12A} \right) / \left(1 + \frac{B}{2A} \right)^3 \\
&\quad + \frac{2A^2}{3B^2} \quad \Delta = 0
\end{aligned} \tag{184}$$

where $\Delta = 4AC - B^2$

$$M_2 = \int_0^1 \frac{t^2}{x^2} dt = - \frac{1}{A(A+B+C)} + \frac{C}{A} M_0 \tag{185}$$

The parametrized linear element formulation presented in Chapter III is corrected for analytic derivative calculations by substituting the following terms into Equations (65) - (68).

$$H_j = 2(m_n I_1 - 2E(A_n M_2 + B_n M_1)) \tag{186}$$

$$H_i = 2(m_n I_0 - 2E(A_n M_1 + B_n M_0)) - H_j$$

$$G_j = A_n I_2 + B_n I_1 \tag{187}$$

$$G_i = A_n I_1 + B_n I_0 - G_j$$

$$L_j = 2(2E(A_n I_2 + B_n I_1) + m_n (L_1 - \frac{1}{2})) \tag{188}$$

$$L_i = 2(2E(A_n I_1 + B_n I_0) + m_n (L_0 - 1)) - L_j$$

$$K_j = A_n L_2 + B_n L_1 - \left(\frac{A_n}{3} + \frac{B_n}{2} \right) \quad (189)$$

$$K_i = A_n L_1 + B_n L_0 - \left(\frac{A_n}{2} + B_n \right) - K_j$$

where $n = 1, 2$ corresponds to the x derivative or the y derivative formulation, respectively. The constants A_n , B_n , and m_n are given as

$$\begin{aligned} A_1 &= A_x & A_2 &= A_y \\ B_1 &= B_x & B_2 &= B_y \\ m_1 &= n_x & m_2 &= n_y \end{aligned} \quad (190)$$

Domain integrations required in the nonhomogeneous form of the equations used to calculate derivatives at internal points are evaluated analytically for a special form of the function $f(x,y)$, given in Equation (171). By substituting the appropriate form of the Green's functions and the special version of $f(x,y)$ into Equations (161) and (162) domain integrals are transformed into a series of boundary integrations. If the surface is described by linear elements, the transformed analytic relationships over each element are defined as

$$\begin{aligned} \int_0^1 f(x,y) \frac{\partial G_2}{\partial x_i} dV &= \frac{1}{32\pi} \sum_e \left(-\frac{Q_1 L_4}{2} + (EP_1 - \frac{Q_2}{2}) L_3 \right. \\ &+ (EP_2 - \frac{Q_3}{2}) L_2 + (EP_3 - \frac{Q_4}{2}) L_1 + (EP_4 - \frac{Q_5}{2}) L_0 \\ &- \frac{3E}{2} \left(\frac{P_1}{4} + \frac{P_2}{3} + \frac{P_3}{2} + P_4 \right) \\ &\left. + \frac{5}{4} \left(\frac{Q_1}{5} + \frac{Q_2}{4} + \frac{Q_3}{3} + \frac{Q_4}{2} + Q_5 \right) \right) \end{aligned} \quad (191)$$

$$\begin{aligned}
\int_V f(x,y) \frac{\partial G_1}{\partial x_i} dV &= \frac{1}{8\pi} \frac{e}{\sum} (2E(P_1 I_3 + P_2 I_2 + P_3 I_1 + P_4 I_0) \\
&+ (R_1 n_i - S_1 A_i) L_2 + (R_2 n_i - (S_1 B_i + S_2 A_i)) L_1 \\
&+ (R_3 n_i - S_2 B_i) L_0 - n_i \left(\frac{R_1}{3} + \frac{R_2}{2} + R_3 \right) + \frac{1}{3} S_1 A_i \\
&+ \frac{1}{2} (S_1 B_i + S_2 A_i) + S_2 B_i) \quad (192)
\end{aligned}$$

where the function constants R_1 , R_2 , R_3 , S_1 , and S_2 are previously defined in Equations (173) - (175). The remaining constants are given as

$$\begin{aligned}
P_1 &= R_1 A_i & P_2 &= R_1 B_i + R_2 A_i \\
P_3 &= R_2 B_i + R_3 A_i & P_4 &= R_3 B_i
\end{aligned} \quad (193)$$

$$\begin{aligned}
Q_1 &= AS_1 A_i - AR_1 n_i \\
Q_2 &= S_1 (AB_i + BA_i) + AS_2 A_i - n_i (AR_2 + BR_1) \\
Q_3 &= S_1 (BB_i + CA_i) + S_2 (AB_i + BA_i) \\
&\quad - n_i (AR_3 + BR_2 + CR_1) \\
Q_4 &= CS_1 B_i + S_2 (BB_i + CA_i) - n_i (BR_3 + CR_2) \\
Q_5 &= CS_2 B_i - n_i CR_3
\end{aligned} \quad (194)$$

where the subscript "i" is equal to 1 or 2 corresponding to the x or y derivative, respectively. Therefore, the constants A_i , B_i , and the direction cosine n_i are given as

$$\begin{aligned}
A_1 &= A_x & A_2 &= A_y \\
B_1 &= B_x & B_2 &= B_y \\
n_1 &= n_x & n_2 &= n_y
\end{aligned}
\tag{195}$$

Although the analytic expressions defined in Equations (191) and (192) seem cumbersome, they are easily calculated and require less time to execute and are more accurate than integration using numerical quadrature. The analytic analysis of the simple form of the function $f(x,y)$ is justified since it has many applications in a wide range of engineering problems.

The domain integrals for nonhomogeneous analysis may be evaluated for the special case when $\nabla^4 f(x,y) = 0$ by the transformation technique discussed earlier. Transformation of the domain integrals into surface integrations require spatial derivatives for the functions G_2 , G_2' , G_3 , G_3' , G_4 , G_4' . The x and y derivatives of G_2 and G_2' are defined in Equations (19) - (20) and (25) - (26). The remaining x-coordinate derivatives are calculated as

$$\frac{\partial G_3}{\partial x_p} = \frac{1}{64\pi} \left((x-x_p) X \left(\ln X - \frac{5}{2} \right) \right) \tag{196}$$

$$\begin{aligned}
\frac{\partial G_3'}{\partial x_p} &= \frac{1}{64\pi} \left(2(x-x_p) Z \left(\ln X - \frac{3}{2} \right) \right. \\
&\quad \left. + n_x X \left(\ln X - \frac{5}{2} \right) \right) \tag{197}
\end{aligned}$$

$$\frac{\partial G_4}{\partial x_p} = \frac{1}{1536\pi} \left((x-x_p) X^2 \left(\ln X - \frac{10}{3} \right) \right) \tag{198}$$

$$\begin{aligned} \frac{\partial G'_4}{\partial x_p} &= \frac{1}{1536\pi} \left(4(x-x_p) Z X \left(\ln X - \frac{17}{6} \right) \right. \\ &\quad \left. + n_x X^2 \left(\ln X - \frac{10}{3} \right) \right) \end{aligned} \quad (199)$$

The necessary y -coordinate derivatives are determined as

$$\frac{\partial G_3}{\partial y_p} = \frac{1}{64\pi} \left((y-y_p) X \left(\ln X - \frac{5}{2} \right) \right) \quad (200)$$

$$\begin{aligned} \frac{\partial G'_3}{\partial y_p} &= \frac{1}{64\pi} \left(2(y-y_p) Z \left(\ln X - \frac{3}{2} \right) \right. \\ &\quad \left. + n_y X \left(\ln X - \frac{5}{2} \right) \right) \end{aligned} \quad (201)$$

$$\frac{\partial G_4}{\partial y_p} = \frac{1}{1536\pi} \left((y-y_p) X^2 \left(\ln X - \frac{10}{3} \right) \right) \quad (202)$$

$$\begin{aligned} \frac{\partial G'_4}{\partial y_p} &= \frac{1}{1536\pi} \left(4(y-y_p) Z X \left(\ln X - \frac{17}{6} \right) \right. \\ &\quad \left. + n_y X^2 \left(\ln X - \frac{10}{3} \right) \right) \end{aligned} \quad (203)$$

where the variable Z is

$$Z = (x-x_p)n_x + (y-y_p)n_y \quad (204)$$

For a general form of the function $f(x,y)$ the "fanning" domain integration technique is used to approximate the integrals required for the calculation of the derivatives of ψ and ω at internal points. Although the execution time is dramatically increased, the resulting solution is very accurate and generally consistent for well behaved functions. However, if the rate of change of the function $f(x,y)$ becomes large over a small area, the order of the quadrature over that

region should be appropriately increased. Refining the boundary discretization may improve the integration, since the number of quadrature points directly correspond to the number of elements.

Higher Order Elements

The correct form of the integrations required to calculate the values of the field variables ψ , ω , and their derivatives at any internal point for a general element are easily obtained. By substituting the appropriate forms of the shape functions, the Jacobian transformation, and the position vector into Equations (11), (12), (15), (16), (21), and (22), the required forms integral expressions are determined. The reader is referred to Chapter III for the development of these element parameters for both the quadratic and the Overhauser elements.

For a general internal point, the position vector is always non-zero. Therefore, no form of special quadrature is necessary since the logarithmic Green's function is no longer singular. A one-dimensional Gaussian quadrature over the parametrized element is used in the calculation of the values of the field variables and their derivatives at any internal point.

If the geometry is piecewise linear or assumed linear, the integrals required in internal point calculations may be evaluated analytically. The procedure is identical to that presented in Chapter III. The Jacobian becomes a constant and is factored from the integrations. The resulting integrals have components defined in the integration table developed in Chapter III and supplemented in this chapter. For a quadratic element, the required integrations for the calculation of

functions ψ and ω at any internal point are defined in Equations (109) - (116). The corresponding set of relationships for an Overhauser element are given in Equations (149) - (156). Surface integrations defining the values of the derivatives of ψ and ω are also calculated analytically for the subparametric versions of both the quadratic and the Overhauser elements. However, the necessary domain integrations involving the function $f(x,y)$ are evaluated numerically using either the integration transformation technique or the domain "fanning" scheme.

Summary

Two methods for handling domain integrations have been presented. Integrations over the domain may be transformed for harmonic and biharmonic forms of the function $f(x,y)$ into a set of surface integrals. Exact analysis for special cases of the resulting surface integrations were derived. The superior accuracy of an exact formulation may offset any error induced by assuming a linear variation of the geometry. The domain "fanning" technique provided implicit volume quadrature for forms of the function $f(x,y)$ which cannot be transformed. Although evaluated numerically, the domain "fanning" method has inherent sensitivity to the distribution of the Green's function resulting in accurate and consistent solutions.

Internal point calculations for the values of the field variables over several types of elements were defined. An exact expression of an isoparametric linear element and the subparametric versions of the quadratic and the Overhauser element were derived. The derivatives of the field variables were evaluated numerically for all element types.

However, derivative calculations for a special form of the function $f(x,y)$ over a linear element were performed analytically. Numerical calculations were very accurate as long as the point in question remained outside a zone measured by approximately half the element length from the boundary. Inside this zone the calculations became inaccurate. In Chapter V, several numerical examples will be worked demonstrating some of the various methods presented in this chapter.

CHAPTER V

EXAMPLE ANALYSES

The example problems presented in this chapter demonstrate the versatility of the formulation developed in Chapters III and IV over a wide range of engineering problems and also illustrate practical modeling techniques for boundary element analysis.

Example problems will be divided into two categories. The first will be a variety of problems involving the behavior of thin plates with small deflections. The second category will be a study of incompressible viscous fluid flow at low Reynolds numbers. In each case, the governing physical process will be identified along with the engineering applications. All example analyses are compared to existing analytical solutions or current published numerical approximations. The availability of analytical solutions for small deflections of thin plates of simple geometries provide an excellent base upon which to compare the different element types developed in the preceding chapters. Once an element hierarchy is established, most of the proceeding examples will use an element type determined to produce superior results.

Deflections of Thin Plates

The first category to be studied is that of the small deflections of a thin plate. A plate is an initially flat structural element

where the ratio of the thickness, measured normal to the midplane, to the smallest span dimension is less than 1/20 (Ugural, 1981). Unless otherwise denoted, the examples presented will consider thin plates composed of homogeneous isotropic materials. A homogeneous "plate" body has identical elastic properties throughout the material. If the material properties are also equal in all directions, the material is isotropic. The governing equation for the deflection of a thin structural plate under transverse loading $P(x,y)$, first derived by Lagrange in 1811, is given as

$$\nabla^4 w = \frac{P(x,y)}{D} \quad (205)$$

where w is the midplane deflection and D is the flexural rigidity. The resulting nonhomogeneous biharmonic equation requires that two boundary conditions of the form given in Equation (2) be satisfied on each edge.

A clamped or built-in edge condition requires that both the deflection, w , and the slope, $\partial w/\partial n$, be equal to zero at the boundary. This type of edge condition matches directly with the "forced" boundary conditions of the integral representation of the governing equation. Therefore, a clamped or built-in edge may be modeled for any type of geometry.

The second type of boundary conditions allowable with this analysis is a simply supported edge. In this case, the deflection and the normal bending moment, M_n , are both zero. The deflection condition is directly compatible to the "forced" conditions of the governing equation. However, the bending moment edge condition must be converted

into a form which matches one of the remaining three boundary conditions of Equation (2). The normal bending moment, M_n , is defined as

$$M_n = -D \left(\frac{\partial^2 w}{\partial n^2} + \nu \frac{\partial^2 w}{\partial s^2} \right) \quad (206)$$

where ν is Poisson's ratio and the coordinate s is measured tangent to the surface at any point. For any polygonal shape, along each rectilinear simply supported edge of the boundary, the term $\partial^2 w / \partial s^2$ is identically zero. Observing that M_n is specified as zero on a simply supported edge, the remaining term of Equation (206), $\partial^2 w / \partial n^2$, also vanishes. The moment function M is defined as

$$M = \frac{M_x + M_y}{1+\nu} = \frac{M_n + M_s}{1+\nu} \quad (207)$$

where M_x and M_y are the bending moments in Cartesian coordinates and M_s is the tangent bending moment. Rewriting the moment function in terms of the deflection results in the following:

$$M = -D \left(\frac{\partial^2 w}{\partial x^2} + \frac{\partial^2 w}{\partial y^2} \right) = -D \left(\frac{\partial^2 w}{\partial n^2} + \frac{\partial^2 w}{\partial s^2} \right) \quad (208)$$

Therefore, on any simply supported rectilinear edge of a polygonal shape the moment function is identically zero (Timoshenko and Woinowsky-Krieger, 1959). This relationship may be recast in the form of a "forced" boundary condition as

$$\nabla^2 w = -\frac{M}{D} = 0 \quad (209)$$

For the integral formulation developed in this work, a simply supported edge condition is possible for any polygonal shape and is specified by prescribing both the deflection, w , and the Laplacian of the deflection, $\nabla^2 w$, as zero along the boundary.

Numerical solutions will be presented for several different types of transverse loadings on thin plates of various geometries under two types of support conditions. Circular plate analysis will be limited to clamped supports, whereas both clamped and simply supported end conditions are possible for a polygonal shape. Numerical quadrature will be used in evaluating the necessary boundary integrals for all elements, except linear elements, for any curved geometry. All polygonal shapes will be analyzed with the analytical expressions developed for the subparametric version of each element. In each case, the various element types will be compared and their performance evaluated.

Circular Clamped Plates

Various axisymmetric loadings which only depend upon the radial coordinate will be considered. The governing equation for the deflection in terms of the radial coordinate is given as

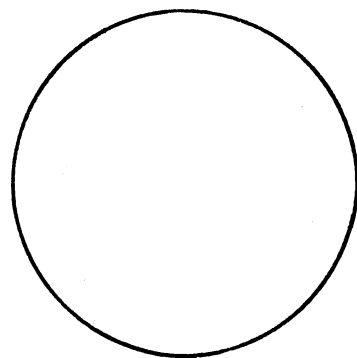
$$\nabla^4 w = \left(\frac{d^2}{dr^2} + \frac{1}{r} \frac{d}{dr} \right) \left(\frac{d^2 w}{dr^2} + \frac{1}{r} \frac{dw}{dr} \right) = \frac{P(r)}{D} \quad (210)$$

where $P(r)$ is the transverse loading function. The outside radius, a , of all the examples will be set equal to the numerical value of two. The clamped boundary conditions have been established and are applied as previously discussed.

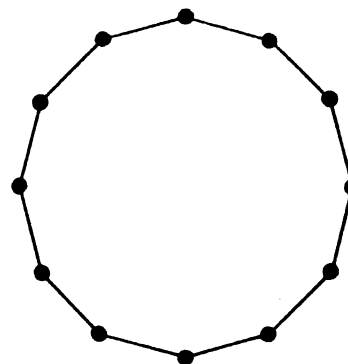
Concentrated Load at Plate Center. The deflection and moment function for a clamped circular plate with a concentrated load at its center are calculated. A concentrated load is one of the simplest loading conditions for any type of boundary element formulation.

Since a concentrated load acts at a point, the loading function $P(r)$ may be replaced by the value of the concentrated load multiplied by the Dirac delta function. Substituting this form of the loading into the necessary domain integrals results in a single evaluation of the integrand at the location of the concentrated load. Therefore, any error in the solution may be attributed directly to the surface integrations of the governing integral equation. This problem will provide an excellent format for the comparison and the evaluation of the three isoparametric elements presented in Chapter III.

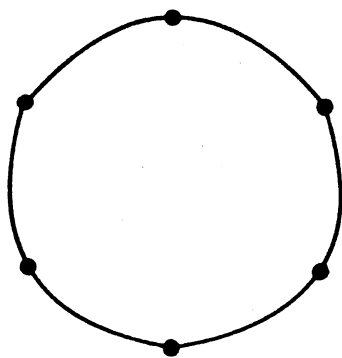
A series of boundary element meshes were used to discretize the circular problem domain. Each of the three elements; linear, quadratic, and Overhauser, are used to describe each mesh. An illustration of the ability of each element type to accurately represent the circular geometry is shown in Figure 9. The Overhauser element models the surface as a C_1 continuous curve, whereas the linear and quadratic element representations of the boundary have discontinuous derivatives between element. To allow for a fair comparison, the number of discrete nodal points and their locations were held constant for each mesh. The absolute percentage error between the boundary element solution and the exact solution, given by Timoshenko and Woinowsky-Krieger (1959), for the center deflection is shown in Figure 10. Several interesting observations may be made from this graph. Even though the linear element analysis was performed using analytical expressions for the integrations the percentage error is much greater than that in both the quadratic and Overhauser element analyses. A solution using just six nodes and six Overhauser elements deviated only 2% from the exact value for the center deflection. Both the



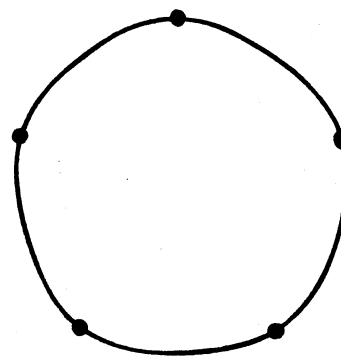
Circle



Linear
12 nodes



Quadratic
6 nodes



Overhauser
5 nodes

Figure 9. Comparison of Example Models Using Various Element Types to a Circle.

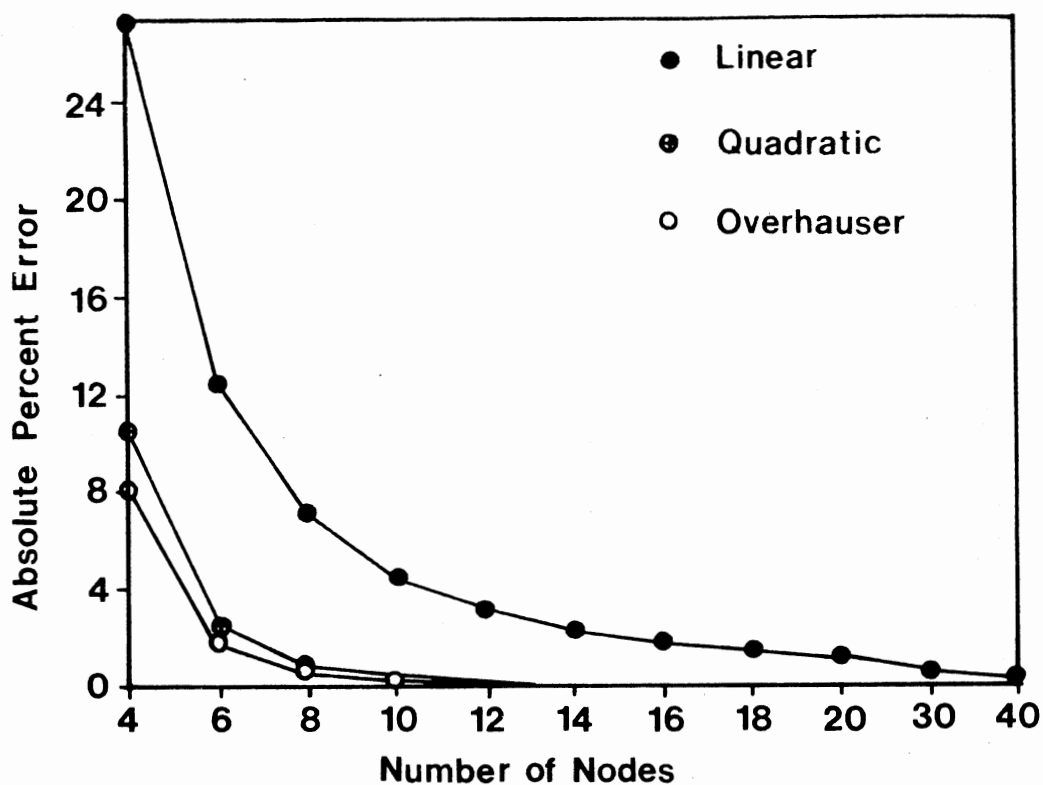


Figure 10. Absolute Percent Error For the Center Deflection of a Clamped Circular Plate With a Concentrated Load at the Center.

TABLE 1.

Deflection and Moment Function for a Clamped Circular Plate with a Concentrated Load P at its Center.

r/a	α	α exact	β	β exact
0.0	0.01989	0.01989	-	-
0.2	0.01653	0.01654	0.17655	0.17657
0.4	0.01087	0.01088	0.06624	0.06625
0.6	0.00541	0.00542	0.00171	0.00172
0.8	0.00147	0.00148	-0.04407	-0.04406

Note: Deflection, $w = \alpha Pa^2/d$, Moment Function $M = \beta P$, and radius a .

quadratic and Overhauser analyses provided excellent solutions when ten or more elements were used. The result of this comparison seems to indicate that the Overhauser element is superior to both the linear and quadratic elements for curved geometries. A boundary mesh using 20 Overhauser elements to describe the circle was used to calculate the deflection, w , and the moment function, M , at several internal points. The results are listed in Table 1.

Uniform Load. Consider an extension of the previous example to that of a plate carrying a uniform transverse load. The domain integrations are transformed into surface integrals using the techniques discussed in Chapter IV. Since the function $P(r) = q$ is a constant, the transformation converts each of the necessary domain integrations into a single corresponding boundary integral. A comparison of the three element types for this problem is shown in Figure 11. The solution obtained from the analytical formulation using linear elements is extremely poor when using less than about 30 nodes. However, the quadratic and the Overhauser elements provide outstanding solutions using only ten elements. Table 2 lists the deflection, w , and moment function, M , at several internal points determined from an analysis using 20 Overhauser elements.

Quadratic Load. A transverse loading of the form $P(r) = q(r/a)^2$ over a clamped circular plate is presented in this example. The domain integrations representing the load are converted into a series of surface integrals by the biharmonic version of the integral transformations discussed in Chapter IV. For this particular loading, each domain integration is transformed into an equivalent set of three sur-

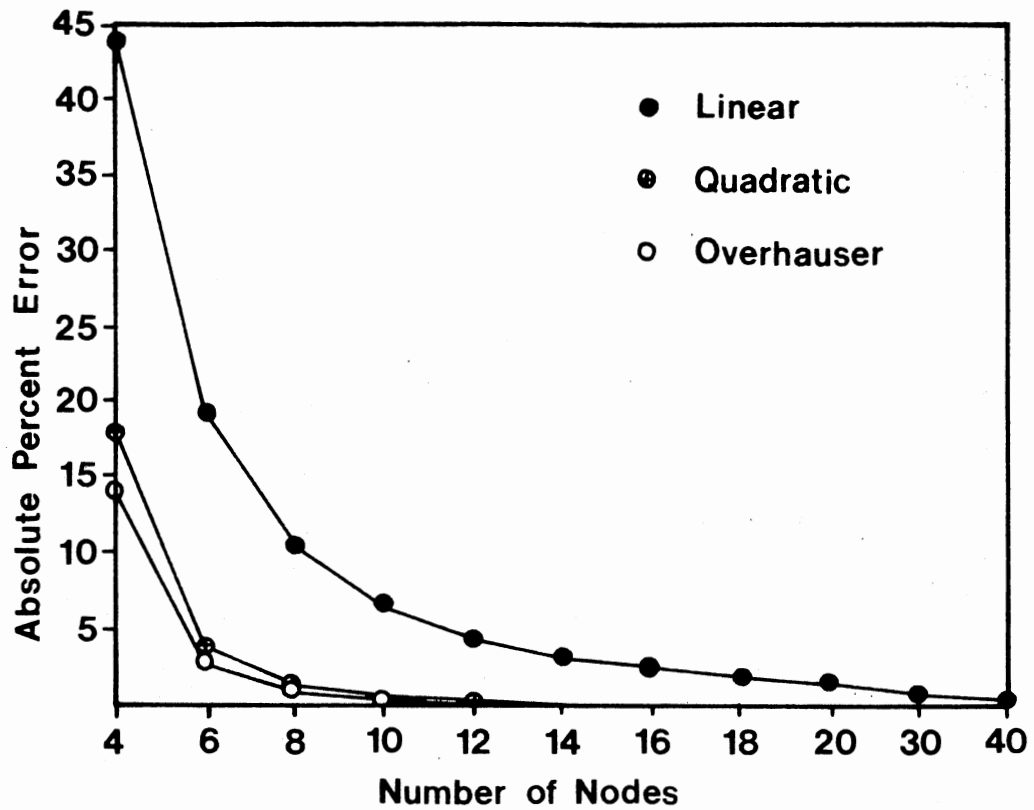


Figure 11. Absolute Percent Error For the Center Deflection of a Clamped Circular Plate Under a Uniform Load.

TABLE 2.

Deflection and Moment Function for a Clamped Circular Plate Under a Uniform Load $P(r)=q$.

r/a	α	α exact	β	β exact
0.0	0.01562	0.01562	0.12499	0.12500
0.2	0.01439	0.01440	0.11499	0.11500
0.4	0.01102	0.01102	0.08499	0.08500
0.6	0.00640	0.00640	0.03499	0.03500
0.8	0.00202	0.00202	-0.03501	-0.03500

Note: Deflection, $w=\alpha qa^4/D$, Moment Function $M=\beta qa^2$, and radius a .

face integrals. The three element types are once again compared for several different boundary discretizations. The results of this analysis are shown in Figure 12 in terms of the absolute percentage error between the numerical solution and the exact value for the center deflection. As the loading function $P(r)$ increases in order, the number of nodes required for an acceptable solution also increases. In Table 3, a solution using 20 Overhauser elements is presented for the deflection and moment function at several internal points.

The three preceding examples demonstrated several important features of the boundary integral formulation presented in this work. Many forms of the loading function $P(r)$ may be rewritten as surface integrals avoiding any type of domain quadrature. The shape functions associated with quadratic and Overhauser elements not only represent the geometry better than a linear element, but also provide a much more accurate solution with far fewer nodes. The decrease in execution time attributed to the analytic expression used in the linear element formulation does not compensate for its lower order approximation of the field variables. However, if a very large number of nodes are required for a particular problem, the difference in the solution obtained using any of the three element types is negligible. In this case the linear element formulation displays a slight advantage over the other two higher order elements in total execution time.

Asymmetric Loading. This example will illustrate the effectiveness of the domain "fanning" technique for a curved geometry. Consider an asymmetric loading of the form $P(r, \theta) = q_0 + q_1(r/a)\cos(\theta)$ acting on

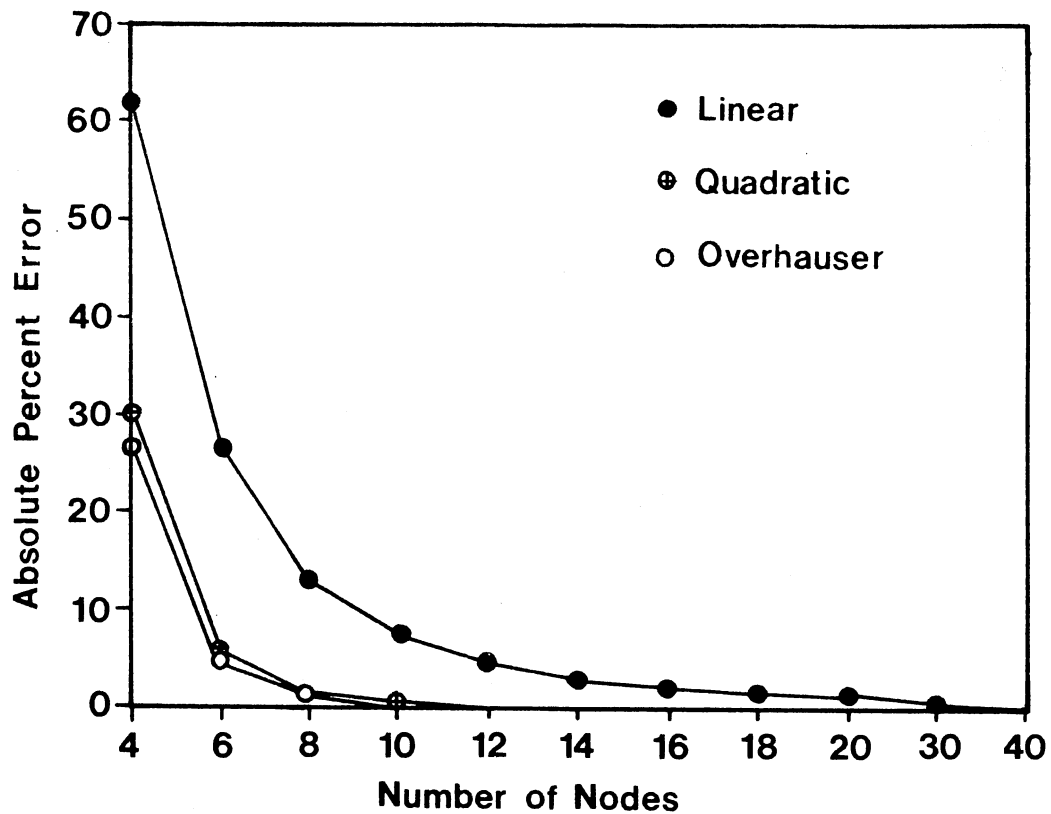


Figure 12. Absolute Percent Error For the Center Deflection of a Clamped Circular Plate Under a Quadratic Load.

TABLE 3.

Deflection and Moment Function for a Clamped Circular Plate Under a Quadratic Load $P(r)=q(r/a)^2$.

r/a	α	α exact	β	β exact
0.0	0.03472	0.03472	0.02083	0.02083
0.2	0.03263	0.03263	0.02073	0.02073
0.4	0.02645	0.02646	0.01923	0.01923
0.6	0.01678	0.01678	0.01273	0.01273
0.8	0.00594	0.00594	-0.00476	-0.00476

Note: Deflection, $w=\alpha qa^4(10^{-1})/D$, Moment Function $M=\beta qa^2$, and radius a .

a clamped circular plate. The domain integrations involving the loading function cannot be transformed into an equivalent set of surface integrals because of the transcendental function $\cos(\theta)$ in the second term. Deflections of the plate at various internal points are calculated using boundary meshes of 10, 20, and 30 Overhauser elements. The results are compared to an exact solution given by Ugural (1981), and listed in Table 4. Previous examples in this section have shown that solutions with a high degree of accuracy are obtainable with minimal boundary discretization when the loading function is "well behaved". When coupled with the domain "fanning" technique the Overhauser formulation can handle more complex loading functions and still retain all of its modelling advantages.

Elastic Foundations. The behavior of structural plates resting on an elastic foundation was first described by Winkler in 1867. In this model the foundation is replaced by an equivalent spring system and applied as an additional loading. Therefore, the governing equation for the deflection of a thin plate on a Winkler foundation is given as

$$\nabla^4 w = \frac{P(x,y)}{D} - \frac{k}{D} w \quad (211)$$

where k is called the modulus of the foundation. The value of the foundation modulus k may vary from 0 to 200MN/m^3 depending upon the subgrade. A dimensionless form of the foundation modulus was used and is defined as $K = ka^4/D$. As can be seen in Equation 211 the unknown deflection function w is not exclusively dependent on the biharmonic operator. Therefore, an iterative solution technique is required.

TABLE 4.

Deflection of a Clamped Circular Plate Under an Asymmetric Load $P(r)=q_0+q_1(r/a)\cos(\theta)$.

$\theta=45$	r/a	α	α_{10}	α_{20}	α_{30}
	0.0	0.25000	0.24715	0.24967	0.24993
	0.2	0.24126	0.23799	0.24088	0.24118
	0.4	0.19303	0.18974	0.19266	0.19298
	0.6	0.11688	0.11409	0.11659	0.11688
	0.8	0.03850	0.03682	0.03836	0.03854
$\theta=90$	0.2	0.23040	0.22767	0.23009	0.23033
	0.4	0.17640	0.17404	0.17613	0.17634
	0.6	0.10240	0.10062	0.10219	0.10235
	0.8	0.03240	0.03144	0.03228	0.03237

Note: Deflection, $w=\alpha q_0/D$, $q_0=q_1$, and radius $a=2$.

TABLE 5.

Center Deflection for a Clamped Circular Plate Under a Uniform Load q , on a Winkler Elastic Foundation.

Dimensionless Foundation Modulus, K	α , Results from Ng	α , Results from Costa and Brebbia	α Using 20 Overhauser Elements
0	0.01562	-	0.01562
20	0.01301	0.01279	0.01314
40	0.01112	0.01096	0.01133
60	0.00969	0.00957	0.00989
80	0.00858	0.00846	0.00878
100	0.00768	0.00760	0.00791
120	0.00695	0.00688	0.00717
140	0.00633	0.00628	0.00656
160	0.00581	0.00577	0.00603
180	0.00537	0.00533	0.00558
200	0.00498	0.00495	0.00518

Note: Deflection $w=\alpha q a^4/D$ and radius $=a$.

This particular example demonstrates the combined effect of several of the developments featured in Chapter IV of this work. The boundary of the circular plate was discretized with 20 Overhauser elements. Since the loading terms are a function of the deflection, an iterative solution procedure was used combining the domain "fanning" integration and "solution map" techniques. The results for different values of the dimensionless foundation modulus K , shown in Tables 5 and 6, are compared with analytical results obtained by Ng (1969) and a boundary element solution presented by Costa and Brebbia (1985). As can be seen in Tables 5 and 6 accurate results can be obtained using just 20 Overhauser elements. It is interesting to note that the results were conservative when compared to either the analytical or the constant element solution. This type of behavior is not unexpected considering that the initial iteration of the solution is that of a plate without an elastic foundation. When the maximum percent change in the deflection between corresponding solution map points was less than a prescribed value, the solution was considered to have converged. A relaxation factor of 0.5 was found to be effective and solutions were obtained in an average of seven iterations.

Simply Supported Rectangular Plates

Several different rectangular plates under various loading functions will be presented in this section. Unless otherwise specified, the dimensions of each plate will be $0 \leq x \leq a$, $0 \leq y \leq b$. The discontinuity of the surface geometry will require "double noding" of the "extra" node when using Overhauser elements at corners. However, the linear nature of the geometry will allow implementation of the analy-

TABLE 6.

Edge Moments for a Clamped Circular Plate Under a Uniform Load q , on a Winkler Elastic Foundation.

Dimensionless Foundation Modulus, K	α , Results from N_g	α , Results from Costa and Brebbia	α Using 20 Overhauser Elements
0	-0.12500	-	-0.12498
20	-0.10858	-0.10914	-0.10875
40	-0.09666	-0.09746	-0.09700
60	-0.08760	-0.08851	-0.08765
80	-0.08047	-0.08144	-0.08040
100	-0.07470	-0.07471	-0.07450
120	-0.06993	-0.07095	-0.06960
140	-0.06592	-0.06694	-0.06545
160	-0.06249	-0.06352	-0.06188
180	-0.05953	-0.06054	-0.05993
200	-0.05694	-0.05760	-0.05722

Note: Deflection $w = \alpha a^2 q$ and radius $= a$.

TABLE 7.

Center Deflection and Moment Function for a Simply Supported Rectangular Plate Bent by Moments Distributed Along Two Parallel Edges.

b/a	α	α exact	β	β exact
0.5	0.0966	0.0964	0.8912	0.8900
1.0	0.0369	0.0368	0.5009	0.5000
1.5	0.0281	0.0280	0.2390	0.2385
2.0	0.0174	0.0174	0.1100	0.1100

Note: Deflection, $w = \alpha M_0 b^2 / D$ for $b/a < 1$,
 $w = \alpha M_0 a^2 / D$ for $b/a > 1$, and Moment Function
 $M = \beta M_0$.

tic expressions developed in Chapter III, for the subparametric form of the element. The order of the loading function is increased with each example in an effort to demonstrate the flexibility of the presented formulation. Element performance is evaluated only in selected examples to be compared with corresponding circular plate analysis.

Edge Moments. The bending of a rectangular plate by uniform moments distributed along two parallel sides is considered. This type of loading condition is extremely easy to model. The homogeneous form of the biharmonic equation is solved with the deflection specified at zero along each edge. The Laplacian of w , $\nabla^2 w$ is specified as zero at $x = 0$ and $x = a$, and set equal to $-M_n/D$ at $y = 0$ and $y = b$. Results for the deflection $w(a/2, b/2)$ and the moment function $M(a/2, b/2)$ at several ratios of b/a , shown in Table 7, compare very well with analytical results obtained by Timoshenko and Woinowsky-Krieger (1959). The number of Overhauser elements used for this example ranged from 20 for $b/a = 0.5$ to 40 for $b/a = 2.0$ maintaining approximately the same element length throughout the analysis.

Thermal Loads. Consider the special case of a simply supported rectangular plate bent by uniform edge moments which are caused by a temperature variation in the plate. Assume the upper surface of the plate is held at a different temperature than the lower surface. The resulting form of the normal edge moment for the linear temperature distribution is given as

$$M_n = \frac{\alpha t(1+\nu)}{h} \quad (212)$$

where t is the temperature difference between the upper and lower surfaces, α is the coefficient of thermal expansion, h is the plate thickness, and ν is Poisson's ratio. The center deflection of the plate for several ratios of a/b are compared to an analytical solution given by Timoshenko and Woinowsky-Krieger (1959) and listed in Table 8. The modelling procedure was identical to that of the previous example.

Concentrated Load. This example will demonstrate the accuracy of the boundary element solution for concentrated loads over rectangular geometries. As previously discussed in the circular plate example, a concentrated load may be modelled quite easily. The reduction of each domain integral involving the load to a single evaluation combined with the analytic expressions available for linear geometries provide an excellent foundation for a very accurate numerical solution. The results for the center deflection $w(a/2, b/2)$ for various ratios of b/a are given in Table 9. Solutions were obtained using Overhauser elements coupled with a spacing scheme similar to the one used in the preceding example.

The next four examples incrementally increase the order of the loading function. Each domain term representing the loading function is transformed into an equivalent series of surface integrals. Higher order functions for the load correspondingly required more surface integrations to evaluate the effects. The proceeding analysis demonstrates the effectiveness of the integral transformations.

TABLE 8.

Center Deflection for a Simply Supported Rectangular Plate Bent by Thermal Loads.

a/b	α	α exact
0.5	0.02846	0.02847
1.0	0.07367	0.07367
1.5	0.10074	0.10077
2.0	0.11385	0.11387
5.0	0.12489	0.12490
10.0	0.12490	0.12500

Note: Deflection, $w = \alpha t(1+\nu)a^4/h$

TABLE 9.

Center Deflection for a Simply Supported Rectangular Plate Bent by a Concentrated Load, P, Located at its Center.

b/a	α	α exact
1.0	0.01160	0.01160
1.2	0.01355	0.01354
1.4	0.01486	0.01484
1.6	0.01570	0.01570
1.8	0.01621	0.01620
2.0	0.01652	0.01651

Note: Deflection, $w = \alpha Pa^2/D$.

Uniform Load. The behavior of a uniformly loaded square plate is presented in this example. For a linear element formulation, the domain integrals representing the effects of the transverse load are evaluated using the analytical expressions derived in Chapters III and IV. For quadratic and Overhauser analyses, the surface integral terms are also evaluated from analytical expressions developed previously. However, the transformed surface integral representing the load effects and the "corner" Overhauser element are calculated using numerical quadrature.

Absolute percentage error for the center deflection between the results obtained using each element type and the analytical solution given by Szilard (1974) is shown in Figure 13 for various boundary mesh sizes. The Overhauser element formulation was determined to be superior to the other two types of elements. However, it should be noted that a quadratic solution using 18 nodes had a lower absolute percent error than an equivalent Overhauser analysis. For meshes of 24 nodes and above, the solutions given by either of the two elements were indistinguishable. The absolute percent error for this solution over a linear geometry when compared at equivalent sized meshes is lower than the circular geometry presented earlier in Figure 11. This result is not unexpected considering the ability of each element type to exactly represent linear geometries. Furthermore, the analytic expressions developed in Chapter III for the surface integrations over linear geometries provide additional accuracy in the approximation.

The solution presented here will also serve to verify the accuracy of the deflection and its first derivative, also the moment function and its derivatives. The results using 24 Overhauser elements

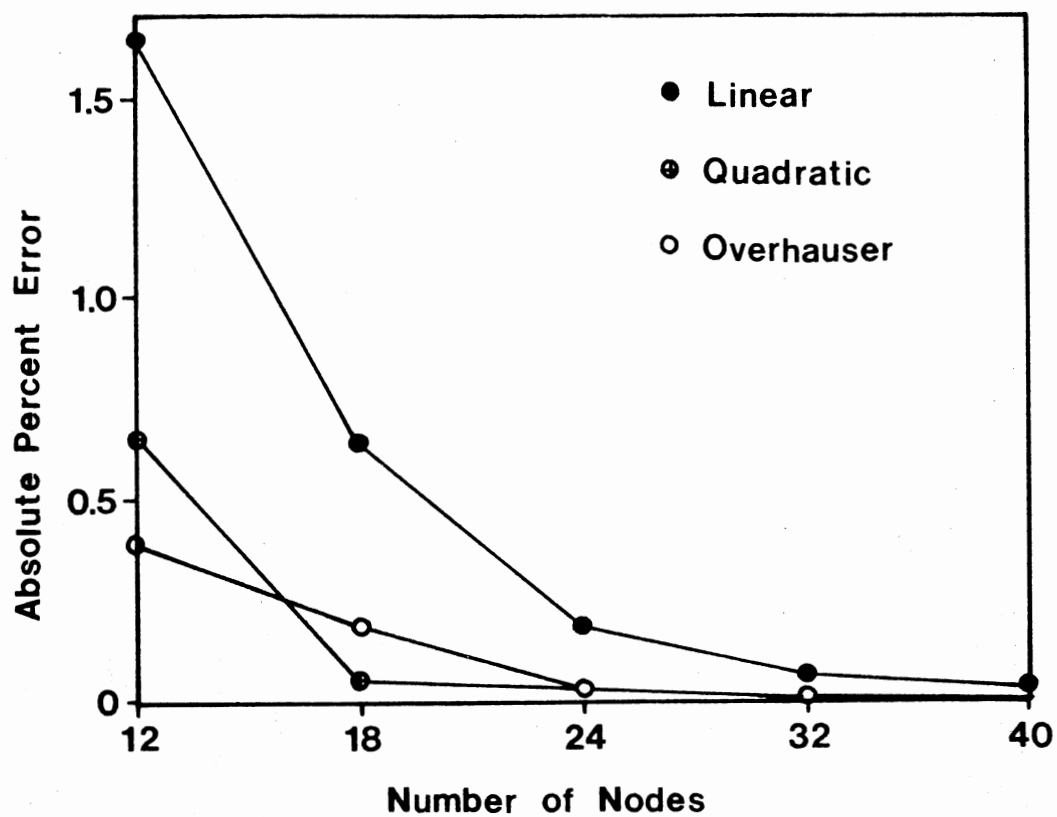


Figure 13. Absolute Percent Error For the Center Deflection of a Simply Supported Square Plate Under a Uniform Load.

are compared with analytical solutions given by Ugural (1981) and listed in Table 10. The accuracy of the derivatives will be important in evaluating more complex domain terms presented in later examples.

Hydrostatic Load. Consider a simply supported square plate loaded by a hydrostatic load of the form $q(x/a)$. The loading function is transformed using the harmonic form of the integral transformation described in Chapter IV. Results for the deflection, the moment function, and their derivatives obtained using 24 Overhauser elements are given in Table 11. The domain integrals for this type of loading are replaced by a set of two surface integrals each evaluated numerically.

Quadratic Load. A simply supported square plate under a quadratic load of the form $q(x/a)^2$ is presented as the third example illustrating the integral transformation technique. Each domain integral representing the loading function is transformed into a series of three surface integrals. Results for the deflection, the moment function, and their derivatives using an identical discretization as the preceding two examples are listed in Table 12. Absolute percent error between this solution and the analytic results given by Timoshenko and Woinowsky-Krieger (1959) is shown in Figure 14 for several mesh sizes. The scale of the error is smaller than corresponding circular plate examples of the same order loading function due to the intrinsic advantages of modelling linear geometries. For a small number of elements the accuracy of the Overhauser formulation suffers from the influence of the "corner" element. However, as more nodes are used to describe the boundary the "corner" effect is negligible and the Overhauser again demonstrates its superiority over the other two elements.

TABLE 10.

Deflection, Moment Function, and Their Derivatives at Various Points on a Uniformly Loaded Square Plate.

(x,y)	(a/2,b/4)	(a/2,b/2)	(3a/4,b/4)	(3a/4,b/2)
α	0.00295	0.00406	0.00213	0.00294
α exact	0.00294	0.00406	0.00213	0.00294
α_1	0.00000	0.00000	-0.00631	-0.00877
α_1 exact	0.00000	0.00000	-0.00630	-0.00876
α_2	0.00875	0.00001	0.00629	0.00000
α_2 exact	0.00876	0.00000	0.00630	0.00000
β	0.05734	0.07368	0.04531	0.05734
β exact	0.05733	0.07367	0.04529	0.05733
β_1	0.00000	0.00000	-0.10189	-0.13639
β_1 exact	0.00000	0.00000	-0.10196	-0.13637
β_2	0.13639	0.00000	0.10196	0.00000
β_2 exact	0.13637	0.00000	0.10196	0.00000

Note: Deflection $w = \alpha qa^4/D$, $\partial w/\partial x_i = \alpha_i qa^3/D$, Moment Function $M = \beta qa^2$, and $\partial M/\partial x_i = \beta_i qa$.

TABLE 11.

Deflection, Moment Function, and Their Derivatives at Various Points on a Square Plate Under a Hydrostatic Load.

(x,y)	(a/2,b/4)	(a/2,b/2)	(3a/4,b/4)	(3a/4,b/2)
α	0.00147	0.00203	0.00119	0.00163
α exact	0.00147	0.00203	0.00119	0.00163
α_1	0.00071	0.00093	-0.00309	-0.00431
α_1 exact	0.00071	0.00093	-0.00308	-0.00431
α_2	0.00437	0.00001	0.00345	0.00001
α_2 exact	0.00438	0.00000	0.00346	0.00000
β	0.02867	0.03684	0.02873	0.03579
β exact	0.02867	0.03684	0.02871	0.03578
β_1	0.03122	0.03735	-0.04103	-0.05782
β_1 exact	0.03104	0.03718	-0.04146	-0.05817
β_2	0.06819	0.00000	0.06091	0.00000
β_2 exact	0.06824	0.00000	0.06107	0.00000

Note: Deflection $w = \alpha qa^4/D$, $\partial w/\partial x_i = \alpha_i qa^3/D$, Moment Function $M = \beta qa^2$, and $\partial M/\partial x_i = \beta_i qa$.

TABLE 12.

Deflection, Moment Function, and Their Derivatives at Various Points on a Square Plate Under a Quadratic Load.

(x,y)	(a/2,b/4)	(a/2,b/2)	(3a/4,b/4)	(3a/4,b/2)
α	0.00867	0.01200	0.00761	0.01038
α exact	0.00867	0.01200	0.00761	0.01038
α_1	0.00706	0.00927	-0.01756	-0.02471
α_1 exact	0.00711	0.00933	-0.01750	-0.02463
α_2	0.02585	0.00006	0.02181	0.00006
α_2 exact	0.02591	0.00000	0.02191	0.00000
β	0.01642	0.02121	0.01994	0.02460
β exact	0.01642	0.02121	0.01992	0.02460
β_1	0.03122	0.03735	-0.01433	-0.02366
β_1 exact	0.03119	0.03733	-0.01439	-0.02364
β_2	0.03985	0.00000	0.04075	0.00000
β_2 exact	0.03984	0.00000	0.04082	0.00000

Note: Deflection $w = \alpha qa^4(10^{-1})/D$, $\partial w / \partial x_i = \alpha_i qa^3(10^{-1})/D$, Moment Function $M = \beta qa^2$, and $\partial M / \partial x_i = \beta_i qa$.

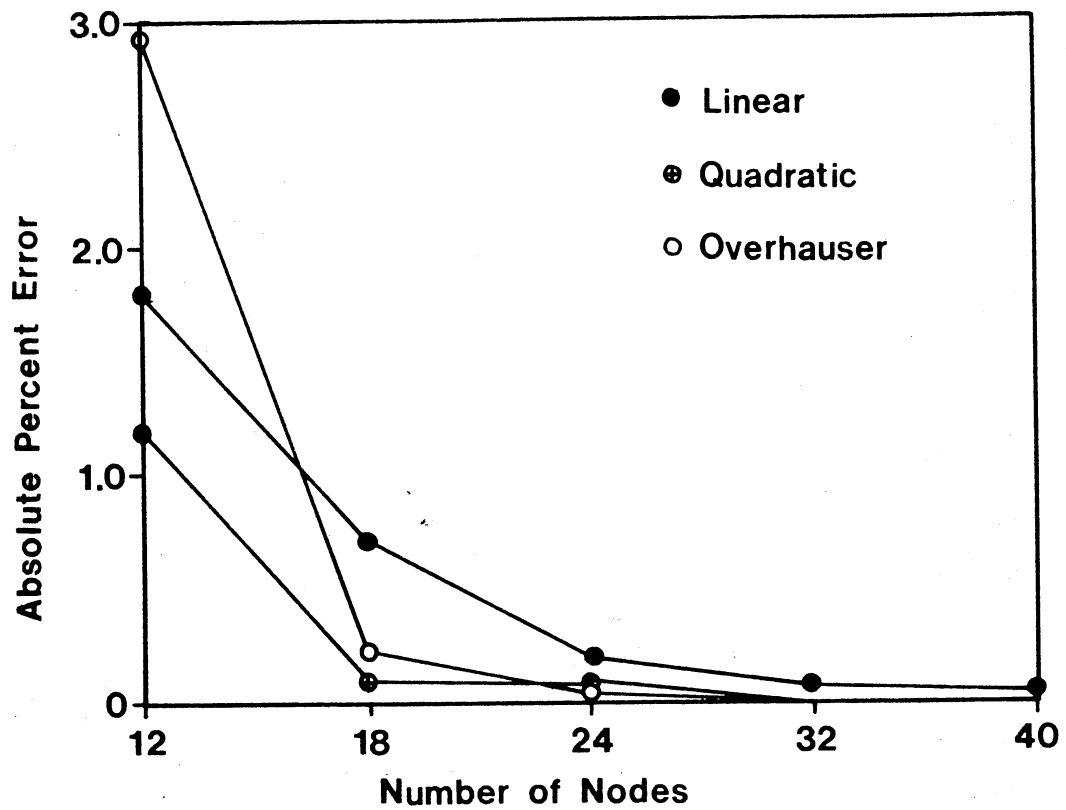


Figure 14. Absolute Percent Error For the Center Deflection of a Simply Supported Square Plate Under a Quadratic Load.

Cubic Loading. The final example illustrating the accuracy of the integral transformation technique will be that of a simply supported square plate with a transverse loading function of the form $q(x/a)^3$. Both of the domain integrals representing the effects of the cubic loading function are converted into a series of four surface integrations using the biharmonic form of the transformation. This example demonstrates a limiting case of the integral transformation technique for the formulation presented in this work. Any loading function of a higher order will be integrated using the domain "fanning" quadrature scheme. Results for the deflection, moment function, and their derivatives using a 24 element Overhauser formulation are given in Table 13.

The results of the four preceding analyses listed in Tables 10, 11, 12, and 13 are in excellent agreement with existing analytic solutions. Calculations for the derivatives of the deflection and the moment function are determined to be very accurate. This analysis is important in validating the ability of the formulation presented in Chapter III and IV in calculating the derivatives of the field variables ψ and ω . The next series of example problems involve complex "loading" functions for which accurate values of the field variables and their derivatives are required to evaluate the necessary domain integrals.

Elastic Foundations. Consider the behavior of a uniformly loaded simply supported square plate resting on an elastic foundation. The governing equation defined in Equation (211) has the unknown deflection as part of the "loading" function. An iterative solution using

TABLE 13.

Deflection, Moment Function, and Their Derivatives at Various Points on a Square Plate Under a Cubic Load.

(x,y)	(a/2,b/4)	(a/2,b/2)	(3a/4,b/4)	(3a/4,b/2)
α	0.00566	0.00784	0.00529	0.00719
α exact	0.00565	0.00784	0.00528	0.00719
α_1	0.00591	0.00777	-0.01091	-0.01552
α_1 exact	0.00597	0.00783	-0.01086	-0.01536
α_2	0.01691	0.00007	0.01503	0.00007
α_2 exact	0.01697	0.00000	0.01510	0.00000
β	0.01029	0.01340	0.01459	0.01790
β exact	0.01029	0.01340	0.01457	0.01789
β_1	0.02557	0.03072	-0.00142	-0.00703
β_1 exact	0.02555	0.03070	-0.00147	-0.00702
β_2	0.02568	0.00000	0.02914	0.00000
β_2 exact	0.02567	0.00000	0.02920	0.00000

Note: Deflection $w = \alpha qa^4(10^{-1})/D$, $\partial w / \partial x_i = \alpha_i qa^3(10^{-1})/D$, Moment Function $M = \beta qa^2$, and $\partial M / \partial x_i = \beta_i qa$.

both the domain "fanning" and solution map techniques was used to solve this problem. The center deflection for various values of the K , the dimensionless foundation modulus, are compared to analytical results given by Ugural (1981) in Table 14. The number of iterations necessary to meet specified convergence criteria varied from 4 to 15 for the values of K equal to 16 and 240 respectively. The analysis was extended to include a hydrostatic loading of the form $q(x/a)$ and a quadratic load given as $q(xy/a^2)$. Results obtained for these cases are compared to analytical expressions and presented in Tables 15 and 16. The increase in order of the loading functions had little or no effect on the number of iterations required for convergence.

In-Plane Forces. Consider the flexural behavior of a simply supported rectangular plate under the combined action of a uniform lateral load and uniform in-plane force. The governing equation for deflection is defined as

$$\nabla^4 w = \frac{1}{D} \left(q + N_x \frac{\partial^2 w}{\partial x^2} + N_y \frac{\partial^2 w}{\partial y^2} + 2N_{xy} \frac{\partial^2 w}{\partial x \partial y} \right) \quad (213)$$

where N_x and N_y are normal forces in the x and y directions respectively and N_{xy} is the shearing force. If N_x and N_y are equal to N_f and N_{xy} is zero, the governing equation reduces to

$$\nabla^4 w = \frac{q}{D} (1 + N \nabla^2 w) \quad (214)$$

where N is a parameter defined as N_f/q . The right hand side of the equation contains the term $\nabla^2 w$ and requires an iterative solution procedure when solved by the technique presented in Chapter II. Results for various values of N for several ratios of a/b are compared to an analytical solution given by Timoshenko and Woinowsky-Krieger, (1959),

TABLE 14.

Center Deflection for a Simply Supported Plate
Under a Uniform Load q , on a Winkler
Elastic Foundation

Dimensionless Foundation Modulus, K	α , Exact Results	α Using 24 Overhauser Elements
0	0.04062	0.04064
16	0.03898	0.03904
32	0.03747	0.03759
48	0.03607	0.03614
64	0.03476	0.03482
80	0.03354	0.03371
160	0.02853	0.02888
240	0.02479	0.02484

Note: Deflection $w = \alpha a^4 q (10^{-1}) / D$.

TABLE 15.

Center Deflection for a Simply Supported Plate
Under a Hydrostatic Load $q(x/a)$, on a
Winkler Elastic Foundation.

Dimensionless Foundation Modulus, K	α , Exact Results	α Using 24 Overhauser Elements
0	0.02031	0.02032
16	0.01949	0.01956
32	0.01873	0.01881
48	0.01803	0.01810
64	0.01738	0.01746
80	0.01677	0.01687
160	0.01426	0.01432
240	0.01240	0.01245

Note: Deflection $w = \alpha a^4 q (10^{-1}) / D$.

TABLE 16.

Center Deflection for a Simply Supported Plate Under a Quadratic Load $q(xy/a^2)$, on a Winkler Elastic Foundation. Deflection $w=\alpha a^4 q(10^{-2})/D$.

Dimensionless Foundation Modulus, K	α , Exact Results	α Using 24 Overhauser Elements
0	0.10156	0.10160
16	0.09746	0.09757
32	0.09367	0.09381
48	0.09016	0.09030
64	0.08690	0.08713
80	0.08382	0.08417
160	0.07132	0.07153
240	0.06198	0.06220

TABLE 17.

Center Deflection for a Simply Supported Rectangular Plate Under the Combined Action of Uniform Lateral and Uniform In-Plane Forces. Deflection $w=\alpha qa^4/D$.

a/b	0.5		1.0	
N	α	α exact	α	α exact
3	0.000508	0.000506	0.002501	0.002501
2	0.000541	0.000542	0.002895	0.002870
1	0.000586	0.000584	0.003376	0.003365
0	0.000633	0.000633	0.004062	0.004062
-1	0.000689	0.000691	0.005083	0.005115
-2	0.000757	0.000760	0.006785	0.006888
-3	0.000839	0.000844	0.010163	0.010499
a/b	1.5		2.0	
3	0.004197	0.004126	0.005024	0.005018
2	0.004879	0.004891	0.006140	0.006042
1	0.006036	0.005994	0.007584	0.007633
0	0.007724	0.007724	0.010129	0.010129
-1	0.010731	0.010814	0.014973	0.015165
-2	0.017377	0.017878	0.028447	0.029603
-3	0.044809	0.050074	-	-

and presented in Table 17. At large negative values of the parameter N , the numerical solution experienced difficulty in converging. In fact, the last case where $N = -3$ and the ratio $a/b = 2.0$ the iterative solution technique diverged. These results were not completely unexpected, since for values of $N_x = 4.46D$, $N_y = 0$, and no transverse loading, a square plate reaches its first buckling mode.

Variable Thickness. A simply supported square plate of variable thickness is considered. Assuming no discontinuous changes in the thickness, the governing equation for bending is given as

$$\begin{aligned}
 D\nabla^4 w + 2 \frac{\partial D}{\partial x} \frac{\partial}{\partial x} \nabla^2 w + 2 \frac{\partial D}{\partial y} \frac{\partial}{\partial y} \nabla^2 w - \nabla^2 D \nabla^2 w \\
 - (1-\nu) \left(\frac{\partial^2 D}{\partial x^2} \frac{\partial^2 w}{\partial y^2} - 2 \frac{\partial^2 D}{\partial x \partial y} \frac{\partial^2 w}{\partial x \partial y} \right. \\
 \left. + \frac{\partial^2 D}{\partial y^2} \frac{\partial^2 w}{\partial x^2} \right) = P(x,y)
 \end{aligned} \tag{215}$$

The flexural rigidity is no longer a constant. For this example it was considered a function of y only and given as $D = D_0 + D_1 y$. The relationship between D_0 and D_1 for this example was $D_1 = 7D_0/b$. Equation (215) reduces to the following form

$$\nabla^4 w = \frac{q_0}{D_0} \left(1 - \frac{2 \left(\frac{\partial \nabla^2 w}{\partial y} \right)}{q_0 \left(1 + 7 \frac{y}{b} \right)} \right) \tag{216}$$

The deflection and the moment function at points along $x = a/2$, shown in Figures 15 and 16 respectively, are compared to numerical results

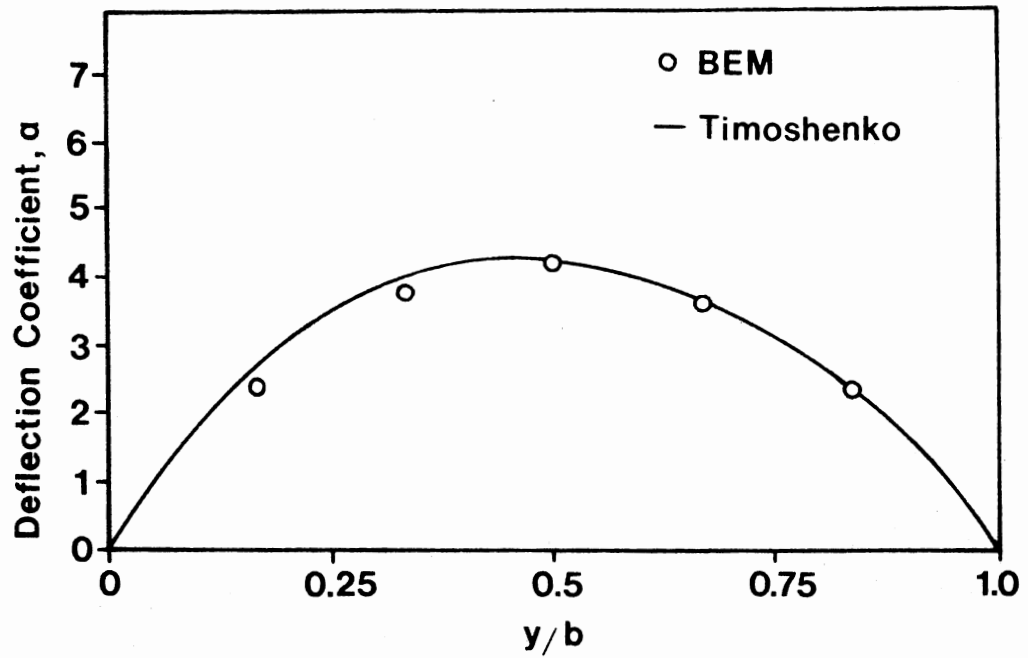


Figure 15. Deflection Along the Centerline, $x=a/2$, for a Simply Supported Plate of Variable Thickness. Deflection $w=\alpha q_0 a^4 (10^{-3})/D_0$.

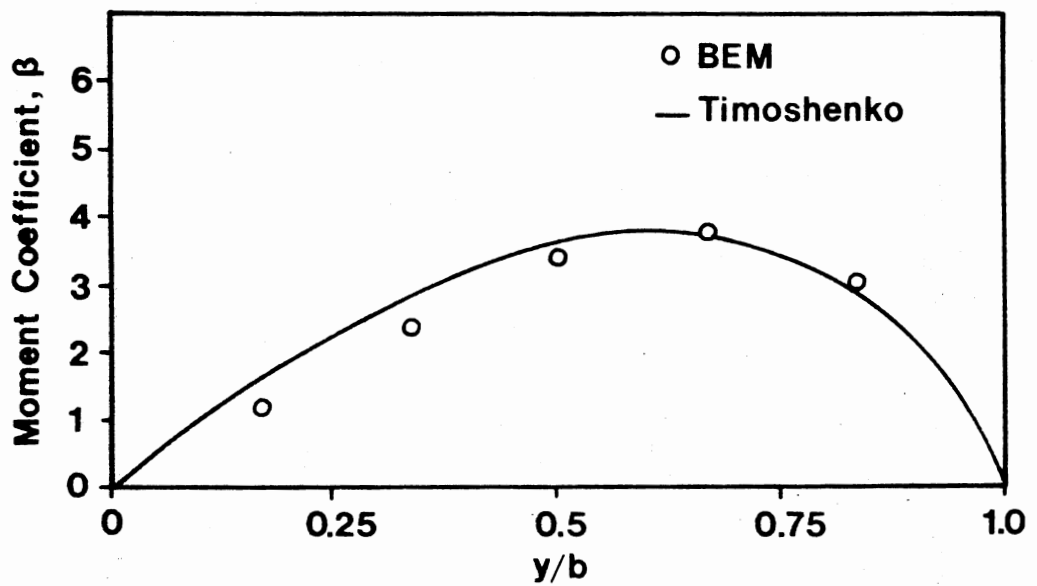


Figure 16. Moment Function Along the Centerline, $x=a/2$, for a Simply Supported Plate of Variable Thickness. Moment Function $M=\beta q_0 a^2 (10^{-2})$.

presented in Timoshenko and Woinowsky-Krieger (1959). The numerical solution given by Timoshenko is very difficult to obtain, whereas the boundary element formulation developed in this work provided accurate results in only four iterations.

Rectangular Plates with Various Edge Conditions

A series of examples combining simple and clamped edge conditions for rectangular plates will be presented in the following section. In each case the boundary was described by Overhauser elements using analytical expressions for the necessary surface integrations. At points where the boundary condition abruptly changes from a simple support to a clamped edge, "double" noding was used to accurately model its effects. Numerical quadrature was used to evaluate any integrations over the corner version of the Overhauser element and the transformed domain integrals involving the loading function. Results for each example are compared to analytical solutions given by Timoshenko and Woinowsky-Krieger (1959) and are presented in the tabular form.

One Clamped Edge. The flexural response of a rectangular plate with three edges simply supported and the edge at $y = 0$ clamped are presented here. Values for the deflection and moment function at the center of the plate for various ratios of b/a for both a uniform and a hydrostatic loading are given in Tables 18 and 19 respectively.

Two Opposite Edges Clamped. Consider a rectangular plate where two opposite edges are simply supported and the other two edges are clamped. Two loading cases were examined: a uniform load q , and a

TABLE 18.

Center Deflection and Moment Function for a
Simply Supported Rectangular Plate with One
Edge Clamped Bent by a Uniform Load q .

b/a	α	α exact	β	β exact
0.5	0.0049	0.0049	0.0648	0.0638
1.0	0.0028	0.0028	0.0562	0.0561
1.5	0.0064	0.0064	0.0899	0.0900
2.0	0.0093	0.0093	0.1084	0.1085

Note: Deflection, $w=\alpha qb^4/D$ for $b/a < 1$, $w=\alpha qa^4/D$
for $b/a > 1$, Moment Function $M=\beta qb^2$ for
 $b/a < 1$, and $M=\beta qa^2$ for $b/a > 1$.

TABLE 19.

Center Deflection and Moment Function for a
Simply Supported Rectangular Plate with
One Edge Clamped Bent by a Hydrostatic
Load $q(x/a)$.

b/a	α	α exact	β	β exact
0.5	0.0045	0.0045	0.0533	0.0538
1.0	0.0013	0.0013	0.0266	0.0269
1.5	0.0019	0.0019	0.0298	0.0300
2.0	0.0022	0.0023	0.0300	0.0308

Note: Deflection, $w=\alpha qb^4/D$ for $b/a < 1$, $w=\alpha qa^4/D$
for $b/a > 1$, Moment Function $M=\beta qb^2$ for
 $b/a < 1$, and $M=\beta qa^2$ for $b/a > 1$.

hydrostatic of the form $q(x/a)$. For both cases each corner is "double" noded to handle the discontinuous boundary conditions. A boundary element solution using an Overhauser formulation for both loading cases is compared to a corresponding analytical solution and listed in Tables 20 and 21.

All Edges Clamped. In this example the deflection of a rectangular plate with all edges clamped is presented. As with the preceding examples, two loading cases were examined: a uniform load q , and a hydrostatic load $q(x/a)$. The deflection and the moment function at the center of the plate is calculated for several ratios of b/a and compared to exact solutions in Tables 22 and 23.

All Edges Clamped on Elastic Foundation. A solution for the deflection and moment function of a uniformly loaded rectangular plate with clamped edges on a Winkler type elastic foundation is presented. The governing equation for the deflection, given by Equation (211), was solved using an iterative solution technique identical to that used for the preceding elastic foundation problems. Results for the center deflection and maximum value of the moment function at the edge for a dimensionless foundation modulus of $K = 200(kb^4/D)$ for various aspect ratios are shown in Figures 17 and 18. These results are in excellent agreement with numerical solutions of Costa and Brebbia (1985), and results using a Galerkin variational method given by Ng (1969).

TABLE 20.

Center Deflection and Moment Function for a Rectangular Plate with Two Opposite Edges Clamped and the Other Two Simply Supported Bent by a Uniform Load q .

b/a	α	α exact	β	β exact
0.5	0.00257	0.00260	0.04291	0.04321
1.0	0.00191	0.00192	0.04423	0.04431
1.5	0.00532	0.00531	0.08029	0.08038
2.0	0.00844	0.00844	0.10323	0.10331

Note: Deflection, $w=\alpha qb^4/D$ for $b/a < 1$, $w=\alpha qa^4/D$ for $b/a > 1$, Moment Function $M=\beta qb^2$ for $b/a < 1$, and $M=\beta qa^2$ for $b/a > 1$.

TABLE 21.

Center Deflection and Moment Function for a Rectangular Plate with Two Opposite Edges Clamped and the Other Two Simply Supported Bent by a Hydrostatic Load $q(x/a)$.

b/a	α	β	β exact
0.5	0.00128	0.02146	0.02154
1.0	0.00096	0.02212	0.02308
1.5	0.00266	0.04015	0.04077
2.0	0.00422	0.05164	0.05154

Note: Deflection, $w=\alpha qb^4/D$ for $b/a < 1$, $w=\alpha qa^4/D$ for $b/a > 1$, Moment Function $M=\beta qb^2$ for $b/a < 1$, and $M=\beta qa^2$ for $b/a > 1$.

TABLE 22.

Center Deflection and Moment Function for a
Rectangular Plate with All Edges Clamped
Bent by a Uniform Load q .

b/a	α	α exact	β	β exact
0.5	0.00016	0.00016	0.00109	0.00109
1.0	0.00127	0.00126	0.03526	0.03554
1.5	0.00220	0.00220	0.04388	0.04392
2.0	0.00253	0.00254	0.04382	0.04385

Note: Deflection, $w=\alpha qa^4/D$ and Moment Function $M=\beta qa^2$.

TABLE 23.

Center Deflection and Moment Function for a
Rectangular Plate with All Edges Clamped
Bent by a Hydrostatic Load q .

b/a	α	α exact	β	β exact
0.5	0.00008	0.00008	0.00548	0.00548
1.0	0.00063	0.00063	0.01763	0.01769
1.5	0.00110	0.00110	0.02194	0.02200
2.0	0.00127	0.00128	0.02191	0.02192

Note: Deflection, $w=\alpha qa^4/D$ and Moment Function $M=\beta qa^2$.

TABLE 24.

Center Deflection for a Simply Supported
Skewed Plate Bent by a Uniform Load q .

θ	m	α exact	α
0	2.00	0.01013	0.01013
30	2.02	0.01046	0.00989
45	2.00	0.00938	0.00895
60	2.00	0.00796	0.00653
75	2.00	0.00094	0.00097

Note: Deflection $w=\alpha qa^4/D$.

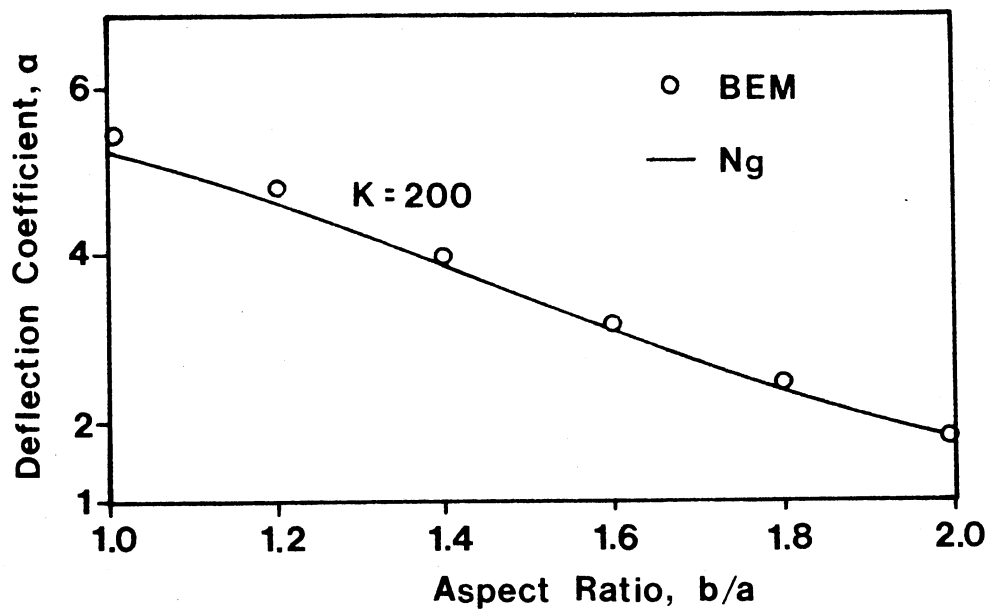


Figure 17. Center Deflection for a Clamped Rectangular Plate on an Elastic Foundation. Deflection $w = \alpha qb^4(10^{-3})/D$.

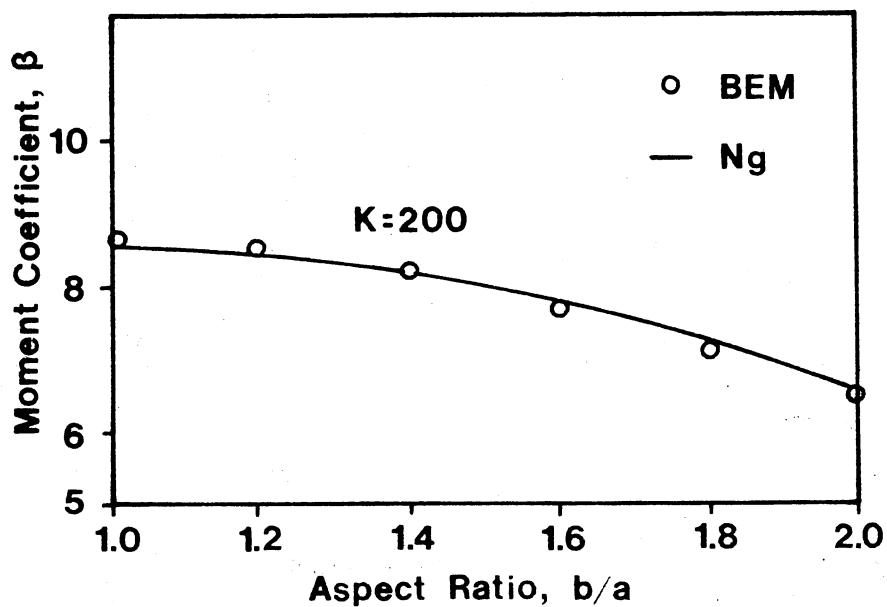


Figure 18. Maximum Edge Moment for a Clamped Rectangular Plate on an Elastic Foundation. Edge Moment $M = \beta qb^2(10^{-2})$.

Plates of Various Shapes

In this example several polygonal shaped plates with both simply and clamped edge supports for various loading functions are presented. In each case the boundary element formulation with the Overhauser element developed in Chapters III and IV of this work was used to obtain solutions for the deflection and the moment function. Results are compared to analytical or published numerical solutions to verify their accuracy.

Simply Supported Triangular Plates. Consider a simply supported equilateral triangular plate under two loading conditions: a uniformly distributed moment M_n applied along the boundary and a uniform load q . The deflection along a line, of length a , that bisects one side and passes through the opposite vertex for each loading condition is shown in Figures 19 and 20 and compared to an analytical solution given by Timoshenko and Woinowsky-Krieger (1959).

Triangular Plate with Two or Three Edges Clamped. In this example the deflection of an equilateral triangular plate along the centerline defined in the previous problem for both a uniform load q and hydrostatic load $q(x/a)$ are presented. In Figure 21, the deflection for a plate where the two sides are clamped while the remaining side is simply supported is shown for both loading functions. Results for the deflection of an equilateral triangular plate where all edges are clamped is presented in Figure 22. Corners where the edge conditions changed from clamped to simple supports were modelled effectively by using the "double" noding technique describe earlier.

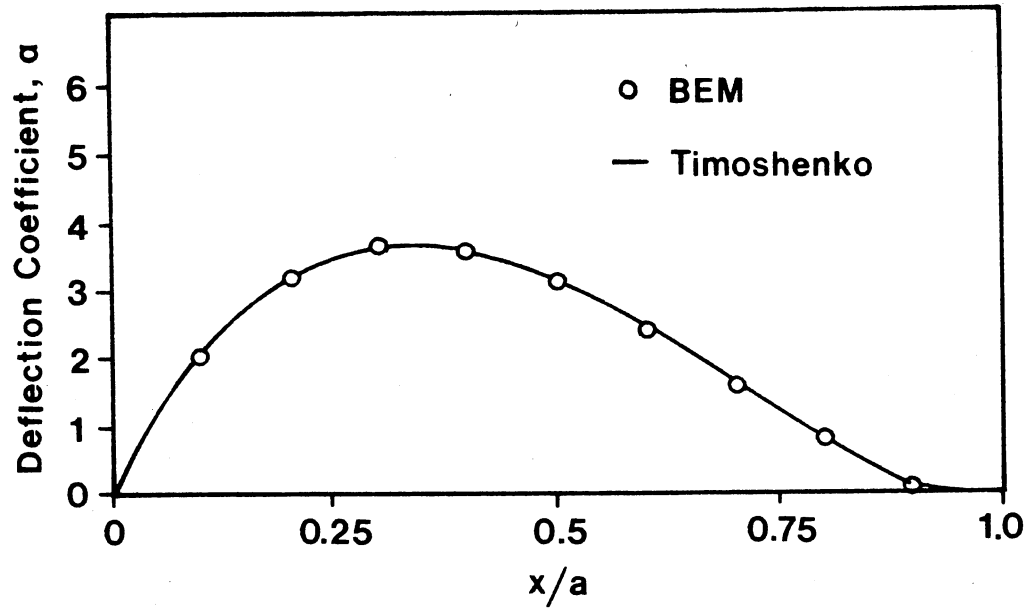


Figure 19. Deflection Along the Centerline of a Simply Supported Triangular Plate Bent by Uniform Edge Moments. Deflection $w = \alpha M_{\eta} a^4 (10^{-2}) / D$.

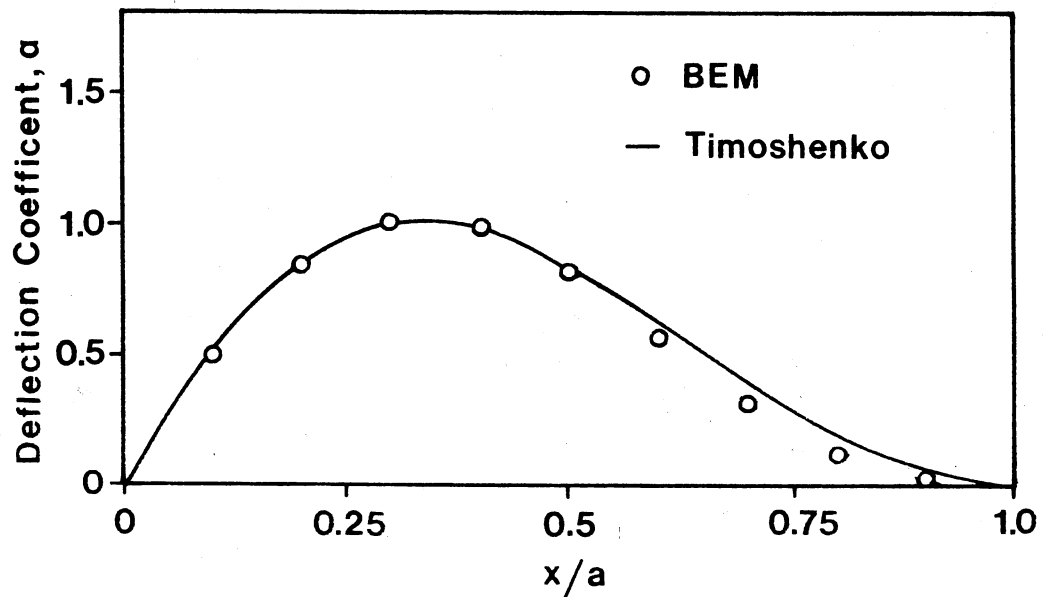


Figure 20. Deflection Along the Centerline of a Simply Supported Triangular Plate Bent by a Uniform Load. Deflection $w = \alpha q a^4 (10^{-3}) / D$.

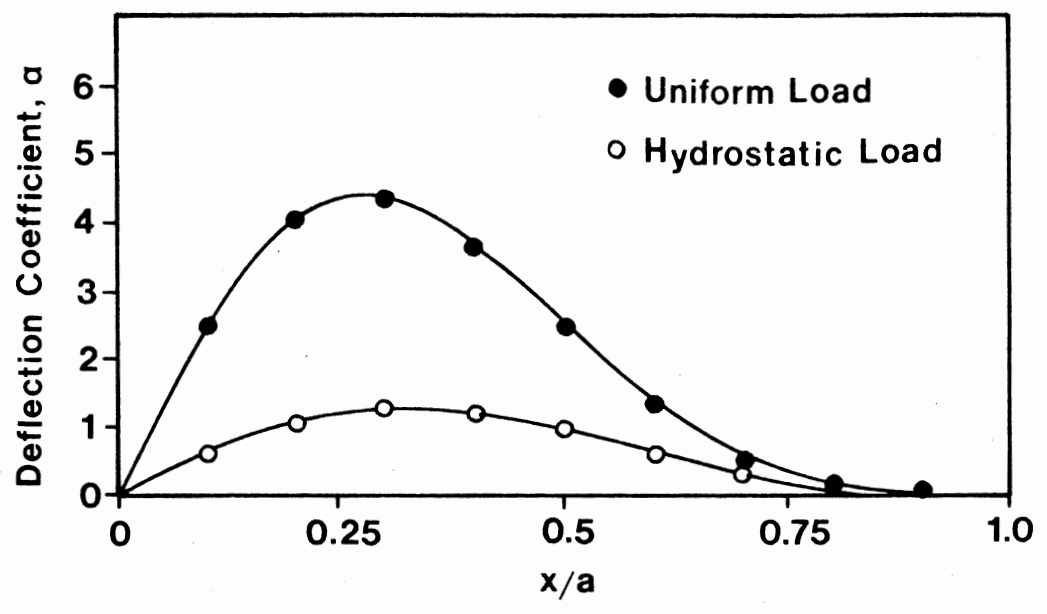


Figure 21. Deflection Along the Centerline of a Triangular Plate with Two Sides Clamped. Deflection $w = \alpha q a^4 (10^{-4}) / D$.

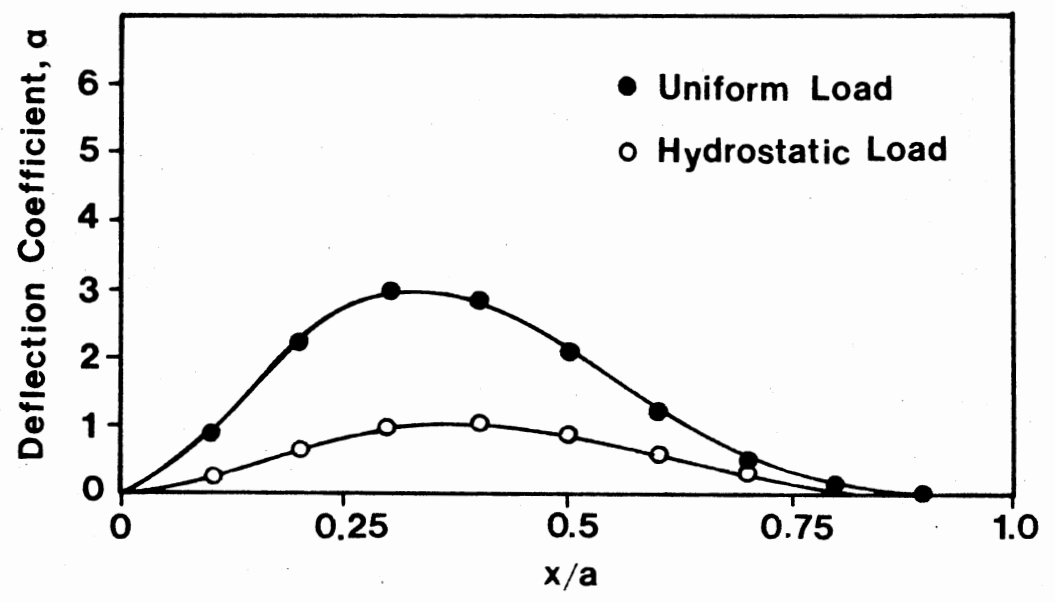


Figure 22. Deflection Along the Centerline of a Triangular Plate with All Edges Clamped. Deflection $w = \alpha q a^4 (10^{-4}) / D$.

Skewed Plates. In this example the deflection at the center of a simply supported oblique parallelogram shaped plate, shown in Figure 23, is presented. This type of plate has applications as floor slabs in skewed bridges. Results for various angles θ are compared with numerical solutions given by Timoshenko and Woinowsky-Krieger (1959) and listed in Table 24.

Rhombic Plates. This case will examine the flexural behavior of a simply supported rhombic plate shown in Figure 24(a). Results for the deflection and bending moment at the center of the plate for various values of the angle r are listed in Table 25. It can be seen that the results using 12 Overhauser elements are in excellent agreement with those of Maiti and Chakrabarty (1974) using 32 constant elements or Leissa (1965) obtained by a variational approach.

Hexagonal Plates. A uniformly loaded simply supported hexagonal plate, shown in Figure 24(b), is considered in this example. Results for several mesh sizes are compared to a published numerical solution given by Maiti and Chakrabarty (1974) and a solution obtained by Leissa (1965) using a variational method. A comparison of the values of the deflection and the moment function at the center of the hexagonal plate, presented in Table 26, indicates the formulation developed in this work is in excellent agreement with existing solutions.

Corner Plate. Corner plates are used to analyze polygonal shaped plates with a polygonal cut-out. Triangular and many polygonal shaped plates are defined by the angle between linear segments as shown in Figure 25. By invoking symmetry, only the corner section of each limb

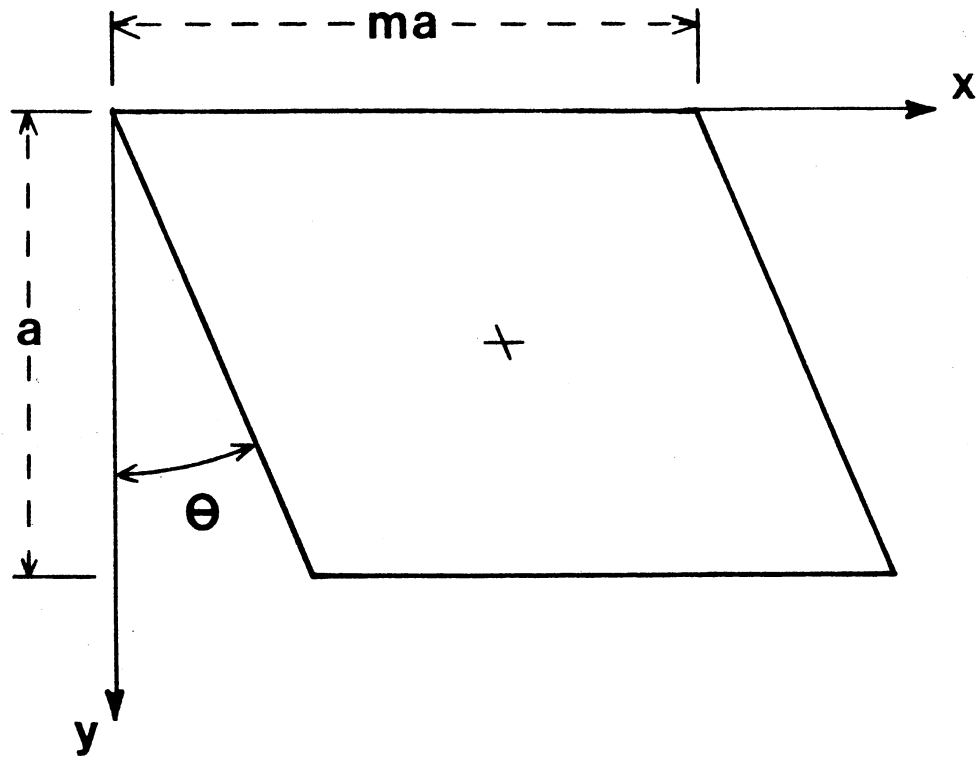


Figure 23. Skewed Plate Geometry.

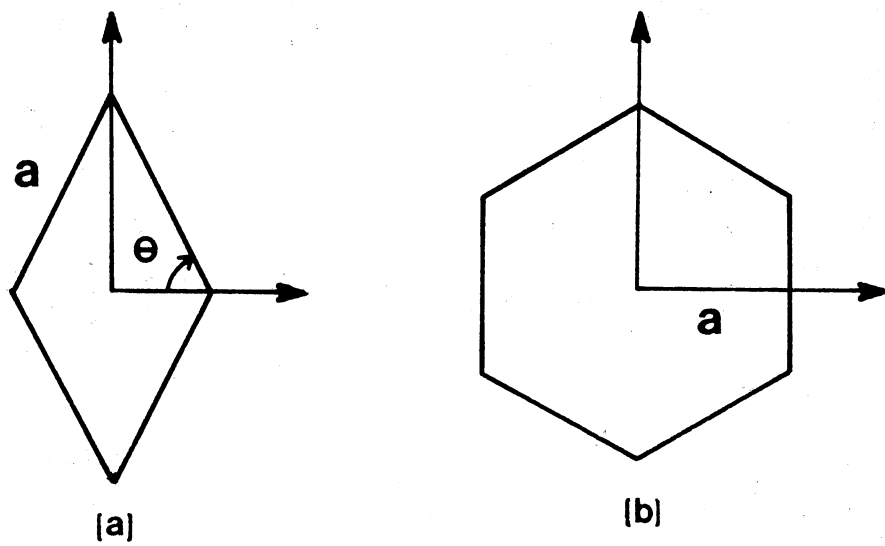


Figure 24. Rhombic and Hexagonal Plate Geometries.

TABLE 25.

Center Deflection and Moment Function for a Simply Supported Rhombic Plate Under a Uniform Load q .

	Angle θ	Using 24	Using 32	Variational
		Overhasuer Elements	Constant Elements	Approach
α	45	0.00408	0.00408	-
	60	0.00256	0.00256	0.00256
	75	0.00041	0.00038	0.00041
β	45	0.07387	0.07385	-
	60	0.05838	0.05838	0.05831
	75	0.02315	0.02292	0.02300

Note: Deflection $w=\alpha qa^4/D$ and Moment Function $M=\beta qa^2$.

TABLE 26.

Center Deflection and Moment Function for a Simply Supported Hexagonal Plate Under a Uniform Load q .

Number of Nodes	Results using Overhauser Formulation		Results from Maiti and Chakrabarty (1974)	
	α	β	α	β
12	0.0573	0.27256	0.0550	0.27077
24	0.0548	0.27019	0.0547	0.27023
48	0.0546	0.26989	-	-
Results of Leissa (1965)	0.0548	0.27077	0.0548	0.27077

Note: Deflection $w=\alpha qa^4/D$ and Moment Function $M=\beta qa^2$.

is modelled, see Figure 26. At lines of symmetry the normal derivatives of both the deflection, $\partial w/\partial n$, and the Laplacian of the deflection, $\partial(\nabla^2 w)/\partial n$, are set equal to zero. The rest of the boundary is simply supported. Values of the deflection and the moment function along the diagonal, for different angles, are shown in Figures 27 and 28. The results compare with good accuracy to those presented by Segedin and Brickell (1968).

Incompressible Viscous Fluid Flow at Low Reynolds Numbers

The governing equation for steady, two-dimensional viscous flow of an incompressible fluid is written in terms of the stream function ψ and the vorticity ω as:

$$\nabla^4 \psi = R \left(\frac{\partial \psi}{\partial y} \frac{\partial \omega}{\partial x} - \frac{\partial \psi}{\partial x} \frac{\partial \omega}{\partial y} \right) \quad (217)$$

where R is the Reynolds number of the motion (Mills, 1977). This equation may be thought of as a nonhomogeneous biharmonic equation wherein the nonhomogeneous function (the right-hand side of Equation (217) is itself a nonlinear function of the field variables. Equation (217) may be transformed to an equivalent set of coupled Poisson-type equations by introducing the relationship between the stream function and the vorticity. For non-zero values of the Reynolds number Equation (217) is solved using the iterative solution technique described in Chapter IV.

Four examples are presented in this section for the purpose of demonstrating the versatility of this formulation. The first case is a moving-wall problem in which the domain is completely enclosed. The second example is a study of the flow field of inflow-outflow in a

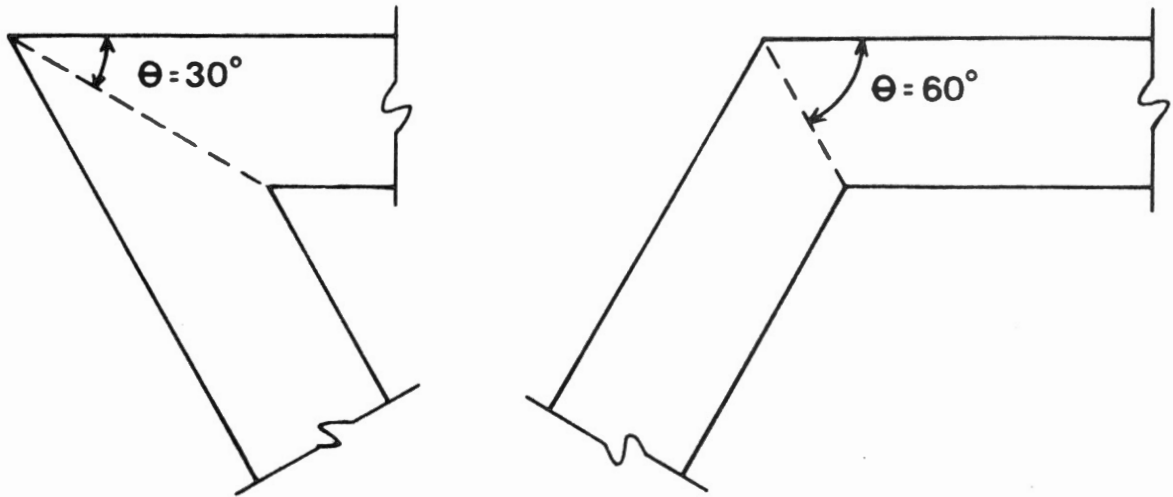


Figure 25. Corner Plates of Different Angles.

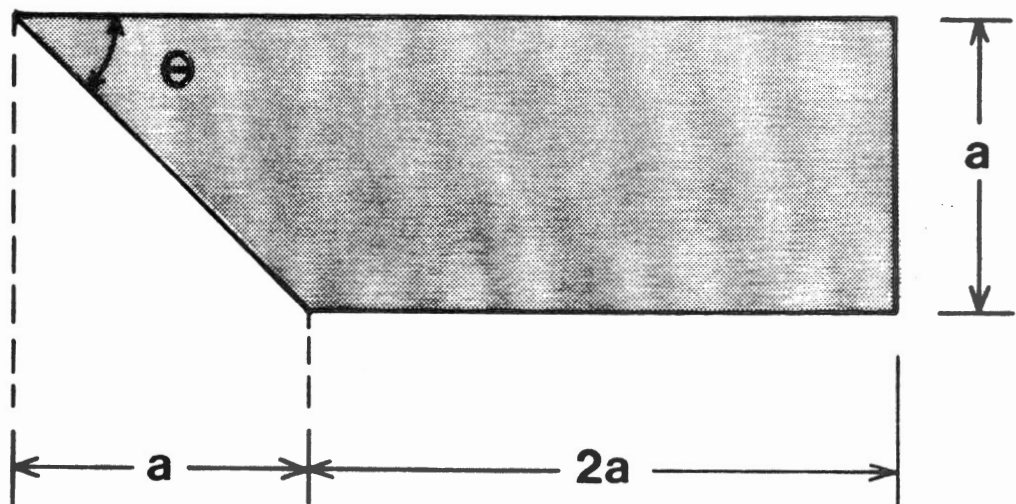


Figure 26. Corner Plate Problem Domain Incorporating Symmetry.

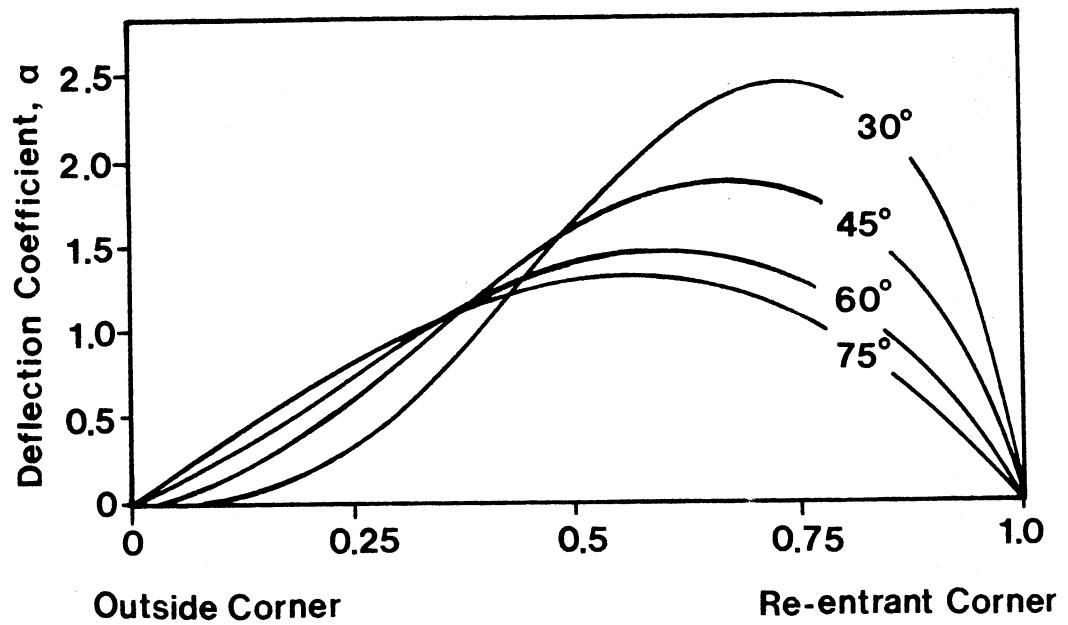


Figure 27. Deflection Across the Diagonal for Corner Plates of Different Angles. Deflection $w = \alpha b^4 (10^{-2}) / D$.

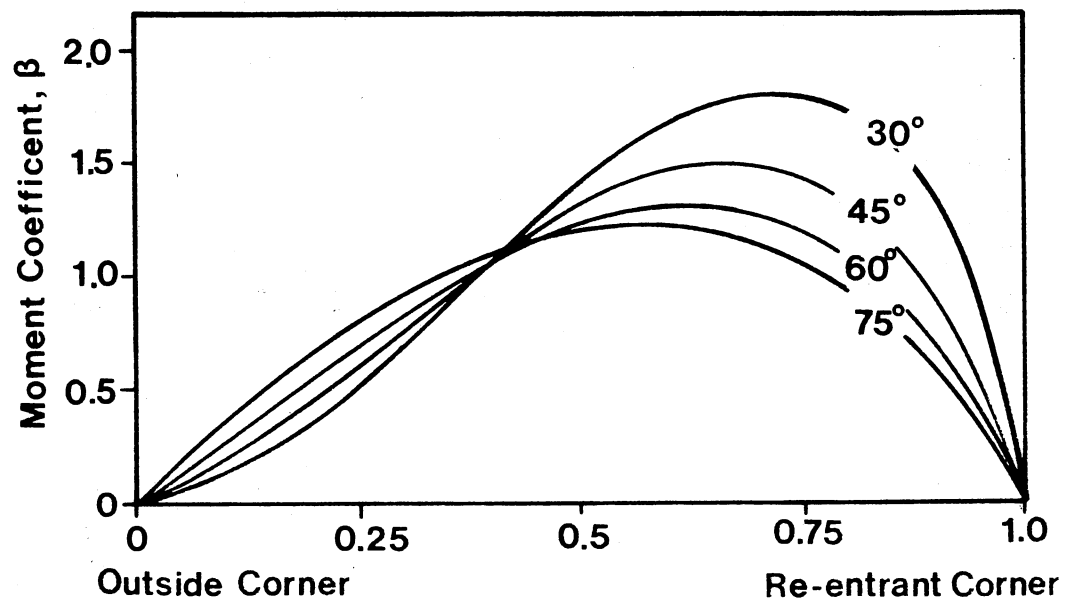


Figure 28. Moment Function Across the Diagonal for Corner Plates of Different Angles. Moment Function $M = \beta q b^2 (10^{-1}) / D$.

cylinder. These two problems were originally analyzed by Mills (1977). The third case will examine fluid flow through an array of impermeable cylindrical fibers. This same example was presented by Hildyard, et al (1985) for a zero value of the Reynolds number. The final example is a study of creeping flow of an incompressible viscous fluid in bearing geometries and is compared to work of Ingham and Kelmanson (1984).

Moving-Wall Problem

Shown in Figure 29 are the geometry and boundary conditions for a circular moving-wall problem. The motion is completely enclosed and is generated by the rotation of part or all the boundary of the cylinder. This type of problem is important in the study of recirculating motion in cavities. The radius of the cylinder r , the constant speed of the moving surface U , and the kinematic viscosity ν , will be used to define the Reynolds number as $R_1 = Ur/\nu$. Plots of the streamlines generated by the rotation of the upper half of the cylinder are shown in Figures 30, 31, and 32 for various Reynolds numbers. The flow at $R_1 = 0$ calculated from a closed form solution given in Mills (1977) and the numerical solution for the same flow conditions, shown in Figure 30, show excellent agreement. Streamline plots for other values of Reynolds number compared favorably with similar solutions presented by Mills (1977).

Inflow-Outflow Problem

The inflow-outflow problem considered in this example is defined as shown in Figure 33. The motion is generated by a viscous fluid

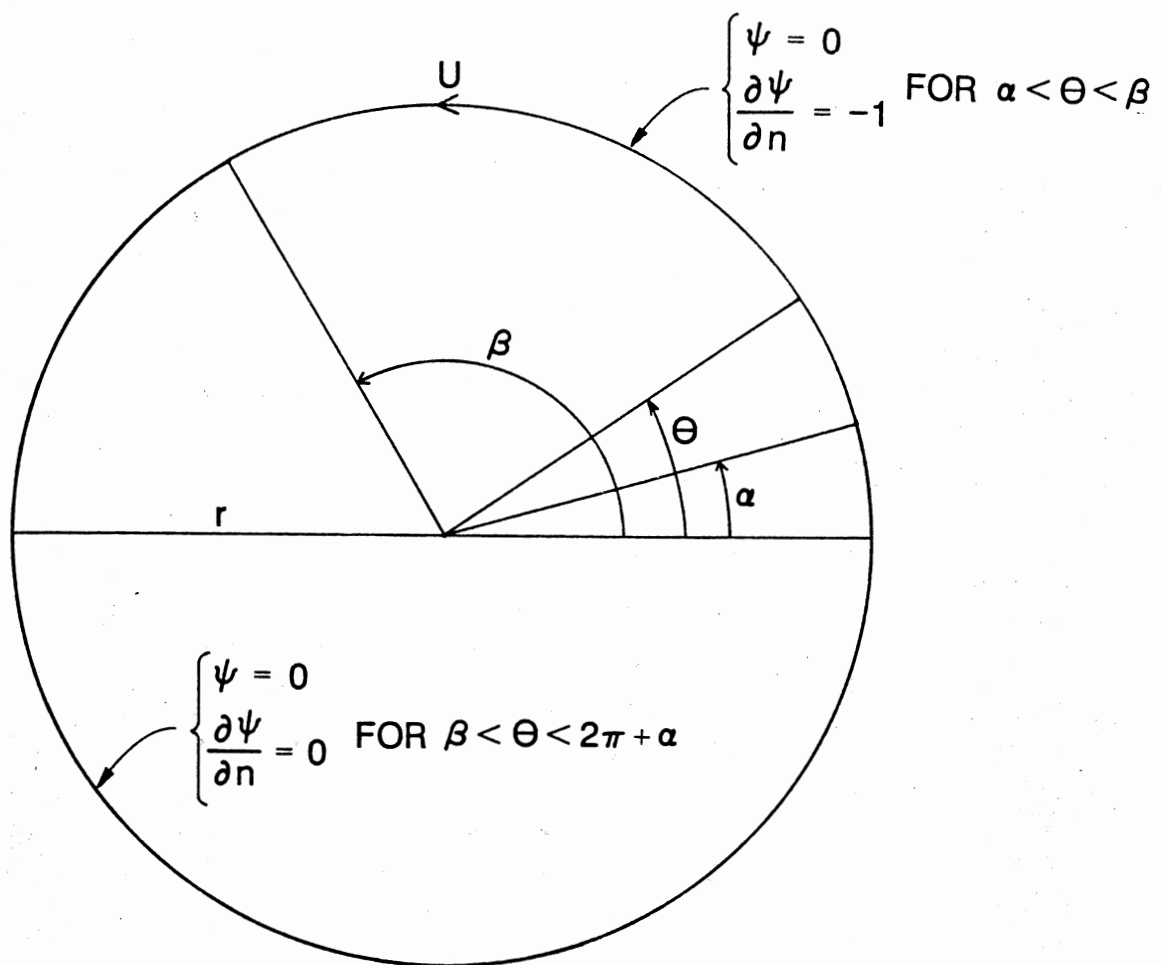


Figure 29. Moving-Wall Problem Definition,
 $r=2.0$, $\alpha=0.0$, and $\beta=\pi$.

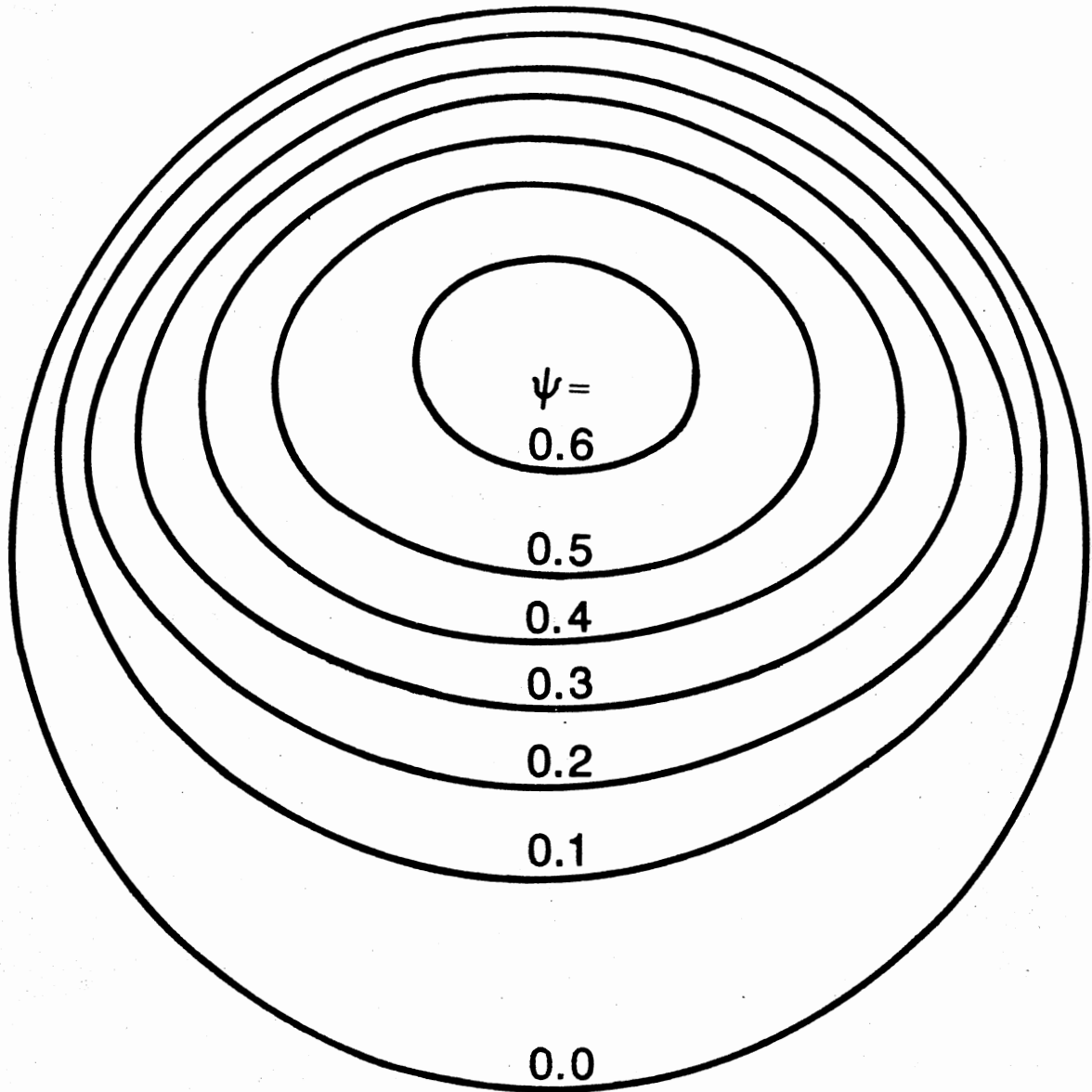


Figure 30. Streamline Plot for the Moving-Wall Problem, $R_1=0.0$.

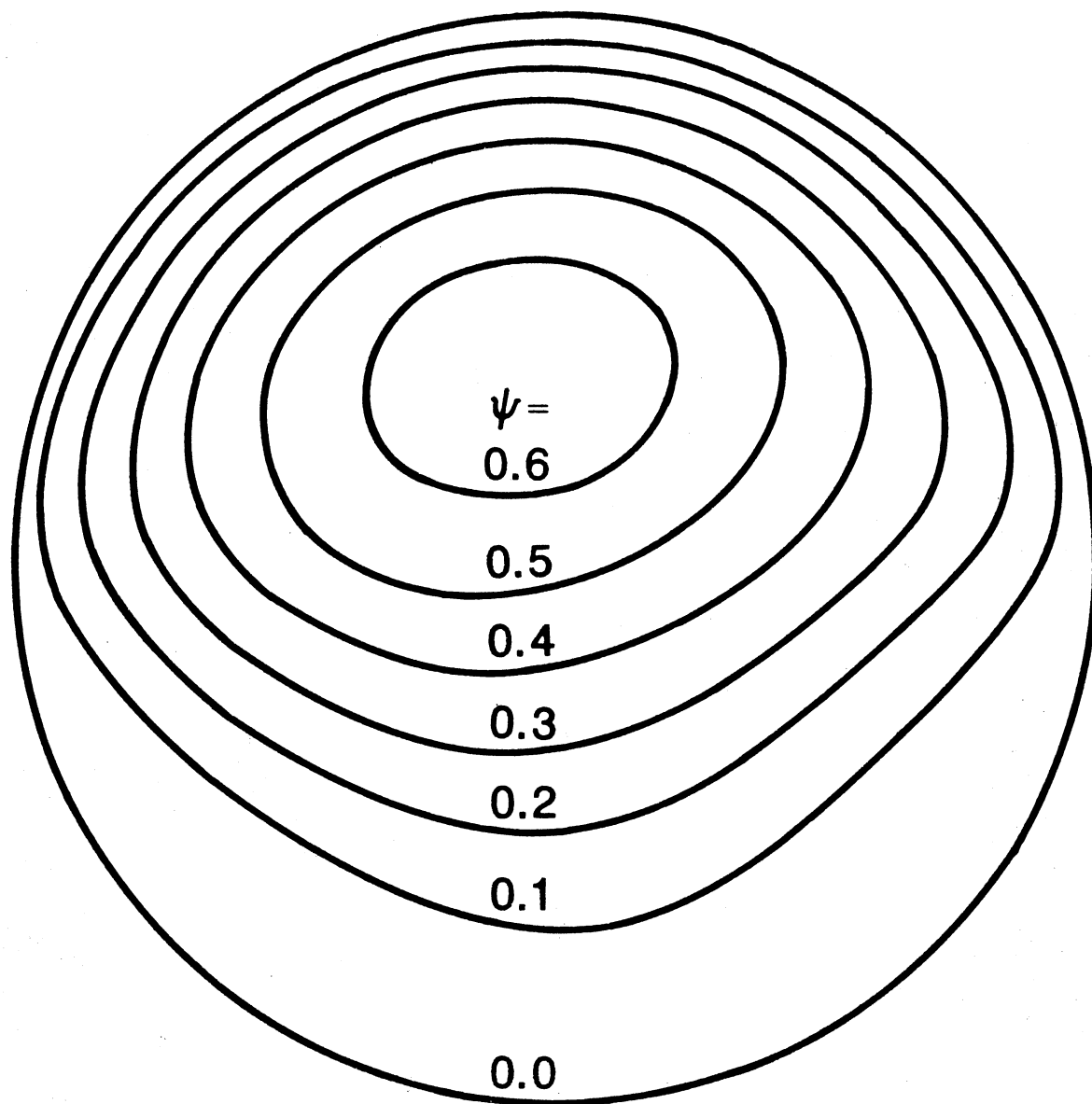


Figure 31. Streamline Plot for the Moving-Wall Problem, $R_1=10.0$.

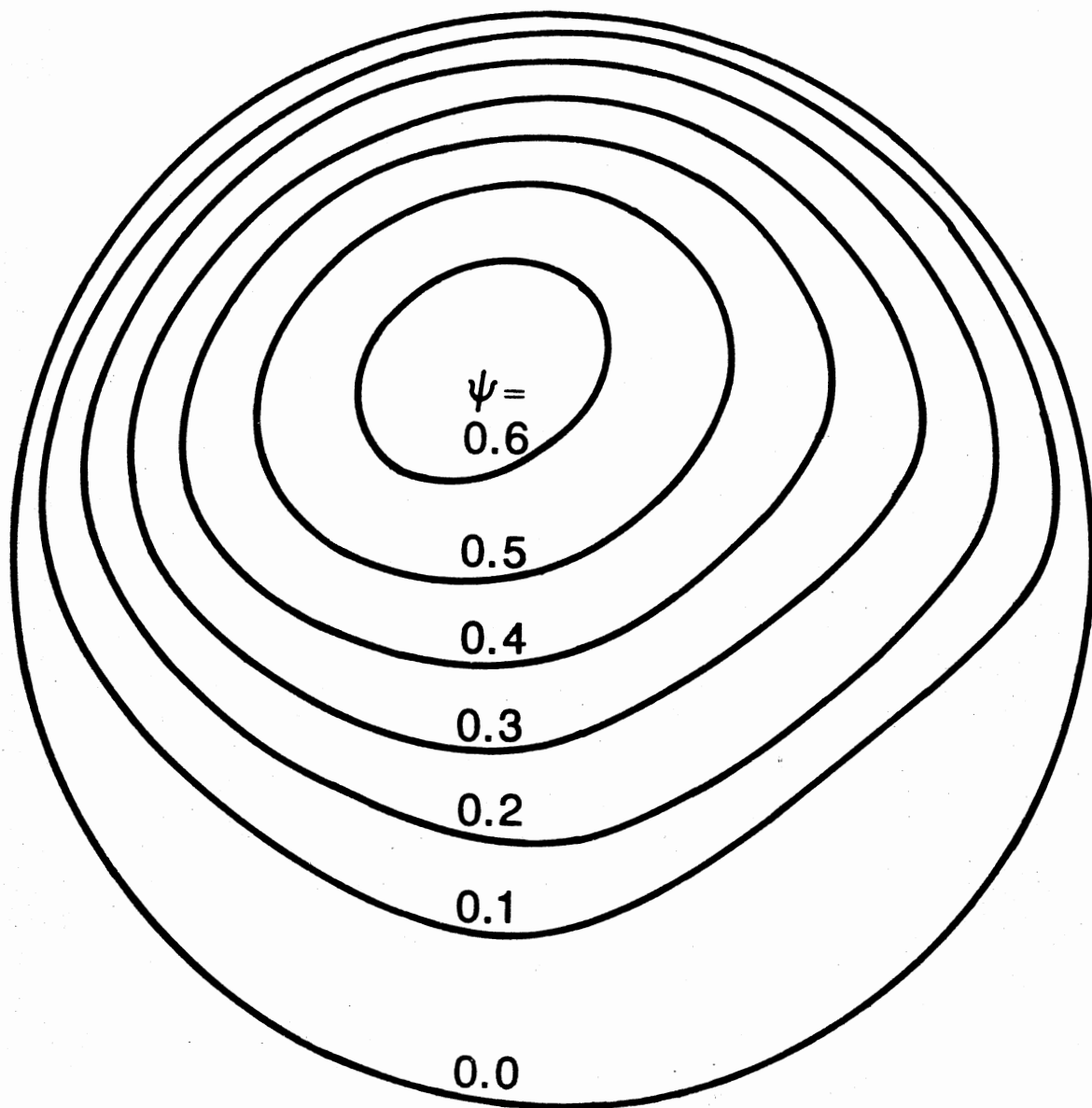


Figure 32. Streamline Plot for the Moving-Wall Problem, $R_1=20.0$.

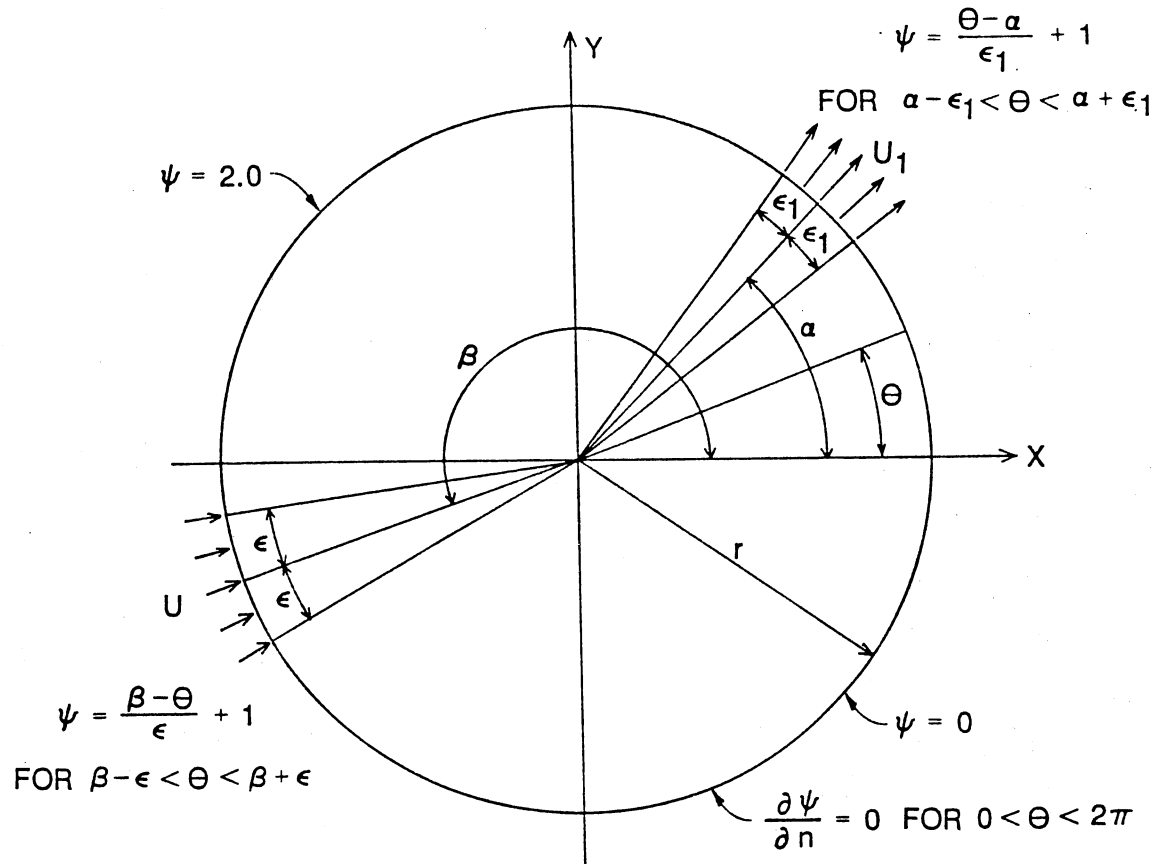


Figure 33. Inflow-Outlet Problem Definition,
 $r=2.0$, $\alpha=\pi/8$, $\beta=\pi$, and $\epsilon=\epsilon_1=\pi/32$.

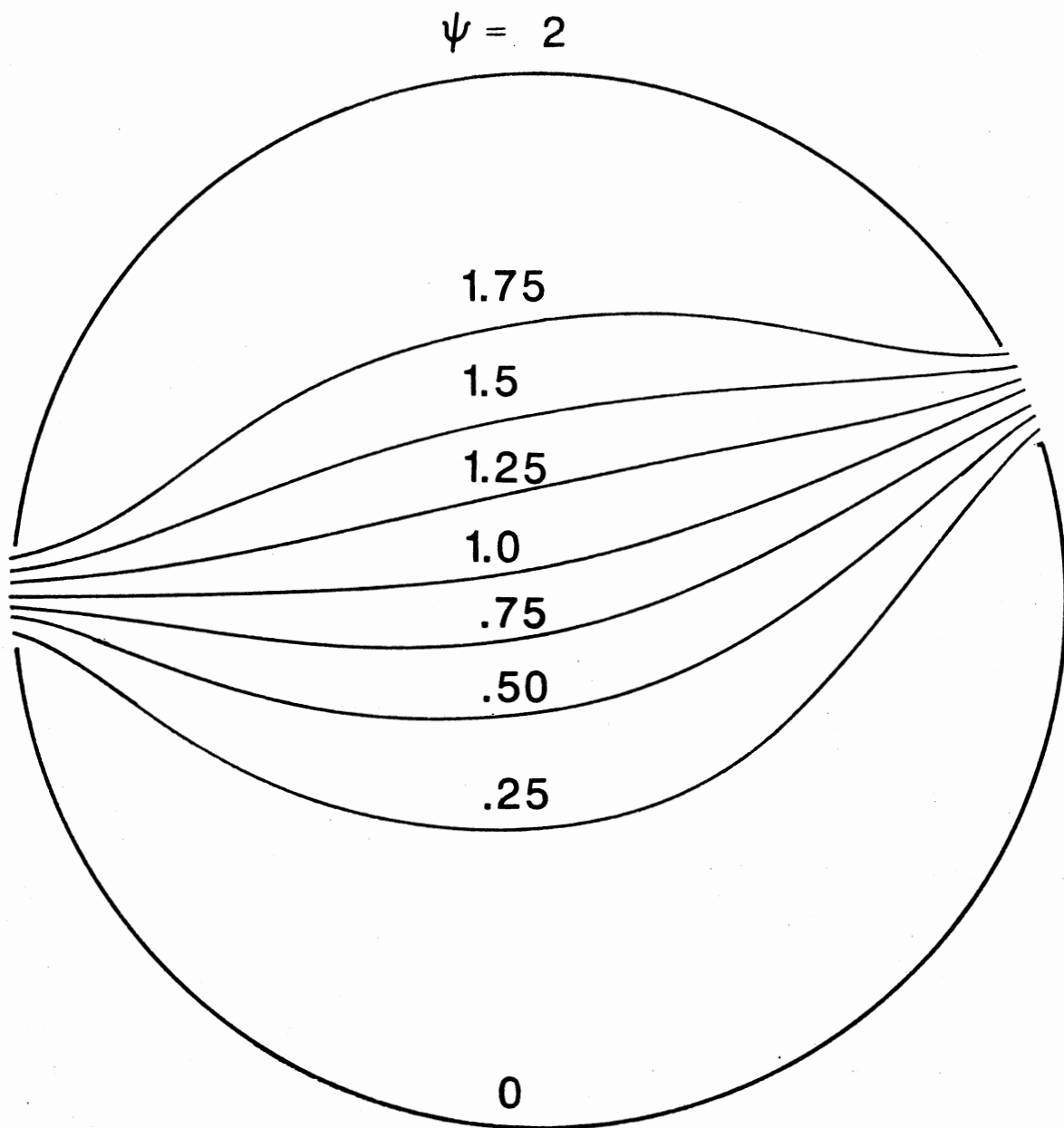


Figure 34. Streamlines Plot for the Inflow-Outflow Problem, $R=0.0$.

entering and leaving the cylinder normal to the walls. The Reynolds number is defined in terms of the radius r , the entrance velocity U , the angle ϵ , and the kinematic viscosity ν , and given as $R = Ur\epsilon/\nu$. In Figure 34, the solution of the flow field for a Reynolds number equal to zero is presented. The accuracy of this result, when checked by computing the exact infinite series solution given by Mills (1977), is excellent. As the Reynolds number increases, regions of recirculation develop as the flow becomes more unsteady. At the entrance and exit, the rate of change of the vorticity becomes large and the iterative solution technique will not converge to an appropriate solution.

Flow Through a Fibrous Filter

Flow through an infinite rectangular array of cylinders is considered in this example. Symmetry reduces the problem geometry and boundary conditions to those shown in Figure 35. The solution for a Reynolds number of zero shows good agreement when compared to the results presented by Hildyard et al (1985). Shown in Figures 36, 37, and 38 are plots of the streamlines for flows characterized by Reynolds numbers of 0.0, 10.0 and 20.0 respectively.

Flow in Bearings of Arbitrary Geometries

In this example slow incompressible viscous flow in bearing geometries at zero Reynolds number are presented. The problem is defined by the region between an inner cylinder rotating at a constant angular velocity and an outer surface of arbitrary shape. The value of the stream function at the inner cylinder, ψ_1 , is an unknown constant. An additional equation for ψ_1 may be obtained from the periodic nature of

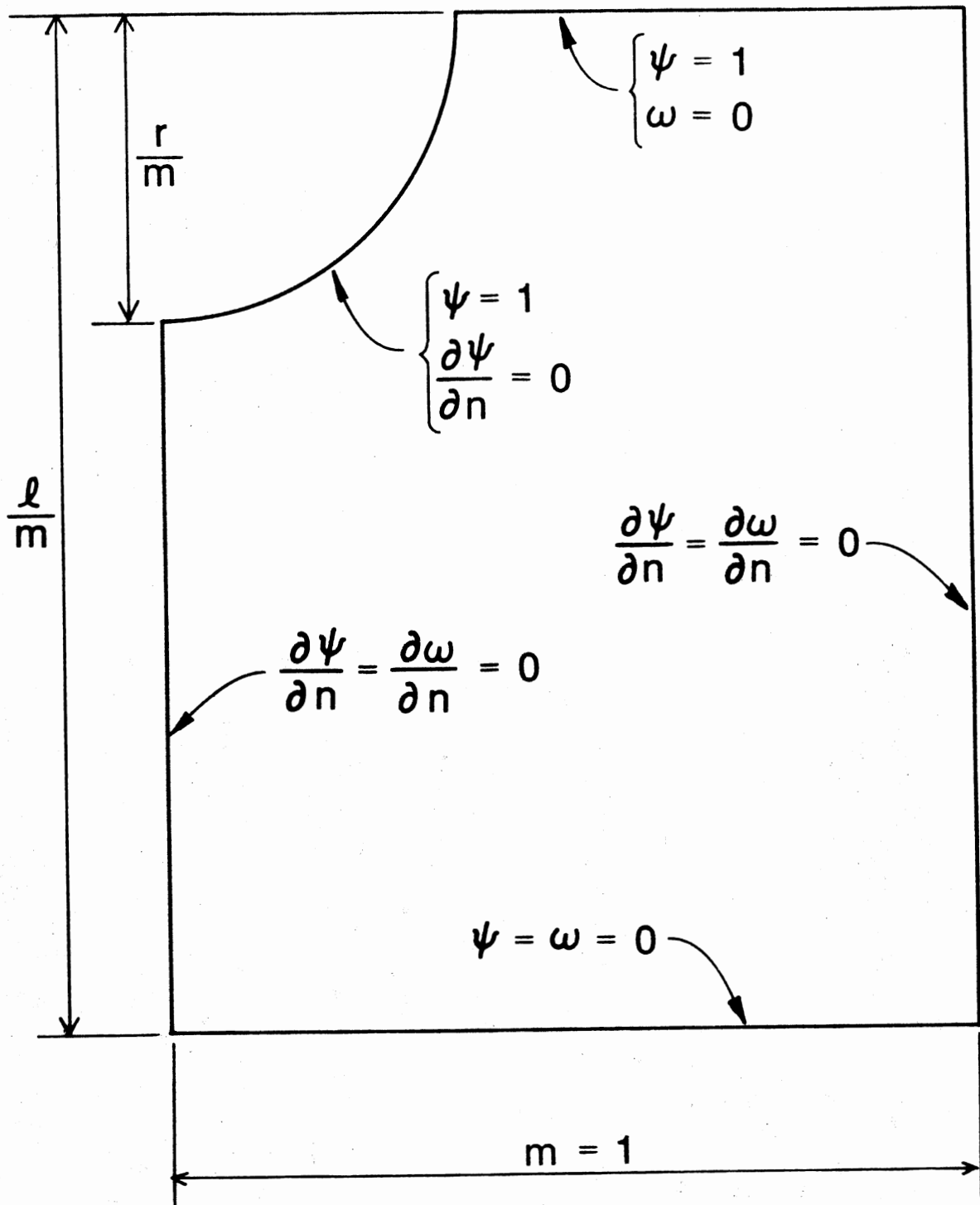


Figure 35. Problem Definition for Flow Through an Infinite Rectangular Array of Cylinders.

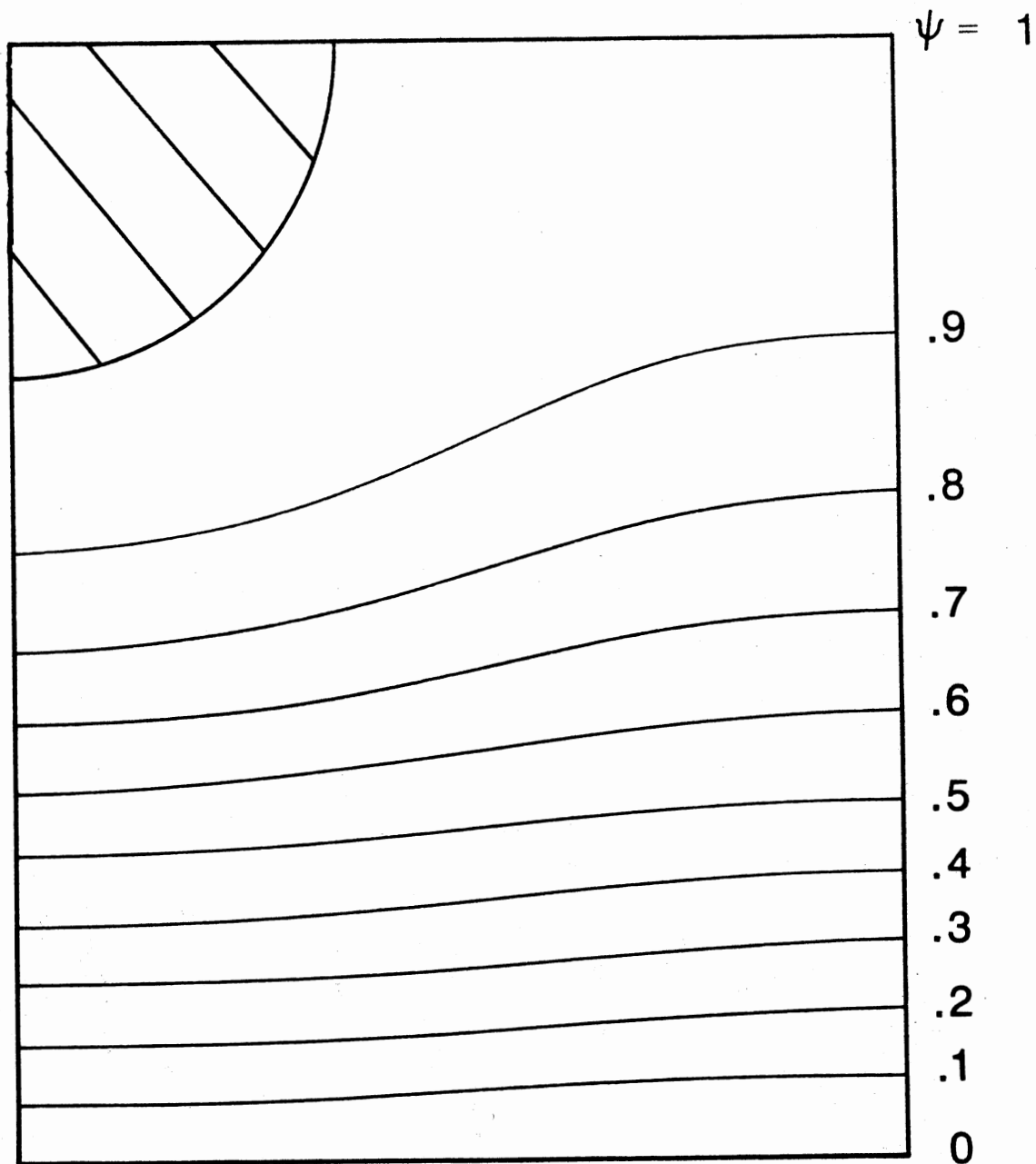


Figure 36. Streamline Plot for Flow Through an Infinite Rectangular Array of Cylinders, $R=0.0$.

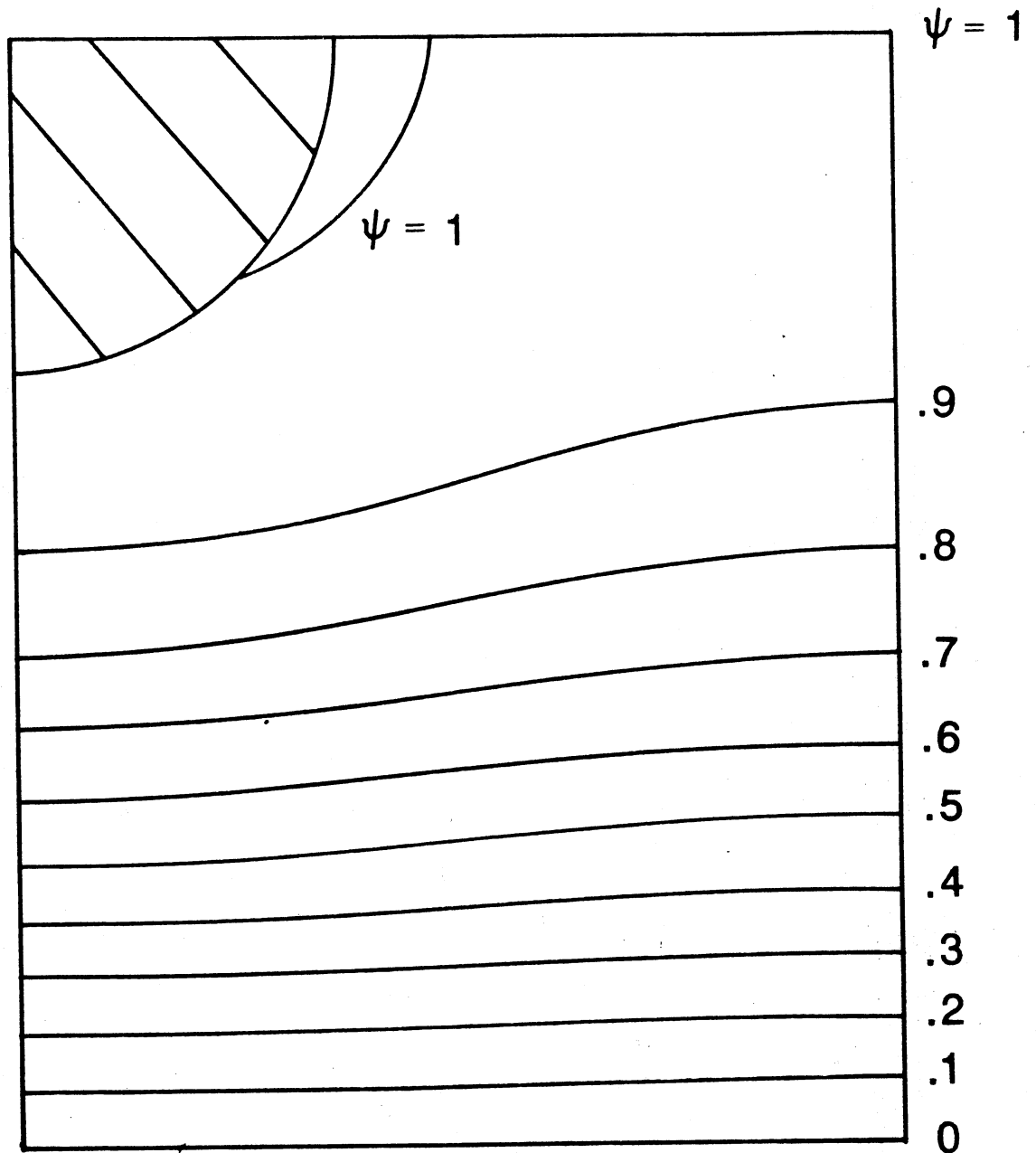


Figure 37. Streamline Plot for Flow Through an Infinite Rectangular Array of Cylinders, $R=10.0$.

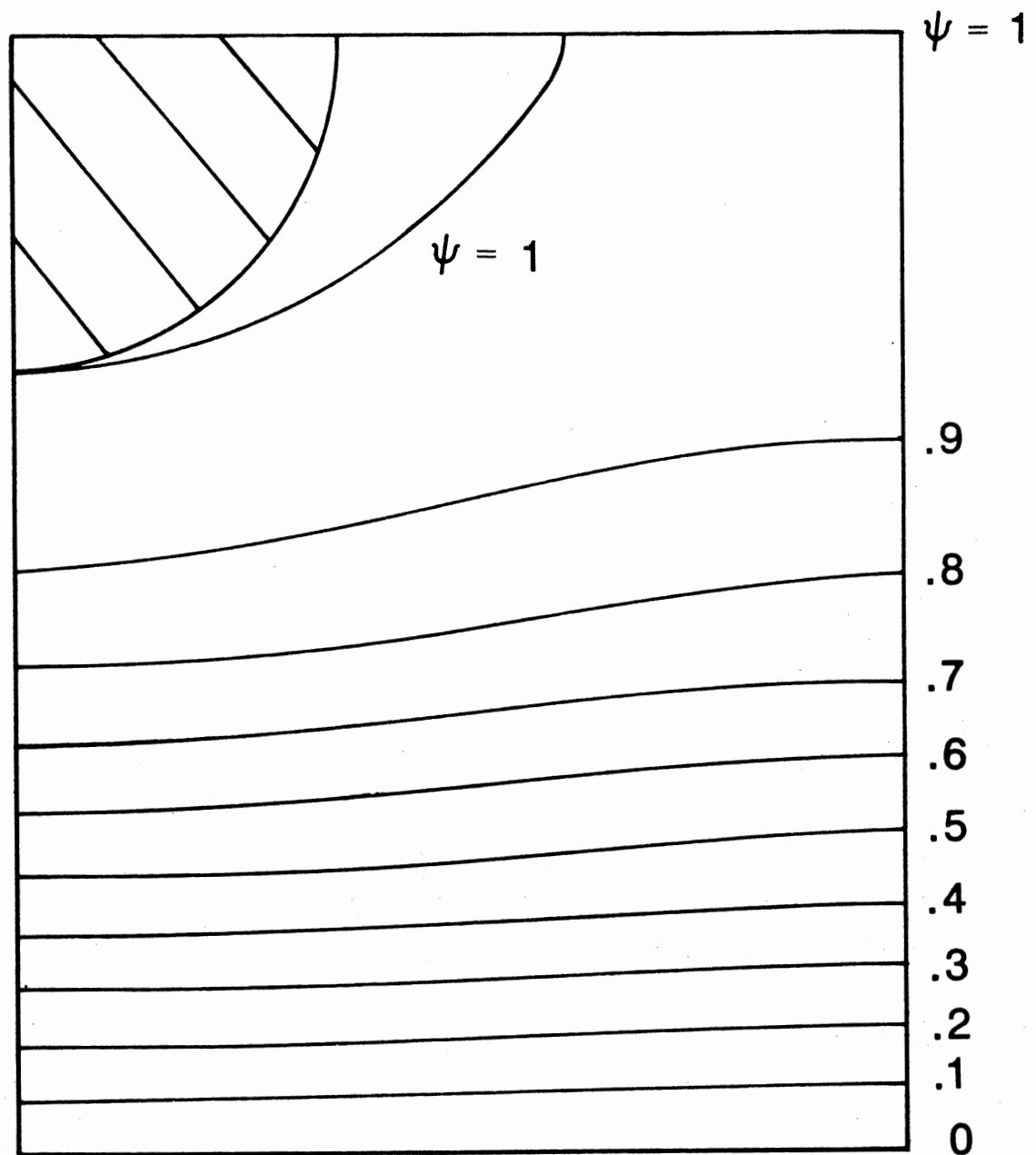


Figure 38. Streamline Plot for Flow Through an Infinite Rectangular Array of Cylinders, $R=20.0$.

the pressure around the inner cylinder C_1 (Ingham and Kelmanson, 1984)

$$\int_{C_1} \frac{\partial P}{\partial S} dS = 0 \quad (218)$$

Equation (218) may be rewritten in terms of the vorticity as

$$\int_{C_1} \frac{\partial \omega}{\partial n} dS = \int_{C_1} \omega' dS = 0 \quad (219)$$

Equation (219) provides the additional relationship required for a solution while accurately enforcing the pressure condition. Results given in the form of plots of streamlines and vorticity contours for cylindrical bearings with eccentricities of 0.5 and 0.8 are shown in Figures 39 and 40. Streamlines and vorticity contours for elliptical bearings with eccentricities of 0.5 and 0.8 are shown in Figures 41 and 42, respectively. Eccentricity for cylindrical geometries is defined as $e = \epsilon(r_2 - r_1)$ and as $e = \epsilon(a_2 - r_1)$ for elliptical bearings. In each case the results are in excellent agreement with those given by Ingham and Kelmanson (1984).

Concluding Remark

The examples presented in this chapter consistently showed that the boundary element formulation developed in this work accurately predicted the solution for a wide range of engineering problems of various geometries. In the next chapter a complete summary of the various techniques developed in this work will be presented along with some general conclusions and recommendations.

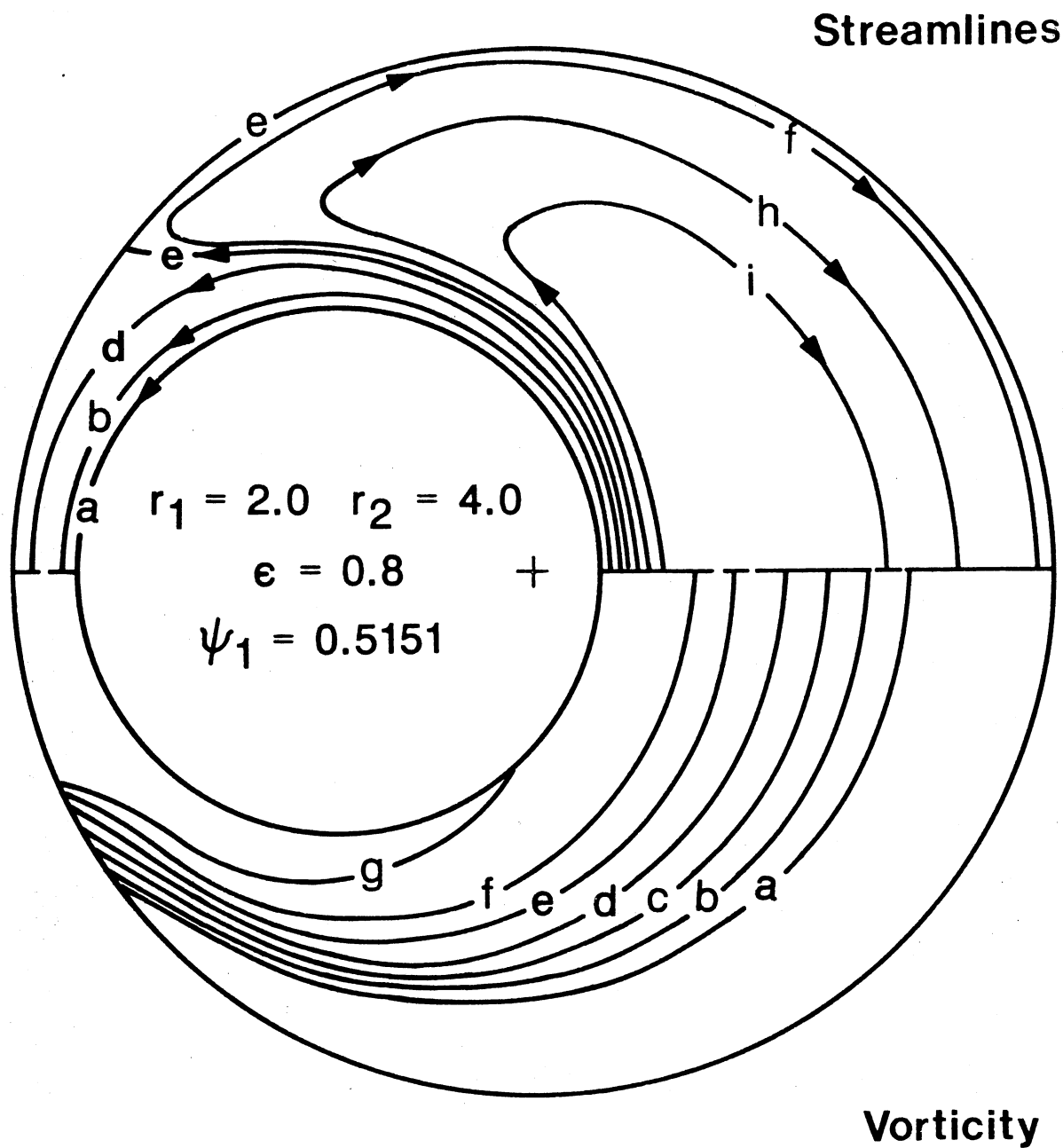


Figure 40. Streamline and Vorticity Contours for an Eccentric Bearing, $e=0.8$. Streamline are at Values of ψ_1/N , where N is (a) 1; (b) 1.5; (c) 3; (d) 10; (e) ∞ ; (f) -60; (g) -30; (h) -5; (i) -2. Vorticity are at Values of N Equal to (a) 0; (b) 0.3; (c) 0.6; (d) 1; (e) 1.5; (f) 2 (g) 4.

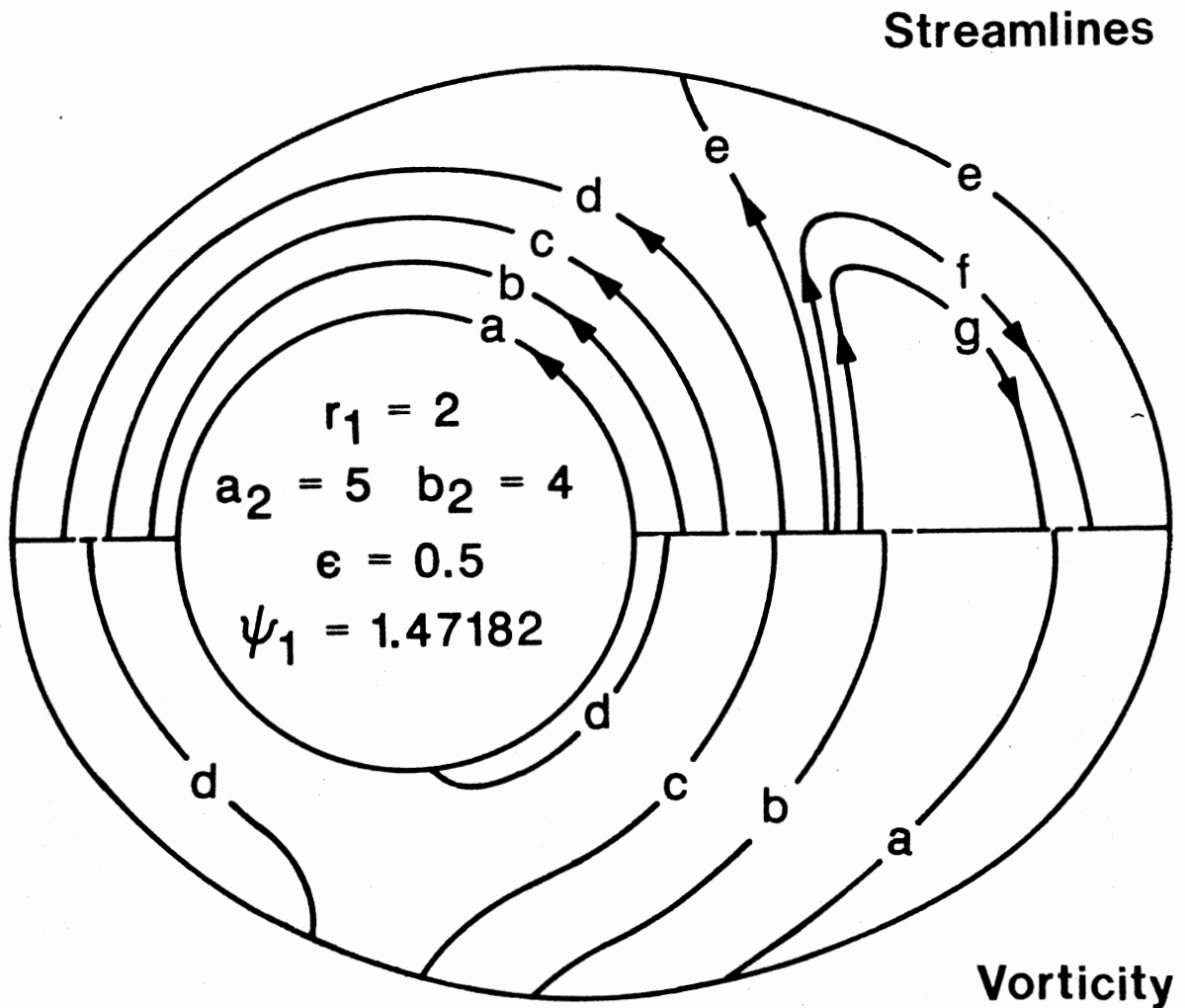


Figure 41. Streamline and Vorticity Contours for an Elliptical Eccentric Bearing, $e=0.5$. Streamline are at Values of ψ_1/N , where N is (a) 1; (b) 1.5; (c) 3; (d) 10; (e) ∞ ; (f) -60; (g) -30 (h) -5; (i) -2. Vorticity are at Values of N Equal to (a) 0; (b) 0.3; (c) 0.6; (d) 1; (e) 1.5; (f) 2 (g) 4.

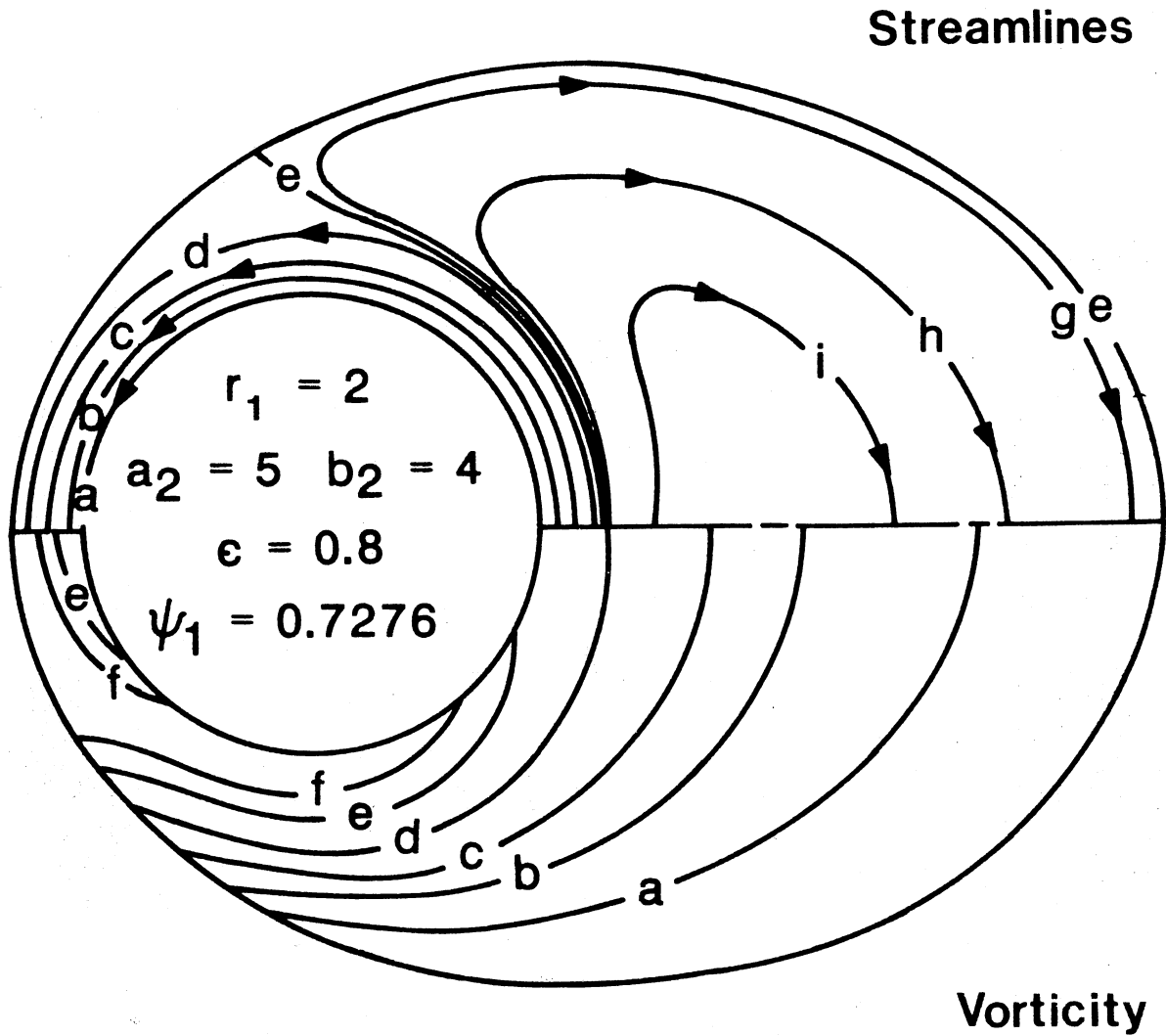


Figure 42. Streamline and Vorticity Contours for an Elliptical Eccentric Bearing, $e=0.8$. Streamline are at Values of ψ_1/N , where N is (a) 1; (b) 1.5; (c) 3; (d) 10; (e) ∞ ; (f) -60; (g) -30 (h) -5; (i) -2. Vorticity are at Values of N Equal to (a) 0; (b) 0.3; (c) 0.6; (d) 1; (e) 1.5; (f) 2.

CHAPTER VI

SUMMARY AND CONCLUSIONS

Summary

In this work the objective was to develop an accurate and more computationally efficient boundary element formulation of the nonhomogeneous biharmonic equation. This goal was achieved, in part, by improving the representation of the boundary through the use of numerical and analytical forms of the Overhauser element. In addition, the domain was efficiently modeled by a "fanning" integration technique characterized by an implicit discretization of the domain coupled with an intrinsic sensitivity to the singularity of the fundamental solution. It was shown that the formulation developed in the previous chapters implementing both the Overhauser element and the "fanning" domain integrator can be used to solve a wide range of biharmonic problems. By incorporating an iterative solution technique which takes advantage of an interpolating map storage scheme, the formulation was shown to be accurate in solving a diverse group of problems in which the nonhomogeneous term was a function of the field variables and their derivatives. The examples, presented in Chapter V, demonstrate the accuracy and versatility of the formulation and give a good indication of its ability to solve similar problems.

Conclusions

The piecewise representation of the boundary geometry and the distribution of the function over each segment are of the utmost importance in the boundary element method. Many times the domain integrations may be transformed into an equivalent set of surface integrals. The resulting boundary element solution is entirely dependent on the accurate and efficient evaluation of the surface integrals. A series of analytical expressions for the required surface integrations were developed for a general isoparametric linear element and the subparametric forms of the quadratic and the Overhauser elements. For a variety of geometries and boundary conditions, the Overhauser element was found to be superior when compared with the lower order elements. At present, the main disadvantage of the Overhauser element is its general inability to handle discontinuous geometries, e.g., corners. This particular problem may be avoided by double noding at corners or coupling the Overhauser element with a nonspline type of element. For rectilinear geometries, the subparametric versions of both the quadratic and the Overhauser elements significantly reduce the total execution time while providing excellent solutions. However, the Overhauser formulation was generally superior to its quadratic counterpart, especially on the boundary at points where discontinuity cusps formed between quadratic elements.

The most common approach used in evaluating domain integrations is the discretization of the domain into a series of cells over which some type of numerical quadrature is performed. In this type of analysis it may be necessary to explicitly define the location of each

cell describing the domain. Recently, several other techniques have eliminated the need for explicit cell definition. The Monte Carlo quadrature technique does not require domain discretization; however, this method is inherently slow to converge and the random characteristic of the quadrature point distribution generally requires a large number of points. Several methods involving multidimensional Gaussian quadrature over the entire domain are possible alternatives if the behavior of the function over the region is known beforehand. In areas where the function is "strongly peaked," the integral may be subdivided into a set of small regions over which the integrand is considered more "well behaved". The "fanning" domain integration technique developed in this work draws on the advantages of implicit domain discretization while automatically concentrating quadrature points in a way that is sensitive to the singular nature of the integrand. The number of quadrature points is directly related to the number of surface elements which define the boundary of the problem.

The most effective and accurate form of evaluating domain integrations is through the use of integral transformations where the domain integrals are converted into a series of surface integrations. The power and accuracy of higher order elements, such as the Overhauser element, make this technique very attractive. However, the main drawback is a loss of generality in the type of functions that may be evaluated. In theory, the transformation may be extended to any order harmonic function. General transcendental functions may be represented by a finite series approximation and transformed by the appropriate form of the Green's identity. This method was shown to

obtain very accurate results with relatively small boundary discretizations using Overhauser elements.

The iterative solution technique employing the interpolating map storage scheme was quite efficient in solving the form of the equation in which the nonhomogeneous term was a function of the field variables and their derivatives. A variety of examples, presented in Chapter V, demonstrated the ability of this formulation in solving very complex problems for which solutions are difficult to obtain by any other treatment. The interpolating nature of the map storage formulation reduces the amount of time required to update each map while providing an accurate representation of the solution over the domain. Each map is automatically generated and updated for arbitrary regions without any additional information other than that required to define the discrete boundary of the problem. The major disadvantage associated with this type of procedure, as with all iterative methods, is a significant increase in the total execution time of the formulation.

Recommendations

The Overhauser element and the "fanning" domain integration technique presented in this work have been shown to be notable improvements in the practical implementation of the boundary element method to the biharmonic equation. The increase in accuracy and the reduction in execution time associated with the analytical expression derived for the surface integrations show promise for future research. New methods for approximating the Jacobian part of the integrand will allow the development of analytical expressions for higher order isoparametric elements. The effectiveness of the Overhauser element is

due to its representation of first derivative continuity in both the geometry and the distribution of the function. Development of elements which provide second and third derivative continuity seems an appropriate area for further research.

REFERENCES

- Abramowitz, M., and Stegun, I. A., eds. Handbook of Mathematical Functions. Dover Publications, Inc., New York, 1972.
- Altiero, N. J., and Sikarskie, D. L. "A Boundary Integral Method Applied to Plates of Arbitrary Plan Form." Computers and Structures, Vol. 9, 1978, pp. 163-168.
- Banerjee, P. K., and Butterfield, R. Boundary Element Methods in Engineering Science. McGraw-Hill, New York, 1981.
- Bezine, G., and Gamby, D. "A New Integral Equation Formulation for Plate Bending Problems." Recent Advances in Boundary Element Methods. C.A. Brebbia, ed. Pentech Press, London, 1978.
- Beyer, W. H., ed. CRC Standard Mathematical Tables. CRC Press, Inc., Boca Raton, Florida, 1981.
- Bois, G. P. Tables of Indefinite Integrals. Dover Publications, Inc., New York, 1961.
- Brebbia, C. A., ed. The Boundary Element Method for Engineers. Pentech Press, London, 1978.
- Brebbia, C. A., and Walker S., Boundary Element Techniques in Engineering. Newnes-Butterworths, London, 1980.
- Brebbia, C. A., ed. "Recent Advances in Boundary Element Methods." Proc. of the First Intl. Conference on Boundary Element Methods. Southampton University, CML Publications, London, 1980.
- Brebbia, C. A., ed. "New Developments in Boundary Element Methods." Proc. of the Second Intl. Conference on Boundary Element Methods. Southampton University, CML Publications, London, 1980.
- Brebbia, C. A., ed. "Boundary Element Methods." Proc. of the Third Intl. Conference on Boundary Element Methods. Irvine, California, Springer-Verlag, Berlin, 1981.
- Brebbia, C. A., ed. "Boundary Element Methods in Engineering." Proc. of the Fourth Int. Conference on Boundary Element Methods. Southampton University, Springer-Verlag, Berlin, 1982.

- Brebbia, C. A., Futagami, T., and Tanaka M., eds. "Boundary Elements." Proc. of the Fifth Intl. Conference on Boundary Element Methods. Hiroshima, Japan, Springer-Verlag, Berlin, 1983.
- Brebbia, C. A., ed. Progress in Boundary Element Methods. Vol. 2. Pentech Press, London, 1983.
- Brebbia, C. A., Telles, J. C. F., and Wrobel, L. C. "Boundary Element Techniques. Theory and Applications in Engineering. Springer-Verlag, Berlin, 1984.
- Brebbia, C. A., ed. Boundary Element Techniques in Computer-Aided Engineering. Martinus Nijhoff Publishers, Dordrecht, 1984.
- Brebbia, C. A., ed. Topics in Boundary Element Research. Springer-Verlag, Berlin, 1984.
- Brebbia, C. A., and Maier, G., ed. "Boundary Elements VII." Proc. of the Seventh Intl. Conference on Boundary Element Methods. Lake Como, Italy, 1985; Springer-Verlag, Berlin, 1985.
- Brewer, J. A. "Three-Dimensional Design by Graphical Man-Computer Communication." Ph.D. dissertation, Purdue University, 1977.
- Brewer, J. A., and Anderson, D. C.. "Visual Interaction with Overhauser Curves and Surfaces." Computer Graphics, Vol. 11, 1977, pp. 132-137.
- Butkovskiy, A. G. Green's Functions and Transfer Functions Handbook. L. W. London, trans. Elliss Horwood Ltd., New York, 1982.
- Camp, C. V., and Gipson, G. S. "A Boundary Element Method for Viscous Flows at Low Reynolds Number." Boundary Elements IX: Proc. of the Ninth Intl. Conference on Boundary Element. Stuttgart, West Germany, September, 1987.
- Connor, J. J., and Brebbia, C. A., eds. Betech 86: Proc. of the 2nd Boundary Element Technology Conference. Massachusetts Institute of Technology, June, 1986; Computational Mechanics Publications, Southampton, 1986.
- Costa, J. A., and Brebbia C. A. "The Boundary Element Method Applied to Plates on Elastic Foundations." Engineering Analysis, Vol. 2, No. 4, 1985, pp. 174-183.
- Cowper, G. R. "Gaussian Quadrature Formulas for Triangles." International Journal of Numerical Methods in Engineering, Vol. 7, 1973, pp. 405-408.
- Currie, I. G. Fundamental Mechanics of Fluids. McGraw-Hill, New York, 1974.

- Fairweather, G., Rizzo, F. J., Shippy, D. J., and Wu, Y. S. "On the Numerical Solution of Two-Dimensional Potential Problems by an Improved Boundary Integral Equation Method " Journal of Computational Physics, Vol. 31, 1979, pp. 96-112.
- Gipson, G. S. "The Coupling of Monte Carlo Integration with the Boundary Integral Equation Technique to Solve Poisson Type Equations." Ph.D. dissertation, Louisiana State University, 1982.
- Gipson, G. S. "Coupling Monte Carlo Quadrature with Boundary Elements to Handle Domain Integrals in Poisson Type Problems." Engineering Analysis, Vol. 2, No. 3, 1985, pp. 138-145.
- Gipson, G. S., and Camp, C. V. "Effective Use of Monte Carlo Quadrature for Body Force Integrals Occurring in the Integral Form of Elastostatics." Boundary Elements VII: Proc. of the Seventh Intl. Conference on Boundary Element Methods. September, 1985, Lake Como, Italy, Springer-Verlag, Berlin, 1985.
- Gipson, G. S., and Camp, C. V. "Phreatic Surface and Subsurface Flow With Boundary Elements Using an Advanced Green's Function." Betech 86: Proc. of the 2nd Boundary Element Technology Conference. Massachusetts Institute of Technology, June, 1986; Computational Mechanics Publications, Southampton, 1986.
- Gipson, G. S. "Use of Residue Theorem in Locating Points Within an Arbitrary Multiply-Connected Region." Advances in Engineering Software, Vol. 8, No. 2, 1986, pp. 73-80.
- Gradshteyn I. S., and Ryshik, I. M. Tables of Integrals, Series, and Products. Academic Press, New York, 1980.
- Guo-Shu S. and Mucherjee S. "Boundary Element Method Analysis of Bending of Elastic Plates of Arbitrary Shape with General Boundary Conditions". Engineering Analysis, Vol. 3, NO. 1, 1986, pp. 36-44.
- Hansen E. B. "Numerical Solution of Integro-Differential and Singular Integral Equations for Plate Bending Problems." Journal of Elasticity, Vol. 6, 1976, pp. 39-56.
- Hildyard M. L., Ingham, D. B., Heggs, P. J., and Kelmanson, M. A. "Integral Equation Solution of Viscous Flow Through a Fibrous Filter " Boundary Elements VII: Proc. of the Seventh Intl. Conference on Boundary Element Methods. September, 1985, Lake Como, Italy; Springer-Verlag, Berlin, 1985.
- Hoagland, D. A., and Prud'homme, R. K. "Taylor-Aris Dispersion Arising From Flow in a Sinusoidal Tube." AICHE Journal, Vol. 31, 1985., pp. 236-244.

- Ingham, D. B., and Kelmanson, M. A. "A Boundary Integral Equation Method for the study of Slow Flow Within Bearing Geometries." Proceedings of the 5th International Conference on Boundary Elements. Hiroshima, Japan; Springer-Verlag, Berlin, 1983.
- Ingham D. B., and Kelmanson M. A. "Boundary Integral Equation Analyses of Singular, Potential, and Biharmonic Problems." Lecture Notes in Engineering, Vol. 7, Springer-Verlag, Berlin, 1984.
- Jaswon, M. A., Maiti, M., and Symm, G. T. "Numerical Biharmonic Analysis and Some Applications." International Journal of Solids and Structures, Vol. 3, 1976, pp. 309-332.
- Jaswon, M. A., and Maiti, M. "An Integral Equation Formulation of Plate Bending Problems." Journal of Engineering Mathematics, Vol. 2, 1968, pp. 83-93.
- Jaswon, M. A., and Symm G. T. Integral Equation Methods in Potential Theory and Elastostatics. Academic Press, London, 1977.
- Katsikadelis, J. T., and Armenakas, A. E. "Analysis of Clamped Plates on Elastic Foundation by the Boundary Integral Equation Method." Journal of Applied Mechanics, ASME, Vol. 51, 1984, pp. 574-580.
- Katsikadelis, J. T., and Armenakas, A. E. "Numerical Evaluation of Double Integrals With a Logarithmic of Cauchy-Type Singularity." Journal of Applied Mechanics, ASME, Vol. 50, 1983, pp. 682-684.
- Katsikadelis, J. T., and Armenakas, A. E. "Plates of Elastic Foundation by BIE Method." Journal of Engineering Mechanics, ASCE, Vol. 110, 1984, pp. 1086-1105.
- Katsikadelis, J. T., and Armenakas, A. E. "Numerical Evaluation of Line Integrals With a Logarithmic Singularity." AIAA Journal, Vol. 23, 1984, pp. 1135-1137.
- Katsikadelis, J. T., and Kallivokas, L. F. "Clamped Plates on Pasternak-Type Elastic Foundation by the Boundary Element Method." Journal of Applied Mechanics, ASME, Vol. 53, 1986, pp. 909-917.
- Kellogg, O. D. Foundations of Potential Theory. Dover Publications, Inc., New York, 1954.
- Kelmanson, M. A. "Boundary Integral Equation Solution of Viscous Flows With Free Surfaces." Journal of Engineering Mathematics, Vol. 17, 1983(a), pp. 329-342.
- Kelmanson, M. A. "An Integral Equation Method for the Solution of Singular Slow Flow Problems." Journal of Computational Physics, Vol. 51, 1983(b), pp. 139-158.

- Kerr, A. D. "Elastic and Viscoelastic Foundation Models." Journal of Applied Mechanics, ASME, Vol. 31, 1964, pp. 491-498.
- Kreyszig, E. Advanced Engineering Mathematics. Fifth Ed. Wiley & Sons, New York, 1983.
- Lamb, H. Hydrodynamics. Dover Publications, Inc., New York, 1945.
- Lapidus, L., and Pinder, G. F. Numerical Solution of Partial Differential Equations in Science and Engineering. John Wiley & Sons, New York, 1982.
- Lebedev, N. N., Skalskaya, I. P., and Uflyans, Y. S. Worked Problems in Applied Mathematics. R. A. Silverman, trans. Dover Publications, New York, 1965.
- Lebedev, N. N. Special Functions and Their Applications. R. A. Silverman, trans. and ed. Dover Publications, Inc., New York, 1972.
- Leissa, A. W., Lo, C. C., and Niedenfuhr, F. S. "Uniformly Loaded Plates of Polygonal Shape." AIAA Journal, Vol. 3, 1965, pp. 566-567.
- Liggett, J. A., and Salmon, J. R. "Cubic Spline Boundary Elements." International Journal of Numerical Methods in Engineering, Vol. 17, 1981, pp. 543-556.
- Maiti, M., and Chakrabarty S. K. "Integral Equation Solutions for Simply Supported Polygonal Plates." International Journal of Engineering Science, Vol. 12, 1974, pp. 793-806.
- Mills, R. D. "Computing Internal Viscous Flow Problems for the Circle by Integral Methods." Journal of Fluid Mechanics, Vol. 79, 1977, pp. 609-624.
- Ng, S. S. F. "Influence of Elastic Support on the Behavior of Clamped Plates." Developments in Mechanics, Vol. 5, Proc. 11th Midwestern Mechanics Conference, 1969, pp. 343-371.
- Ortiz, J. C. "An Improved Boundary Element Analysis System for the Solution of Poisson's Equation." M.S. thesis, Louisiana State University, 1986.
- Overhauser, A. W. "Analytic Definition of Curves and Surfaces by Parabolic Blending." Ford Motor Company Technical Report, SL68-40, 1968.
- Press, W. H., Flannery, B. P., Teukolsky, S. A., and Vetterling, W. T. Numerical Recipes. Cambridge University Press, Cambridge, 1986.

- Rouse, H. Elementary Mechanics of Fluids. Dover Publications, Inc, New York, 1978.
- Schlichting, H. Boundary-Layer Theory. J. Kestin, trans. McGraw-Hill, New York, 1979.
- Segedin, C. M., and Brickell, D. G. A., "Integral Equation Method for a Corner Plate." Journal of the Structural Division, ASCE, Vol. 94, No. ST1, 1968.
- Selvadurai, A. P. S. Elastic Analysis of Soil-Foundation Interaction. Elsevier/North-Holland, 1979.
- Slattery, J. C. Momentum, Energy, and Mass Transfer in Continua. Robert E. Krieger Publishing Company, New York, 1981.
- Stern, M. "A General Boundary Integral Formulation for the Numerical Solution of Plate Bending Problems." International Journal of Solids and Structures, Vol. 15, 1979, pp. 769-782.
- Stern, M. "Boundary Integral Equations for Bending of Thin Plates." Progress in Boundary Element Methods. Vol. 2. C.A. Brebbia, ed. Pentech Press, London, 1983.
- Stroud, A. H., and Secrest, D. Gaussian Quadrature Formulae. Prentice-Hall, Englewood Cliffs, New Jersey, 1966.
- Syngellakis, S., and Kang, M. "A Boundary Element Solution of the Plate Buckling Problem." Engineering Analysis, Vol. 4, No. 2, 1987, pp. 75-81.
- Szilard, R. Theory and Analysis of Plates--Classical and Numerical Methods. Prentice-Hall, New York, 1974.
- Telles, J. C. F. "The Boundary Element Method Applied to Inelastic Problems." Lecture Notes in Engineering. Vol. 1. Springer-Verlag, Berlin, 1984.
- Timoshenko, S. T., and Woinowsky-Krieger, S. Theory of Plates and Shells. McGraw-Hill, New York, 1959.
- Tottenham, H. "The Boundary Element Method for Plates and Shells." Developments in Boundary Element Methods 1. P. K. Banerjee and R. Butterfield, ed. Applied Science Publishers, Ltd., London, 1979.
- Ugural, A. C. Stresses in Plates and Shells. McGraw-Hill, New York, 1981.
- Walters, H. G. "Techniques for Boundary Element Analysis in Elastostatics Influenced by Geometric Modelling " M.S. thesis, Louisiana State University, 1986.

- Wu, B. C., and Altiero, N. J. "A Boundary Integral Method Applied to Plates of Arbitrary Plan Form and Arbitrary Boundary Conditions." Computers and Structures, Vol. 10, 1979, pp. 703-707.
- Wylie, C. R., and Barrett, L. C. Advanced Engineering Mathematics. McGraw-Hill, New York, 1982.
- Xu, B., and Hansen, E. B. "Transient Stokes Flow in a Wedge." Journal of Applied Mechanics, Vol. 54, 1987, pp. 203-208.
- Youngren, G. K., and Acrivos, A. "Stokes Flow Past a Particle of Arbitrary Shape: A Numerical Method of Solution." Journal of Fluid Mechanics, Vol. 69, 1975, pp. 377-403.
- Zienkiewicz, O. C. The Finite Element Method. 3rd Ed. McGraw-Hill, Maidenhead, U.K., 1977.

VITA

Charles V. Camp

Candidate for the Degree of

Doctor of Philosophy

Dissertation: A SOLUTION OF THE NONHOMOGENEOUS BIHARMONIC
EQUATION BY THE BOUNDARY ELEMENT METHOD

Major Field: Civil Engineering

Biographical:

Personal Data: Born in Panama City, Florida, on April 23, 1958,
the son of Billy E. and Barbara R. Camp.

Education: Graduated from Hawaii Baptist Academy, Honolulu,
Hawaii, in June 1976; received the Bachelor of Science in
Civil Engineering degree on June 1981; received the Master
of Science degree from Auburn University in June, 1986;
completed requirements for the Doctor of Philosophy degree
at Oklahoma State University in December, 1987.

Professional Experience: Research Engineer, Water Resource
Institute, Auburn University, 1982; Research and Teaching
Assistant, Department of Civil Engineering, Auburn Univer-
sity, 1981-1983; Hydrologist, U.S. Geologic Survey, Baton
Rouge, LA, 1983; Research and Teaching Assistant, Department
of Civil Engineering, Louisiana State University, 1984-1986;
Research Associate, U.S.A.E. Waterways Experiment Station,
Vicksburg, MS, 1986; Graduate Teaching Assistant, School of
Civil Engineering, Oklahoma State University, 1986-1987;
Research Associate, U.S.A.E. Waterways Experiment Station,
Vicksburg, MS, 1987; Teaching Associate, School of Civil
Engineering, Oklahoma State University, 1987.